Sustainable Pre-Treatments for White Spruce Wood-Based Activated Carbon: Impact on Porosity and Aqueous-Phase Adsorption

Kieran Lobo

Under the joint supervision of:
Dr. Reza Foruzanmehr and Dr. Roberto M. Narbaitz

Thesis submitted to the University of Ottawa
in partial Fulfillment of the requirements for the
Master of Applied Science

Department of Civil Engineering
Faculty of Engineering
University of Ottawa

Abstract

Historically, activated carbon (AC) has been widely used in potable water treatment to remove dissolved organic compounds, including taste and odour-causing compounds, harmful pesticides, and herbicides. Its high specific surface area and extensive pore size distribution give AC a high adsorption capacity for various contaminants. There are numerous long-term drinking water advisories in remote and northern Canadian communities that arise from the significant economic, transportation and logistical challenges in constructing and maintaining water treatment infrastructure. A sustainable solution could be to use white spruce wooden pallets, a common waste in the region, to manufacture AC onsite for use in drinking water treatment. However, the economic and technical constraints necessitate cost-effective and simple methodologies for producing high-performance AC.

The primary objective of this thesis is to evaluate the feasibility of producing AC from white spruce wood using phosphoric acid, both with and without three distinct pre-treatment (PT) methods. Part of the novelty of this study is that these PT methods – Torrefaction (TPT), Hydrothermal (HPT) and Alkaline (APT) – have been explored individually in the literature but not comparatively applied to the same materials for this purpose, and this study addresses this gap. A secondary objective is to analyze how these PTs alter the crystalline structure, chemical composition, and macroscopic properties of white spruce wood, and to assess how these changes influence the adsorption capacity and pore size distribution of the resulting ACs. To support the proposed differences in pore development mechanisms, thermogravimetric analysis (TGA) paired with Fourier Transform – Infrared Spectroscopy (FT-IR) was used to analyze the gases produced during the carbonization of phosphoric acid-impregnated samples.

The results showed that all the PT methods promoted a greater degree of pore widening during carbonization, enhancing adsorption capacities, specific surface areas and pore volumes compared to the Untreated sample. Remarkably, the PT methods made it possible to produce AC from white spruce wood with iodine adsorption capacities (Iodine Number, IN) and specific surface areas comparable to those of commercial ACs. The enhanced AC properties were accredited to the PTs removing amorphous

biopolymers (mainly hemicellulose) from white spruce wood, decreasing the apparent density of the wood leading to increased phosphoric acid activating agent permeation into the wood. This removal increased the crystallinity index (CrI) of the wood, favouring phosphoric acid's reaction with amorphous biopolymers, enhancing pore widening. The different PTs affected crystalline cellulose uniquely, which had the most significant impact on pore development in the ACs. Based on the mean size of cellulose crystallites, it was hypothesized that there was a shift in the dominant mechanism of pore development (acid-catalyzed hydrolysis of biopolymers versus cross-link formation) in AC during carbonization. The change in crystallite size due to HPT caused the greatest increase in specific surface area and adsorption capacity of all ACs produced. HPT slightly increased the size of cellulose crystallites, favouring the development of small mesopores during activation by benefitting from both enhanced acid catalyzed-hydrolysis and cross-link formation. On the other hand, TPT decreased the size of crystallites, leading to somewhat smaller pores in the AC by promoting cross-link formation between the smaller crystallites during activation and limiting acid-catalyzed hydrolysis. APT increased crystallite size to the greatest degree, limiting acid-catalyzed hydrolysis of biopolymers, making the AC slightly more microporous than HPT AC. The pore size distributions of the PT ACs suggest their potential suitability for removing taste and odour-causing compounds, cyanotoxins, and natural organic matter (NOM) in potable water, which are concerns in northern Canadian waters. Ultimately, the study highlights the potentially transformative role that simple PT methods have in optimizing AC adsorption capacity, specific surface area and pore size distribution.

Acknowledgements

The author would like to express his sincerest gratitude to the following persons and parties:

Dr. Foruzanmehr, your enthusiasm, creativity, and unwavering support have been a source of motivation through the years; starting in my undergraduate degree and through my graduate research. Your ability to provide clarity and perspective in times of uncertainty is an inspiration. I will remember our long trips to the Université de Sherbrooke during the preliminary phases of this work. Those trips emphasize your dedication to the work and your students.

Dr. Narbaitz, your meticulous attention to detail and commitment to academic quality has challenged me to think critically and refine my ideas. You are the definition of a professional and I feel fortunate to have spent many hours working together, whether during your Directed Studies course or discussing our research.

The Natural Science and Engineering Research Council of Canada (NSERC) for their financial support through Dr. Narbaitz and Foruzanmehr's NSERC Discovery grants.

Dr. Stephanie Guilherme, for your support and guidance at the beginning of this research.

Joseph D. "J.D." Ladouceur, for your technical support, critical review and friendship. Your insightful discussions and shared enthusiasm have been and will continue to be a source of motivation and inspiration. Dr. Patrick D'Aoust, your willingness to support the setup of the research equipment was critical to this work. Dr. Mathieu Robert, for supporting the preliminary data collection at the Université de Sherbrooke.

My family (Mom, Dad, Aidan), for their support and encouragement throughout. Your wisdom and faith have given me the confidence and drive to pursue my goals. Thank you.

Ashley, your constant reassurance, sacrifice and patience have made this process manageable. Thank you for supporting me in every possible aspect from the beginning of my research journey. I am forever grateful for everything you have done along the way.

Table of Contents

Abstract ii
Acknowledgements iv
List of Figures ix
List of Tables xiii
List of Abbreviations xiv
List of Variables xvi
Chapter 1 - Introduction 1
1.1 Background 1
1.2 Research Objectives 5
1.3 Research Methodology 6
1.3.1 Phase 1: Production and Characterization of Untreated and Pre-treated White Spruce Wood Activated Carbons. 6
1.3.2 Phase 2: Characterization of Untreated and Pre-treated Whtie Spruce Wood. 6
1.3.3 Phase 3: Observation of Gaseous Products During Carbonization Step of Activation for Untreated and Pre-treated White Spruce Wood Samples. 7
1.4 Thesis Outline 7
Chapter 2 - Background 9
2.1 Water Treatment Challenges in Remote Communities of Canada 9
2.2 Emerging Water Treatment Challenges 12
2.3 Proposed Solution 14
Chapter 3 - Literature Review 16
3.1 Activated Carbon for Water Treatment 16
3.1.1 Treatment Processes 16
3.1.1.1 Powdered Activated Carbon 17
3.1.1.2 Granular Activated Carbon 18
3.1.2 Adsorption 21
3.1.3 Internal Pore Structure of Activated Carbon 22
3.1.4 Atomic Structure of Activated Carbon 24
3.1.4.1 Carbon Structure 24
3.1.4.2 Surface Function Groups 25
3.2 Activated Carbon Production 27
3.2.1 Physical Activation for Activated Carbon Production 27

3.2.2 Chemical Activation for Activated Carbon Production 29
3.2.3 Lignocellulosic Materials for the Production of Activated Carbon 34
3.2.4 Wood Characteristics 37
3.2.4.1 Anatomy of Wood 37
3.2.4.2 Wood Cell Wall 38
3.2.4.3 Chemical Composition 40
3.2.4.4 Impact of Wood Chemical Structures on Activated Carbon Porosity 47
3.3 Woody Biomass Pre-Treatments 49
3.3.1 Physical Pre-Treatments 50
3.3.1.1 Particle Size Reduction 50
3.3.1.2 Torrefaction Pre-Treatment 50
3.3.1.3 Ultrasonic Pre-treatment 51
3.3.2 Chemical Pre-Treatments 52
3.3.2.1 Hydrothermal Pre-Treatment 52
3.3.2.2 Alkaline Pre-Treatment 53
3.3.2.3 Acid Hydrolysis 53
3.3.3 Comparison of Pre-Treatment Methods 55
3.4 Conclusions and Research Gaps 57
Chapter 4 - Materials and Methods 59
4.1 Materials 59
4.1.1 Lignocellulosic Precursor 59
4.1.2 Chemicals 59
4.2 Wood Pre-Treatment Methods 60
4.2.1 Sample Preparation 60
4.2.2 Pre-Treatments 64
4.2.2.1 Torrefaction Pre-Treatment 64
4.2.2.2 Hydrothermal Pre-Treatment 67
4.2.2.3 Alkaline Pre-Treatment 68
4.3 Activated Carbon Preparation Methods 72
4.4 Experimental and Analytical Methodology 74
4.4.1 Characterization of Activated Carbons 76
4.4.1.1 Adsorption Capacity Analysis by Iodine Number Test for Activated Carbons 76
4.4.1.2 Activated Carbon Surface Area and Pore Size Analysis by Nitrogen Adsorption Test 77
4.4.2 Characterization of Pre-Treated Woods 77

4.4.2.1 Powder – X-Ray Diffraction of Wood Samples 77
4.4.2.2 Fourier Transform – Infrared Spectroscopy of Wood Samples 80
4.4.2.3 Apparent Density of Wood Blocks 81
4.4.2.4 Identifying Differences in Activated Carbon Pore Development Mechanisms 83
4.4.2.5 Carbonization of Phosphoric Acid Impregnated Wood and Analysis of Produced Off-Gases 83
4.4.2.6 FT-IR of Off-Gases Produced During Carbonization of Dry and Impregnated Wood 86
Chapter 5 - Sustainable Pre-Treatments for White Spruce Wood-based Activated Carbon: Impact on Porosity and Aqueous-Phase Adsorption 88
5.1 Abstract 88
5.2 Introduction 88
5.3 Materials and Methods 91
5.3.1 Materials 91
5.3.2 Sample Resizing 91
5.3.3 Pre-Treatment Processes 92
5.3.3.1 Torrefaction Pre-Treatment 92
5.3.3.2 Hydrothermal Pre-Treatment 92
5.3.3.3 Alkaline Pre-Treatment 93
5.3.4 Preparation of Activated Carbon 93
5.3.5 Characterization of Activated Carbons 94
5.3.5.1 Aqueous-Phase Adsorption Capacity by Iodine Number of Activated Carbons 94
5.3.5.2 Surface Area and Pore Size Analysis by Nitrogen Adsorption Tests 94
5.3.6 Methods of Characterizing the Impact of Pre-Treatments on Wood Properties 94
5.3.6.1 Powder X-Ray Diffraction 95
5.3.6.2 Fourier Transform – Infrared Spectroscopy 96
The FT-IR spectra of the 5 × 5 × 2 mm samples were collected before and after each PT using the Nicolet™ iS650 FT-IR Spectrometer (Thermo Fisher Scientific, St. Louis, MO, USA). The spectra were measured between 4000 cm^{-1} and 400 cm^{-1} (average of 64 scans) at a resolution of 4 cm^{-1}. The spectrophotometer's attenuated total reflectance (ATR) crystal was cleaned with alcohol before each sample measurement as per the methods described in the iS50 ATR Module User Guide (Thermo Scientific, 2021). 96
5.3.6.3 Change in Apparent Density of Wood Blocks as an Indirect Indicator of Porosity Development in Wood 96
5.3.7 Gaseous Carbonization Products from Phosphoric Acid Impregnated Wood 98

5.3.7.1 Thermogravimetric Analysis Paired with Fourier Transform – Infrared Spectroscopy 98
5.4 Results and Discussion 98
5.4.1 Characterization of Produced Activated Carbons 99
5.4.1.1 Aqueous Phase Adsorption Capacity of Activated Carbons 99
5.4.1.2 Pore Size Distribution and Surface Area of Activated Carbons 100
5.4.2 Characterization of Pre-Treated White Spruce Wood 103
5.4.2.1 Impact of Pre-Treatments on the Crystalline Structure of Wood 104
5.4.2.2 Impact of Pre-Treatments on the Chemical Composition of Wood 110
5.4.2.3 Impact of Pre-Treatments on Wood Macroscopic Structure 113
5.5 Conclusions 116
5.6 References 117
Chapter 6 - Conclusions 128
6.1 Scientific Contributions 128
6.2 Benefits for Use in Remote and Northern Canadian Communities 129
6.3 Recommendations for Future Work 130
Chapter 7 - References 132
Appendix A – Supplementary Data: Apparent Density of Wood Blocks 154
Appendix B – Supplementary Data: X-Ray Diffraction – Mean Size of Cellulose Crystallites and Crystallinity Index 156
Appendix C – Supplementary Data: Thermogravimetric Analysis and Fourier Transform -Infrared Spectroscopy of Produced Off-Gases 157
Appendix D – Supplementary Data: Nitrogen Gas Adsorption Test 162

List of Figures

Figure 2-1. Active long-term drinking water advisories identified by the Government of Canada (Government of Canada, 2025c). 10
Figure 2-2. Distribution of causes of boil water advisories in Canada between 2011 and 2023 (Government of Canada, 2025b). 11
Figure 2-3. Distribution of community sizes of boil water advisories in Canada between 2011 and 2023 (Government of Canada, 2025b). 12
Figure 2-4. Community march in Attawapiskat First Nation pressuring for an end to their long-term drinking water advisory (Barrera, 2019). 13
Figure 3-1. Process flow diagram showing an example of powdered activated carbon use in a conventional water treatment scheme. 17
Figure 3-2. GAC column configuration for water treatment (Crittenden et al., 2012; Tchobanoglous et al., 2003). 19
Figure 3-3. GAC column adsorption breakthrough schematic (Crittenden et al., 2012; Vermeulen, 1958). 20
Figure 3-4. Simplified liquid-phase adsorption (single solute, mono-layer adsorption). 21
Figure 3-5. Contribution of pore size distribution to adsorption of contaminants in aqueous phase (Kemp, 2017). 23
Figure 3-6. Three graphene layers atop one another (Marsh and Rodriguez-Reinoso, 2006a). 24
Figure 3-7. Two-dimensional crystallite formation of AC (adapted from Franklin, 1951 and Sontheimer et al., 1988b). 25
Figure 3-8. Potential surface functional groups on AC (Casimero et al., 2020). 26
Figure 3-9. Simplified physical activation process. 27
Figure 3-10. Simplified chemical activation process. 30
Figure 3-11. Degradation mechanism of cellulose by zinc chloride into D-glucose (Amarasekara and Ebede, 2009). 31
Figure 3-12. Phosphate ester formation on cellulose size chain during phosphoric acid activation at temperatures < 450°C (Marsh and Rodriguez-Reinoso, 2006d). 33
Figure 3-13. Map showing growth range of native white spruce in Canada (Nienstaedt and Zasada, 1990). 36
Figure 3-14. Anatomy of softwood cellular structure (Arzola-Villegas et al., 2023). 38
Figure 3-15. Tracheid cell wall structure of softwoods (Ansell, 2015). 39

Figure 3-16. Arrangement of cellulose, hemicellulose and lignin in wood cell wall (Ansell, 2015). 40
Figure 3-17. Cellulose molecule consisting of D-glucopyranose rings (adapted from Ansell, 2015). 41
Figure 3-18. Inter- and intramolecular hydrogen bonding shown in the 002 plane (Fengel and Wegener, 1984c). 42
Figure 3-19. 3-Dimensional structure of cellulose molecule with a degree of polymerization equal to three (American Chemical Society, 2022). 42
Figure 3-20. Scanning Electron Micrograph of white spruce wood showing exposed cellulose microfibrils 43
Figure 3-21. Common hemicellulose sugar monomers (Rowell et al., 2012). 44
Figure 3-22. Sample structure of part of softwood lignin (Rowell et al., 2012). 46
Figure 3-23. Phases of torrefaction pre-treatment (Chen et al., 2021). 51
Figure 3-24. Summary of acid hydrolysis of lignocellulosic materials (Lv et al., 2024). 54
Figure 4-1. 15 x 15 x 30 mm white spruce wood block. 61
Figure 4-2. White spruce wood chips with a minimum dimension of 9.5 mm. 61
Figure 4-3. 5 x 5 x 2 mm white spruce wood sample after Torrefaction pre-treatment 62
Figure 4-4. Oven used for drying white spruce wood samples. 63
Figure 4-5. Desiccator used for drying samples 64
Figure 4-6. Thermolyne™ F6020C-60 Atmosphere Controlled Ashing Furnace. 65
Figure 4-7. White spruce wood chips in clean, dry, ceramic crucibles 66
Figure 4-8. White spruce wood chips in atmosphere-controlled ashing furnace chamber. 67
Figure 4-9. Hydrothermal pre-treatment apparatus using hot plate. 68
Figure 4-10. Alkaline pre-treatment apparatus for 5 x 5 x 2 mm sample. 69
Figure 4-11. SEM-EDS image of Alkaline pre-treated white spruce wood charcoal without washing 70
Figure 4-12. Vacuum washing apparatus for Alkaline pre-treatment. 70
Figure 4-13. Alkaline pre-treatment supernatant after one (left) and two (right) vacuum washing cycles. 71
Figure 4-14. Charcoal produced from Alkaline pre-treated wood without washing (left), with vacuum washing (center), and with both vacuum and titration washing (right). 72
Figure 4-15. Clean, dry, powdered, activated carbon in air-tight container. 73
Figure 4-16. Schematic diagram of experimental plan. 75
Figure 4-17. IN Isotherm for activated carbon with the Iodine Number highlighted. 76
Figure 4-18. Bruker D8 Endeavor instrument 78
Figure 4-19. Sample X-Ray Diffraction spectrum with Scherrer Equation parameters highlighted. 79
Figure 4-20. Sample X-Ray Diffraction spectrum with Crystallinity Index parameters highlighted. 80

Figure 4-21. Thermo Scientific™ Nicolet™ iS650 FT-IR Spectrometer equipped with the ATR Module. 81
Figure 4-22. Schematic diagram showing the analysis of off-gases produced during the carbonization step of the phosphoric acid activation of pre-treated samples. 83
Figure 4-23. Chemical impregnation of 5 x 5 x 2 mm sample. 84
Figure 4-24. TA Instruments Discovery SDT 650. 85
Figure 4-25. 5 x 5 x 2 mm phosphoric acid impregnated sample prepared for thermogravimetric analysis. 85
Figure 4-26. Activated carbon produced from carbonization in the thermogravimetric analyzer. 86
Figure 4-27. Thermo Fisher Scientific Nicolet™ iS50 FT-IR Spectrometer. 87
Figure 5-1. Correlation between specific surface areas and Iodine Numbers of produced activated carbons. 102
Figure 5-2. Hypothesized impact of smaller crystallites (left) versus larger crystallites (right) on pore development in wood-based activated carbon. 106
Figure 5-3. Fourier Transform – Infrared Spectroscopy of off-gases produced during the thermogravimetric analysis of the H_3PO_4 impregnated samples. 108
Figure 5-4. FT-IR spectra of Untreated and Pre-Treated white spruce wood. 111
Figure 5-5. Percentage decrease in apparent density of wood blocks due to Pre-Treatments. 114
Figure 5-6. Differential thermogravimetric analysis of impregnated Untreated and Pre-Treated white spruce wood. 115
Figure C-1. Thermogravimetric analysis of Torrefaction Pre-Treatment process……..…..157
Figure C-2. Fourier Transform – Infrared Spectroscopy of off-gases produced during the Torrefaction Pre-Treatment of 5 x 5 x 2 mm sample……..158
Figure C-3. Thermogravimetric analysis of Untreated and Pre-Treated, dry samples…….…..158
Figure C-4. Differential thermogravimetric analysis of Untreated and Pre-Treated, dry samples…..……159
Figure C-5. Fourier Transform – Infrared Spectroscopy of off-gases produced during the thermogravimetric analysis of Untreated and Pre-Treated, dry samples……...159
Figure C-6. Thermogravimetric analysis of Untreated and Pre-Treated H3PO4 impregnated samples…….…..160
Figure C-7. Differential thermogravimetric analysis of Untreated and Pre-Treated H3PO4 impregnated samples……...…160
Figure C-8. Fourier Transform – Infrared Spectroscopy of off-gases produced during the thermogravimetric analysis of the H3PO4 impregnated samples…….…161
Figure D-1. Nitrogen gas adsorption-desorption isotherm plot for Untreated AC……...…162

Figure D-2. Nitrogen gas adsorption-desorption isotherm plot for HPT AC……...……163

List of Tables

Table 3-1. Surface areas of phosphoric acid activated carbons from various lignocellulosic precursors… 35
Table 3-2. Comparison of common sustainable and cost-effective pre-treatment methods. 56
Table 5-1: Iodine Number of activated carbons prepared from Untreated and Pre-Treated white spruce wood..... 99
Table 5-2. Porosity characterization by nitrogen gas adsorption-desorption isotherm of activated carbons produced from Untreated and Pre-Treated white spruce wood..... 101
Table 5-3. Change in mean cellulose crystallite size of white spruce wood due to Pre-Treatments. 104
Table 5-4. Change in CrI of white spruce wood due to Pre-Treatments..... 109
Table A-1. Reduction in apparent density of 30 x 15 x 15 mm wood block samples under different Hydrothermal Pre-Treatment times……...….154
Table A-2. Reduction in apparent density of 30 x 15 x 15 mm wood block samples under different Alkaline Pre-Treatment times……...154
Table A-3. Statistical analysis parameters for the reduction in apparent density of 30 x 15 x 15 mm wood block samples under two hours of treatment…….....…..…155
Table B-1. Parameters used in the calculation of the Mean Size of Cellulose Crystallites……..156
Table B-2. Parameters used in the calculation of the Crystallinity Index……156

List of Abbreviations

AC	Activated Carbon
ACAF	Atmosphere Controlled Ashing Furnace
APT	Alkaline Pre-Treatment
ATR	Attenuated Total Reflectance
AWWA	American Water Works Association
BET	Brunauer-Emmett-Teller
C_0	Influent Concentration
CA	Chemical Activation
CAF	Controlled Atmosphere Furnace
CDWQG	Canadian Drinking Water Quality Guidelines
CEC	Contaminants of Emerging Concern
CrI	Crystallinity Index
DBP	Disinfection Byproduct
DTG	Differential Thermogravimetric Analysis
DP	Degree of Polymerization
FT-IR	Fourier Transform Infrared Spectroscopy
FWHM	Full Width at Half Maximum
GAC	Granular Activated Carbon
HAA	Haloacetic Acid
HPT	Hydrothermal Pre-Treatment
IUPAC	International Union of Pure and Applied Chemistry
IN	Iodine Number
LHW	Liquid Hot Water
ML	Middle Lamella
NOM	Natural Organic Matter
PA	Physical Activation
PAC	Powdered Activated Carbon
PFAS	Per- and Polyfluoroalkyl Substances
PT	Pre-treatment
P-XRD	Powder X-Ray Diffraction
S1	Secondary Wall 1

S2	Secondary Wall 2
S3	Secondary Wall 3
SEM-EDS	Scanning Electron Microscopy and Energy-Dispersive X-Ray Spectroscope
T	Tertiary Wall
THM	Trihalomethanes
TGA	Thermogravimetric Analysis (or Analyzer)
TPT	Torrefaction Pre-treatment
USEPA	United States Environmental Protection Agency

List of Variables

C	Effluent concentration
C_0	Influent concentration
C_f	Free carbon
CI	Confidence interval
CrI	Segal Crystallinity Index
d_{AVE}	Average of differences
d_i	Change in apparent density of dry sample
I_{002}	Intensity of 002 crystalline cellulose plane peak
I_{am}	Intensity of amorphous phase
K	Shape factor
N	Number of paired observations
$N\text{-}1$	Degrees of freedom
s_d	Standard error of the average differences
t	t-statistic
T	Temperature
α	Significance level
β	Full width half maximum of crystalline cellulose peak in the 002 plane
θ_B	Bragg angle
λ	X-ray wavelength
ρ_{dry}	Apparent density of dry sample
$\rho_{dry,\ after\ pre\text{-}treatment}$	Apparent density of dry sample after pre-treatment
$\rho_{dry,\ before\ pre\text{-}treatment}$	Apparent density of dry sample before pre-treatment
σ	Sample standard deviation of differences
σ^2	Sample variance of differences
τ	Mean size of cellulose crystallites

Chapter 1 - Introduction

1.1 Background

Activated carbon (AC) has long been recognized for its effectiveness as a high-performance adsorbent in both gas and liquid-phase separation technologies. A significant early example was in World War I where AC sequestered from birch wood was used by the Russians in iterations of the Zelinsky-Kummant Gas Mask; the first mass-produced gas mask (Kozhevnikov, 2004). The non-selective adsorptive properties of the activated birch used in the masks provided soldiers with protection against the various agents used in chemical warfare. In modern day, AC continues to be used by a range of industries for gas separation and purification processes (Georgiadis et al., 2020). Perhaps the most prolific use of AC is in many forms of water treatment: potable water treatment, domestic wastewater treatment and industrial wastewater treatment. In municipal scale potable water treatment, the popularity of AC (to this point) has been primarily driven by the need to improve the aesthetics of finished water (e.g., taste and odour-causing compound removal) and secondly, to remove low-level residual natural organic matter (NOM) to limit disinfection byproduct formation (DBP) in finished water (Crittenden et al., 2012). Over the past 20 years, AC has gained increased attention for removing contaminants of emerging concern (CEC), including various pharmaceuticals and dyes (Mansour et al., 2018; Demirbas, 2009). Of these contaminants, per- and poly-fluoroalkyl substances (PFAS) have received the most attention with the United States Environmental Protection Agency (USEPA) slated to begin regulating their concentrations nation-wide. Upgrades associated with these regulations are estimated to cost water utilities more than $3.8B per year across the US (Black and Veatch and AWWA, 2023) which further reinforces the importance of AC in potable water treatment. These water treatment challenges are magnified in remote and northern communities of Canada where funding and logistical limitations led to over 113 long-term drinking water advisories in Newfoundland (The Canadian Press, 2025) alone and over 33 active long-term drinking water advisories in remote First Nations communities in Canada (Government of Canada, 2025c). AC proves to be effective

for the management of taste and odour-causing compounds, NOM (Crittenden et al., 2012), cyanotoxins (USEPA, 2025) and PFAS (Black and Veatch and AWWA, 2023; USEPA, 2018) all of which are an increasing threat to remote and northern community waters (Anderson et al., 2023; Gobler, 2020; Ateia et al., 2019). Thus, AC has the potential to be a critical resource in such communities.

As the name suggests, AC is composed predominantly of carbon. Its distinctive utility arises from its unique physical and chemical characteristics. Notably, AC exhibits an exceptionally high internal porosity and a specific surface area often exceeding 1,000 m^2/g, which facilitates the adsorption of contaminants onto its internal surfaces (Marsh & Rodríguez-Reinoso, 2006a). The extensive range of applications attributed to AC is largely due to this high porosity and the complex distribution of pore sizes within the material. The International Union of Pure and Applied Chemistry (IUPAC) classifies pores into three distinct size categories, each of which play critical roles in the adsorption process (Rouquerol et al., 1994). Macropores (diameter greater than 50 nm) and mesopores (diameter between 2 nm and 50 nm) are generally responsible for facilitating intra-particle diffusion and inter-particle diffusion. These larger pores facilitate mass transfer into the AC particles whereas most of the molecular adsorption occurs in the micropores (pores less than 2 nm in diameter) (Sontheimer et al., 1988b). In other words, an AC with an exceedingly high proportion of micropores, may possess a high surface area, but would likely not function as an effective adsorbent because of the limited mass transfer potential offered by the meso- and macropores. Moreover, larger molecular diameter contaminants such as NOM and some cyanotoxins are too large to access micropores and are adsorbed in the mesoporous regions of AC (Gong et al., 2020; Pivokonsky et al., 2021). Thus, the pore size distribution, developed during the manufacturing process, plays a significant role in the adsorption process.

AC is produced using one of two thermo-chemical processes. The elevated temperatures at which these processes are carried out facilitate thermal degradation of feedstock, leading to the restructuring of carbon atoms into graphene sheets (Marsh and Rodriguez-Reinoso, 2006c). The activating agent, a chemical introduced to the structure of the feedstock, imposes imperfections in this restructuring process

leading to the development of porosity. The method by which the activating agent is introduced to the material, gas or liquid, defines the activation method and mechanisms. Physical Activation (PA) refers to the activation of a material using gas or vapour. PA is typically carried out at high temperatures (greater than 500°C) in an atmosphere which is often oxidative (e.g., steam, carbon dioxide, air). The elevated temperature and pressure of the atmospheric gas surrounding the precursor ultimately enters the internal structure of the precursor and expands. The pressure introduced to the inside of the material, paired with the oxidation and thermal degradation of the precursor results in the development of porosity (Marsh and Rodriguez-Reinoso, 2006c; Sontheimer et al., 1988b). On the other hand, Chemical Activation (CA) involves the impregnation of the precursor with a liquid activating agent, often a dehydrating chemical (e.g. phosphoric acid, zinc chloride, potassium hydroxide). The impregnated material is then carbonized (i.e., heated in an inert environment), at lower temperatures, typically around 500°C (Marsh and Rodriguez-Reinoso, 2006d; Sontheimer et al., 1988b). Between PA and CA, CA is much more economical and sustainable due to the lower energy and equipment requirements making CA much more feasible for application in northern and remote communities (Jiao et al., 2025). When comparing the CA agents, phosphoric acid has prevailed as the most versatile and environmentally sustainable (El Qada et al., 2008; Kumar and Jena, 2016; Oginni et al., 2019).

Generally, phosphoric acid is used for producing ACs from lignocellulosic biomass such as (wood, coconut shells and other agricultural waste materials). One of the most common waste materials in northern and remote communities is wood waste; making up 21% of all solid waste in First Nations communities in Canada (Wang et al., 2023). This waste is generated from wooden pallets used to ship goods to these desolate locations and these pallets are built from white spruce wood. Phosphoric acid effectively activates wooden materials (such as white spruce wood) by degrading its lignocellulosic structure through cleavage of glycosidic linkages of hemicellulose and cellulose and breaking aryl-ether bonds in lignin (Marsh and Rodriguez-Reinoso, 2006c). This chemical degradation decreases the degree of polymerization of hemicellulose and lignin, allowing these lignocellulosic components to thermally degrade (volatilize) at

lower temperatures during carbonization. Upon volatilization, pores are formed as their carbon structure reforms. Simultaneously, pores develop throughout the formation of phosphate linkages between cellulose and phosphoric acid products during carbonization (Marsh and Rodriguez-Reinoso, 2006c; Jagtoyen and Derbyshire, 1993).

The resultant AC pore structure, however, relies heavily on the inherent chemical, crystalline and macroscopic properties of the lignocellulosic precursor (Boundzanga et al., 2022; Zuo et al., 2009). Thus, extensive research to optimize the CA parameters (e.g., acid to precursor ratio, carbonization temperature, carbonization duration, etc.) used for various precursors have been carried out (Jjagwe et al., 2021; Dias et al., 2007). However, such optimization studies are less feasible in remote and northern communities due to the extensive experimentation, difficulty in maintaining controlled conditions and high cost of experimentation (Jjagwe et al., 2021). As the production of Ac from white spruce wood seems possible but has not been studied yet, the main novelty of this study is in demonstrating that it is possible.

The inherent limitations of naturally occurring lignocellulosic materials reduce their usefulness not only in AC production but also across various industries, all of which are actively exploring new ways to re-use and re-purpose waste materials. These industries have investigated methods of pre-treating lignocellulosic biomass to modify their chemical, crystalline and macroscopic characteristics to improve their respective utility (Bulkowska and Klimiuk, 2016). It has been established in the research that these characteristics have a significant impact on the properties of resultant ACs (Boundzanga et al., 2022; Zuo et al., 2009). However, research efforts thus far have not sufficiently investigated the effect that lignocellulosic pre-treatments (PT) have on the pore size distribution of the resultant ACs; and perhaps more importantly, why and how this process occurs. This gap represents a significant barrier to sustainably producing AC from waste wooden pallets (made of white spruce wood) in northern and remote communities of Canada.

The present research aims to begin addressing this gap through an in-depth analysis of the changes in the lignocellulosic structure that sustainable PTs have on white spruce wood. The novelty of this work

is that three relatively sustainable and simple PT methods (torrefaction, hydrothermal, alkaline) were studied on the same material. The changes to the chemical, crystalline and macroscopic properties of the white spruce wood precursor due to each PT were identified to try to understand the differences in pore characteristics of the produced ACs. Moreover, the activation process was studied in-depth to better-understand the evolution of the chemical structure of the PT woods as they convert from wood to porous AC. Improving the understanding of the impact that lignocellulosic biomass PTs have on the porosity of these ACs may broaden the re-use and re-purposing potential of lignocellulosic waste materials for AC production while contributing to needed water treatment solutions in northern and remote communities of Canada.

1.2 Research Objectives

The overarching objective of this research is to investigate the impact that changes in the properties of spruce wood, brought on by PTs, have on the CA process and on the subsequent porosity of AC. To adequately accomplish this objective, clear characterization of the spruce wood before and after each PT was detailed to set the framework for the investigation of the activation mechanisms. The specific objectives of this research were the following:

1. **Characterize the Pore Size Distribution and Aqueous-Phase Adsorption Capacity of Produced ACs.**

Evaluate the pore size distributions (including total specific surface area and pore volume, and specific micropore surface area and micropore volume) and adsorption capacity of ACs produced from PT white spruce wood in a water environment.

2. **Elucidate the Effects of Pre-Treatments on White Spruce Wood Characteristics.**

Define the chemical, crystalline and macroscopic characteristics of white spruce wood before and after each PT to explain differences in the pore size distribution of produced ACs. The characterizations included the identification of changes to the chemical composition, crystalline composition and microstructure, and apparent density of white spruce wood.

3. **Identify Differences in Pore Development Mechanisms.**

Identified the gaseous products of the carbonization of Untreated and PT white spruce wood samples impregnated with the phosphoric acid activating agent to try to identify differences in the way pores were formed in the produced ACs.

Together, the final conclusions of the thesis improve the available knowledge of wood PTs to effectively produce highly porous AC for water treatment in remote and northern communities.

1.3 Research Methodology

White spruce wood, of *Picea glauca* variety, was prepared using three (3) common and accessible PT methods: Torrefaction, Hydrothermal, and Alkaline. The Untreated and PT spruce woods were activated by phosphoric acid to produce AC. To accomplish the objectives listed above, the research was carried out in three phases:

1.3.1 Phase 1: Production and Characterization of Untreated and Pre-treated White Spruce Wood Activated Carbons.

ACs were prepared from Untreated and PT white spruce wood using phosphoric acid as the activating agent. The aqueous-phase adsorption capacity was evaluated using the Iodine Number Test and the pore size distribution was evaluated using the Nitrogen Gas Adsorption Test.

1.3.2 Phase 2: Characterization of Untreated and Pre-treated Whtie Spruce Wood.

Changes to the chemical composition, crystalline properties and macroscopic features of white spruce wood due to the PTs were analyzed using Fourier Transform - Infrared Spectroscopy (FT-IR), Powder X-Ray Diffraction (P-XRD) and apparent density measurement, respectively. The identified changes were used to try to explain the differences in the pore size distribution and adsorption capacity of the ACs prepared from PT white spruce wood.

1.3.3 Phase 3: Observation of Gaseous Products During Carbonization Step of Activation for Untreated and Pre-treated White Spruce Wood Samples.

The samples used in Phase 2 were impregnated with phosphoric acid and carbonized (using an identical methodology used for preparing the ACs used in Phase 1). The off-gases produced during the carbonization step of the activation process were measured using FT-IR in parallel with thermogravimetric analysis (TGA) to help explain how pores were formed during the carbonization step of activation.

1.4 Thesis Outline

The present chapter of the thesis provides a brief background of the state of the field, and the justification this research adds value to the field from a practical and research-perspective.

Chapter 2 provides the reader with background, specifically with the purpose of introducing the overarching motivation and use-case for the research from a practical perspective.

Chapter 3 provides the reader with a review of the literature related to the scientific and engineering components necessary for the research. The chapter includes discussion on how AC is used for water treatment, how AC acts to remove contaminants from water, how AC is manufactured and what raw materials are used for its production. The reader is then introduced to the properties of wood, how these properties impact resultant AC properties, and how they may be altered using PTs. The chapter closes with a comparison of the common PT methods for the intended application.

Chapter 4 outlines the materials and methods used to PT the white spruce wood and prepare the resultant ACs. The chapter also covers the characterization and analytical techniques used to conduct the research.

Chapter 5 presents the manuscript to be published using the results obtained from the research. The manuscript follows the standard article format (i.e., Abstract, Introduction, Materials and Methods, Results and Discussion, Conclusion) and presents significant conclusions which contribute to the practical (water treatment) and research (materials science and engineering) fields.

Chapter 6 provides the general conclusions of the research and an opinion on the next steps in the research to improve the understanding of the impact that PTs have on porosity and adsorption capacity of CA ACs.

Chapter 2 - Background

This chapter provides the reader with context to explain the motivation and need for this research at the practical level. The water treatment challenges experienced in northern and remote communities of Canada are discussed first. The chapter then explores some of the imminent threats which may exacerbate these challenges. The chapter closes with a proposed route to a solution. The proposed solution is ultimately investigated through the present study.

2.1 Water Treatment Challenges in Remote Communities of Canada

Potable water treatment challenges in remote and First Nations communities across Canada have dominated news stories for the past 15 years. Funding, construction and operational challenges associated with producing and delivering potable water to these primarily small communities led to over 151 drinking water advisories in Canada in 2016 alone (David Suzuki Foundation, 2017). At the time of the present study, there are 33 active long-term drinking water advisories (i.e., drinking water advisories lasting over 12-months) across Canadian First Nations communities and 113 long-term drinking water advisories in Newfoundland alone (The Canadian Press, 2025). The location of the 33 active long-term advisories in First Nations Communities are shown in Figure 2-1.

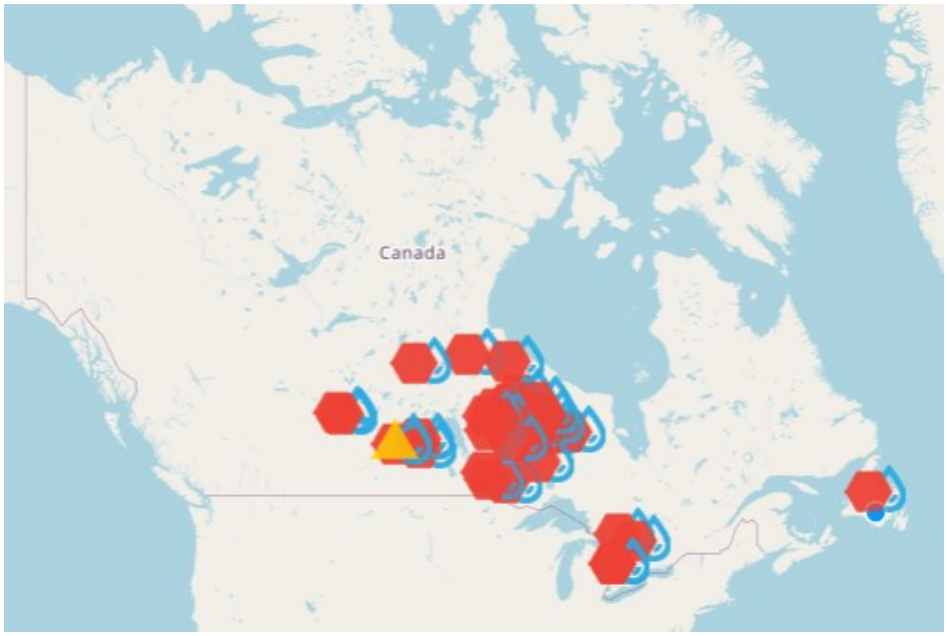

Figure 2-1. Active long-term drinking water advisories identified by the Government of Canada (Government of Canada, 2025c).

The causes of the drinking water advisories do include challenges related to the quality of source water (e.g. microbiological parameters, presence of other deleterious contaminants). However, overwhelmingly, insufficient process and distribution equipment is largely responsible for the inability to provide communities with safe drinking water as shown in Figure 2-2.

The Office of the Parliamentary Budget Officer (2017) evaluated their budget allocation for First Nations water and wastewater infrastructure between the years of 2009 and 2016. It was found that over $2.25B was spent on First Nations water and wastewater infrastructure alone (an average of $322M per year). Based on these results, it was determined that approximately $1.8B would be required between 2017 and 2020 to end drinking water advisories. Despite the high funding support, 33 active long-term advisories persist in Canada at the time of this study (Government of Canada, 2025b).

Figure 2-2. Distribution of causes of boil water advisories in Canada between 2011 and 2023 (Government of Canada, 2025b).

The David Suzuki Foundation (2017) studied the Government of Canada's progress in addressing drinking water advisories in First Nations across Canada. The overarching finding was that providing funding and equipment to sufficiently treat water was not enough to sustainably supply safe potable water to the communities. Ultimately, in addition to providing funding for treatment processes, operator and equipment support is required for a long-term solution. This finding was perhaps best illustrated in Constance Lake First Nation where the long-term drinking water advisory was lifted upon receiving upgraded equipment but was later put back into effect due to approximately $800k in repairs required after operating for approximately one year. Supporting remote and First Nations communities is not as simple as designing and supplying a system but requires ongoing support to be successful.

This additional support is required since most communities (not only including First Nations communities) under drinking water advisories have low populations as shown in Figure 2-3. Low population communities typically have limited construction and operational capacity when compared to

communities with higher populations (Government of Canada, 2025b). Exacerbating this challenge is the fact that these communities are often remote, making it even more challenging and costly to construct infrastructure (Flanagan, 2021).

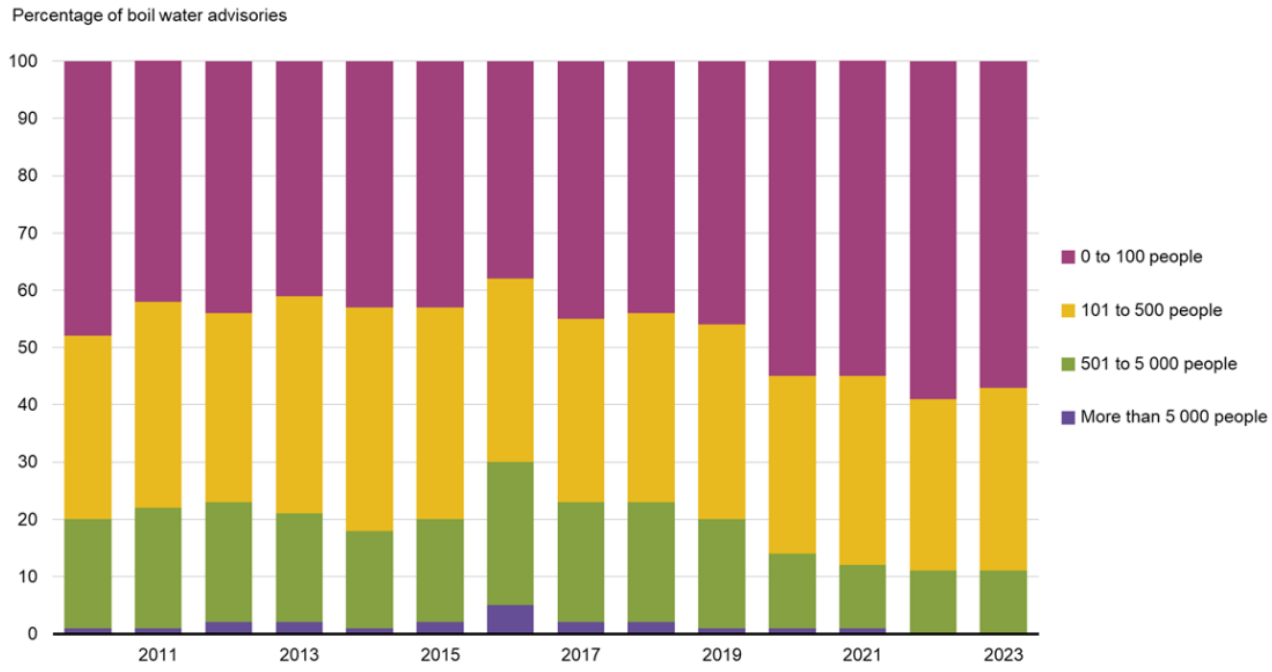

Figure 2-3. Distribution of community sizes of boil water advisories in Canada between 2011 and 2023 (Government of Canada, 2025b).

Two primary roadblocks disrupt the upgrading of treatment process and distribution infrastructure in remote and First Nations communities in Canada. Firstly, the high cost of construction paired with the general lack of economic resources in such communities limits their ability to execute on upgrading infrastructure. The first problem leads to the second problem which is that communities ultimately end up relying on federal funding leading to a drawn-out bureaucratic process that ultimately lengthens the long-term drinking water advisories.

2.2 Emerging Water Treatment Challenges

The emergence of issues involving disinfection byproduct (DBP) formation have left communities such as Attawapiskat First Nation in Ontario under a state of emergency (Barrera, 2019). The formation of

DBPs occurs when chlorine in finished water is left to contact NOM, anthropogenic contaminants and/or halides in the distribution system. The most monitored DBPs are trihalomethanes (THM) and haloacetic acids (HAA) (Xiao et al., 2024). Both these DBPs were in exceedance of Canadian Drinking Water Quality Guidelines (CDWQG) in Attawapiskat, and these issues are not limited to just this community. Amarawanshe et al. (2023) monitored THM concentrations in drinking water at three First Nations communities across Manitoba. In all three reserves, regardless of the distribution or storage method used (e.g. piped, cistern, truck), THM concentrations were above the maximum acceptable concentration in 70% of samples collected. These challenges have led to civil unrest in impacted communities who have not had access to potable water supplies for years (Figure 2-4).

Figure 2-4. Community march in Attawapiskat First Nation pressuring for an end to their long-term drinking water advisory (Barrera, 2019).

With funding provided by Climate Change Impacts and Adaptation Program within Natural Resources Canada, the Assembly of First Nations Environmental Stewardship Unit (2008) evaluated the risks and impacts of climate change on First Nations Communities. The analysis showed that climate change will only increase the water treatability challenges faced by remote and First Nations communities. Not only will NOM concentrations become elevated (Delpla et al., 2009), but their composition is likely to

shift to a greater proportion of hydrophobic fractions (Anderson et al., 2023). These changes may impact the performance of existing treatment processes at remote and First Nations communities putting them at an increased risk of inadequate removal of NOM. Moreover, the anticipated higher water temperatures promote algal blooms, increasing their frequency (Gobler, 2020). In more challenging cases blue-green algae develops which can produce cyanotoxins (through cyanobacteria) which damage the liver, nervous system, skin and mucous membranes of humans (USEPA, 2025).

The removal of NOM and cyanotoxins will continue to be a challenge threatening the health of remote and northern communities in Canada. Given the existing problem with laboured solution implementation, the need exists to develop sustainable technologies for the removal of organics at these remote locations. One such material capable of managing both NOM and cyanotoxins AC. In fact, the USEPA lists AC adsorption as one of the leading technologies for the removal of cyanotoxins for drinking water treatment (USEPA, 2025). Given the funding and shipment challenges encountered by remote and northern communities, the requirement to ship such material to site is a considerable and foreseeable stressor and the need exists to produce AC on site to sustainably implement this effective technology.

2.3 Proposed Solution

Taking into consideration the funding and equipment limitations in remote and First Nations communities in Canada, a simple methodology to manufacture a high performing AC must be developed. With the production of high performing AC onsite, the need to purchase and ship material to the location will be removed. Moreover, dependence on entities outside the communities will be reduced. These factors benefit these communities in need and Canada as a whole, two-fold:

1. Improving the overall health and well-being of people in remote and northern communities by sustainably reducing drinking water advisories.
2. Cost savings by locally manufacturing water treatment technologies; avoiding the high cost of shipping and by providing potential employment opportunities onsite.

To logically arrive at a suitable methodology given the manufacturing constraints (e.g. limited resources and equipment), there are two fundamental steps:

1. The identification of a sustainable AC precursor material at the location.
2. The development of a simple activation methodology which is affordable and effectively produces a high performing AC.

The following sections of the literature review describe how AC is used for potable water treatment and what makes it a high performing water treatment material. The reader is then introduced to what AC is manufactured from and how it is manufactured.

Chapter 3 - Literature Review

This literature review summarizes the utility of AC for water treatment, adsorption theory, AC properties, AC production methods and the properties of wood. The chapter closes by revealing the gap in research surrounding the impact of wood PTs on AC porosity and how this can benefit northern and remote communities of Canada.

3.1 Activated Carbon for Water Treatment

AC gained popularity for water treatment applications in the mid-1970s due to its effectiveness in the removal of large organics such as natural organic matter (NOM), pesticides, and taste and odour-causing compounds (Crittenden et al., 2012). While known as a highly reliable material for removal of organics, since then, it has recently gained increased popularity for its effectiveness in per- and polyfluoroalkyl substance (PFAS) removal (USEPA, 2018). This section introduces AC as it is used for potable water treatment. The treatment processes, contaminant removal mechanisms, and physical and chemical properties of AC are discussed.

3.1.1 Treatment Processes

AC is used as powdered AC (PAC), which typically has a mean particle diameter between 20 um and 50 um, and granular AC (GAC), which typically has a mean particle diameter of 0.5 mm to 3 mm (Crittenden et al., 2012). In 1985, the American Water Works Association (AWWA) concluded that 29% of public potable water treatment utilities in the USA used PAC (Seidel, 1985). Merely four to five years later (1989), a survey revealed that 63% of plants across the world used PAC, and 7% were using GAC for taste and odour-causing compound removal (Suffet et al., 1996). The uses of AC are only expected to increase with its emergence as a leading technology for the treatment of PFAS from potable water (Black and Veatch and AWWA, 2023). PAC and GAC are used differently for water treatment, and their processes are summarized in Sections 3.1.1.1 and 3.1.1.2, respectively.

3.1.1.1 Powdered Activated Carbon

PAC is often slurried and then injected directly into channels or existing treatment units, such as rapid mix tanks, and allowed to contact the water in subsequent treatment units, such as flocculation basins, to remove contaminants as shown in Figure 3-1.

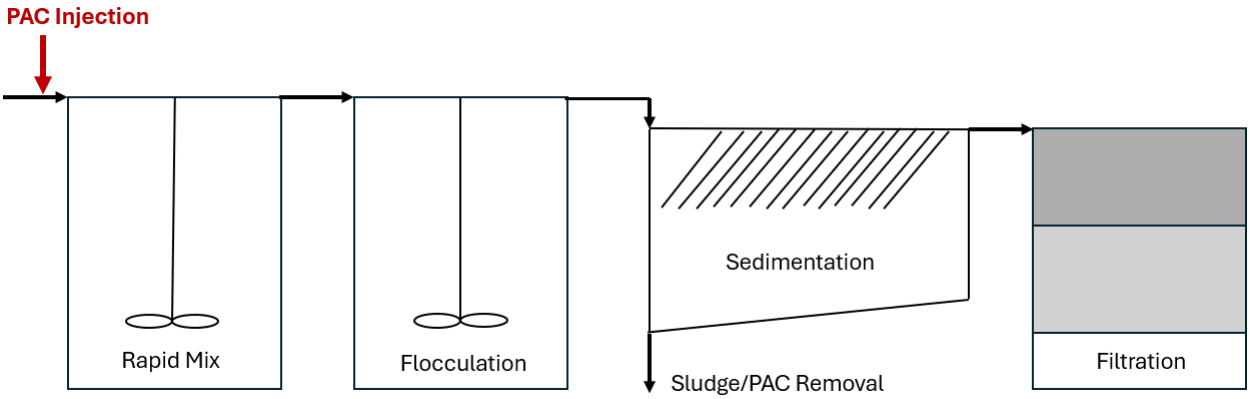

Figure 3-1. Process flow diagram showing an example of powdered activated carbon use in a conventional water treatment scheme.

The spent PAC is finally removed by either sedimentation or filtration. Perhaps one of the main reasons that PAC was used more frequently than GAC at the time of the aforementioned studies is that PAC does not require high capital investment for building new processes. PAC is particularly practical for plants which experience contaminant spills in the raw water or seasonal organics loading for this reason (Sontheimer et al., 1988a; Crittenden et al., 2012). The most common locations for introducing PAC to treatment schemes are at the intake, rapid mix, filter inlet and/or following rapid mix (Crittenden et al., 2012). Contaminant removal by AC relies on sufficient contact time, which varies based on the existing treatment configuration, process sizing and operational parameters; meaning that the optimal location for PAC addition is decided on a case-by-case basis. The kinetics of PAC adsorption (contaminant removal) are relatively fast, leading to the exhaustion of its usable surface area driving high usage rates when compared to GAC (Crittenden et al., 2012).

3.1.1.2 Granular Activated Carbon

GAC is used in contactors such as the pressure filter shown in Figure 3-2, the GAC media is often 3 to 3.6 m deep. These contactors are generally located after the traditional gravity-driven multimedia deep bed filtration. GAC can also be used as the top layer within an existing gravity-driven multimedia deep bed filter. However, most existing filters do not allow for a sufficiently deep GAC layer for it to be effective. Purposely designed gravity-driven multimedia filters can be effective, but the gravity-driven nature of the filters limits the depth of the GAC layer to approximately 1.5m, and this may not provide sufficient contact time for some applications. The configurations of such processes vary from gravity-fed, pressurized or even fluidized bed contactors (Crittenden et al., 2012). The required contact time, nature and concentration of the target contaminant, the level of removal required, and the existing treatment equipment are the primary factors contributing to the selection of the process configuration.

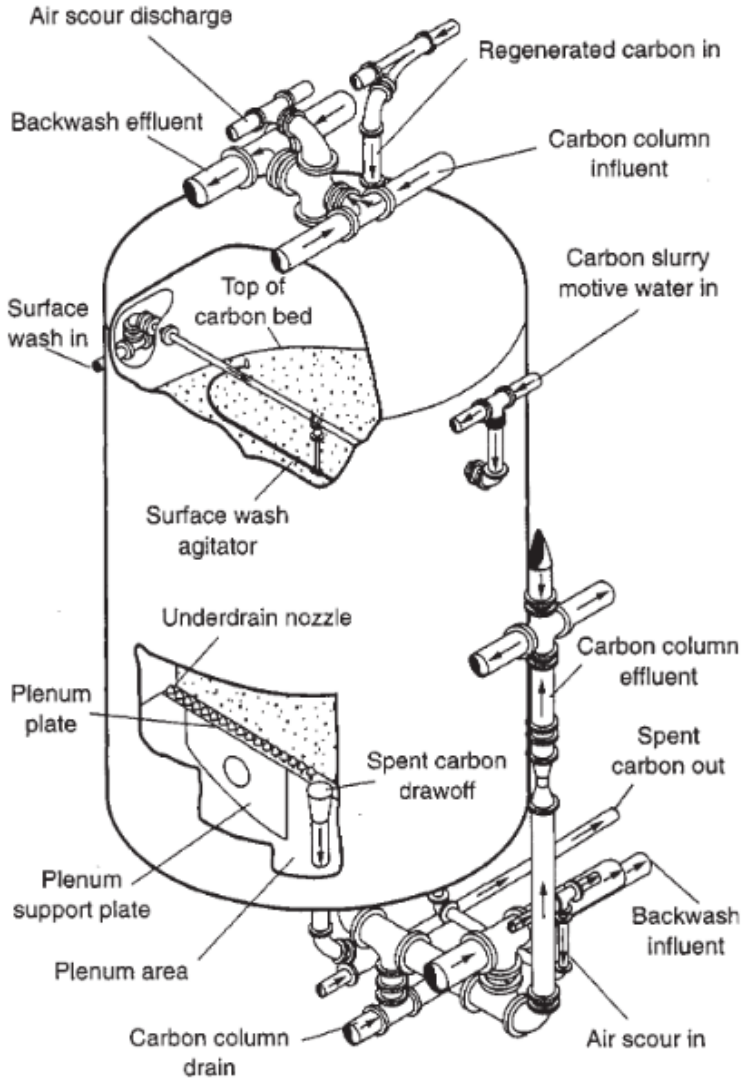

Figure 3-2. GAC column configuration for water treatment (Crittenden et al., 2012; Tchobanoglous et al., 2003).

In traditional multi-media deep bed filtration processes, particles (and contaminants) are removed by size exclusion, and head loss through the filter is the limiting parameter for filtration time before backwash. The same backwashing requirement applies when GAC is a layer with the plant's gravity-driven multimedia filter. However, the contaminants removed by GAC are much smaller than the flocs/particles removed by conventional multimedia filtration, and the limiting factor for GAC contactors is the saturation of the GAC with contaminants that leads to a decrease in performance. In all cases, the GAC gradually

becomes saturated with contaminants with greater operation time as shown in Figure 3-3. The contaminant removal by the column diminishes as the GAC becomes loaded with contaminants (illustrated by the dashed areas) and ultimately equilibrates with the influent concentration (C_0).

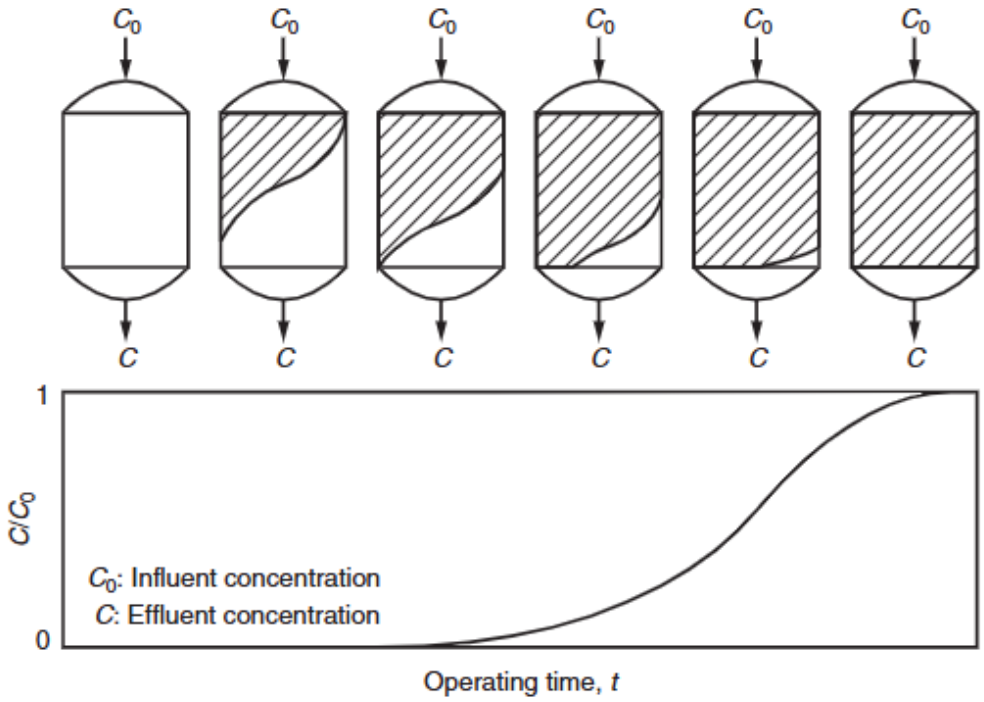

Figure 3-3. GAC column adsorption breakthrough schematic (Crittenden et al., 2012; Vermeulen, 1958).

At the point at which the GAC column's effluent exceeds the maximum contaminant concentration allowed, the GAC must be replaced by regenerated or virgin GAC. Because of mass transfer limitations the GAC approaches saturation but it is not fully equilibrated with the feed (i.e., somewhere between the fourth and fifth column schematic in Figure 3-3). The exhaustion mentioned above for both PAC and GAC are due to the mechanism by which AC removes contaminants from water: adsorption. The following section (Section 3.1.2) describes this phenomenon specifically as it pertains to how AC is used in an aqueous medium.

3.1.2 Adsorption

AC removes contaminants from water by way of adsorption. Adsorption is defined as the agglomeration of a substance at the interface between two phases (e.g. solid and liquid, solid and gas) as shown in Figure 3-4 for liquid-phase adsorption. Generally, adsorption occurs due to unbalanced forces imposed on the atoms at the surface of a solid material. This imbalance attracts molecules or atoms in the liquid or gas phase to the surface of the solid material where adsorption occurs (Faust and Aly, 1987a). In water treatment, the target adsorbate molecules or ions are dissolved, and the adsorption process brings the adsorbate from the liquid phase (in the bulk solution) to the solid phase (onto the surface of the AC).

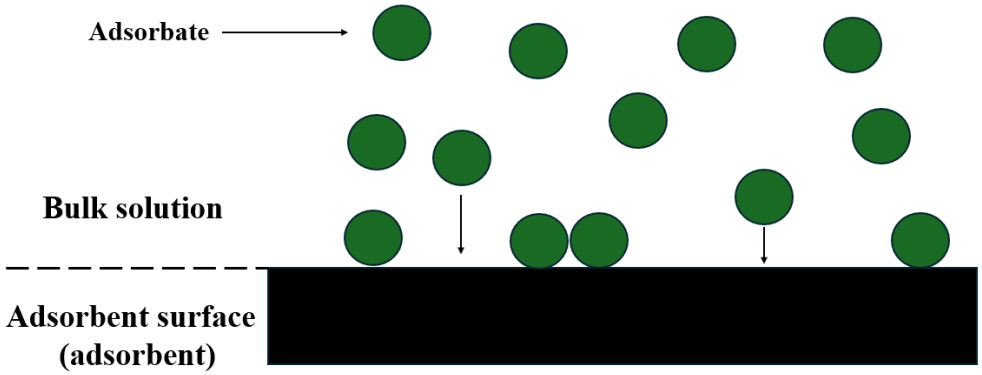

Figure 3-4. Simplified liquid-phase adsorption (single solute, mono-layer adsorption).

Adsorption processes are simply classified into two categories: Physical adsorption and chemical adsorption. Both physical and chemical adsorption take place on the surfaces of AC. Adsorption occurs on the external surface of AC particles and the much greater surface area within the internal pores of the AC particles. AC is a powerful water treatment adsorbent because of its high internal surface area (often in exceedance of 1000 m^2/g). It is often challenging to distinguish the precise mechanism of adsorption of a specific contaminant or contaminants onto a surface. Physical adsorption relies on attraction through intermolecular forces and can occur anywhere on the adsorbent surface. On the other hand, chemical adsorption involves primary bonding between the adsorbent itself and the adsorbate or the functional groups on the surface of the adsorbent and the adsorbate. In this manner, chemical adsorption can only take place at a compatible site on the adsorbent surface and is generally 'irreversible' for most practical purposes

(Faust and Aly, 1987a). For most AC water treatment applications, contaminants are removed by way of physical adsorption (Crittenden et al., 2012).

The previously illustrated example (in Figure 3-4) is simplified because it shows, presumably, a single-solute system and so-called mono-layer adsorption (i.e., where only a single layer of adsorbate accumulates on the surface of the adsorbent). In reality, natural waters contain multiple dissolved constituents which have varying molecular sizes and affinities for the ACs surface. These differences impose so-called 'competitive adsorption' (i.e., the competition between adsorbate molecules of different species to adsorb onto the adsorption sites on the adsorbent) (Sontheimer et al., 1988c). Moreover, the adsorbates do not only form a single layer on the ACs surface, but possibly 'stack' atop one another to form several layers, which often fill the pores of the AC. Given the nature of physical adsorption used in water treatment, attractive forces diminish with increased layer thickness leading to AC exhaustion (Faust and Aly, 1987b).

Most of the surface area on ACs is internal surface area (within countless pores within the AC). In fact, it is estimated that over 99% of the adsorption sites available on ACs are on the internal surface area (Faust and Aly, 1987c). Thus, it is implied that the adsorbate molecules must first diffuse into the internal pore network of the AC before they can be adsorbed onto its surface. Pores of different sizes are critical to both the diffusion and adsorption of contaminants. The roles that pore structure and pore size distribution play in the adsorption process are discussed in Section 3.1.3.

3.1.3 Internal Pore Structure of Activated Carbon

The International Union of Pure and Applied Chemistry (IUPAC) defined three pore size ranges (Rouquerel et al., 1994). The largest of the pores are termed macropores (greater than 50 nm in diameter). Macropores are primarily responsible for facilitating the diffusion of adsorbate molecules into AC pore network. An AC with too low a proportion of macropores would be at risk of having slow kinetics of adsorption and would be limited to adsorbing contaminants of small molecular size. In water treatment, macropores are essential for the adsorption of large molecular mass NOM fractions, for example

(Sontheimer et al., 1988b; Crittenden et al., 2012). The role of macropores in the diffusion of adsorbate into the pore network of AC and the adsorption of large organics is clearly illustrated in Figure 3-5.

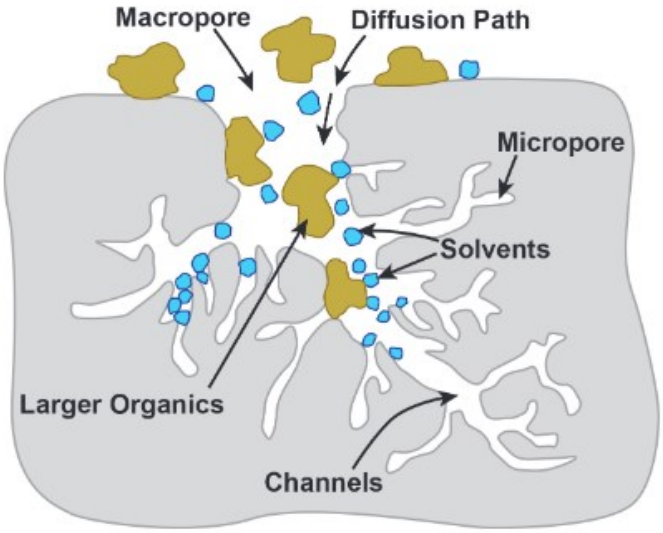

Figure 3-5. Contribution of pore size distribution to adsorption of contaminants in aqueous phase (Kemp, 2017).

Pores with diameters between 50 nm and 2 nm are termed mesopores. Mesopores play a hybrid role in the adsorption process. They can facilitate the diffusion of smaller molecular mass molecules further into the pore network of the AC and adsorb larger organic and inorganic contaminants. Cyanotoxins, for example, are most adsorbed in pores 8.5 nm to 14 nm in diameter, making mesoporosity crucial to this water treatment application (Pivokonsky et al., 2021). It is partially for this reason that wood-based ACs are preferred for such applications due to their innate macro- and mesoporous structure (Sontheimer et al., 1988b). The smallest diameter fraction of pores (diameters less than 2 nm) are called micropores. ACs micropores are generally responsible for the high specific surface area of AC. The micropores are also where smaller contaminants such as some taste and odour-causing compounds and PFAS are predominantly adsorbed to the ACs surface (Park et al., 2020). The pore size distribution of ACs is related to its micro- and macrostructure. The physical and chemical structure of AC is discussed in Section 3.1.4.

3.1.4 Atomic Structure of Activated Carbon

The high specific surface area of AC (often over 1000 m^2/g) is what gives it its high adsorption capacity for a vast range of contaminants (Sontheimer et al., 1988a). ACs high specific surface area is granted by its advanced microstructure discussed in the previous section. This section aims to take a closer look at the atomic structure of AC.

3.1.4.1 Carbon Structure

At the atomic level, carbon atoms within AC are formulated in graphene layers (graphite). The carbon atoms within each layer are organized in hexagonal unit cells as shown in Figure 3-6.

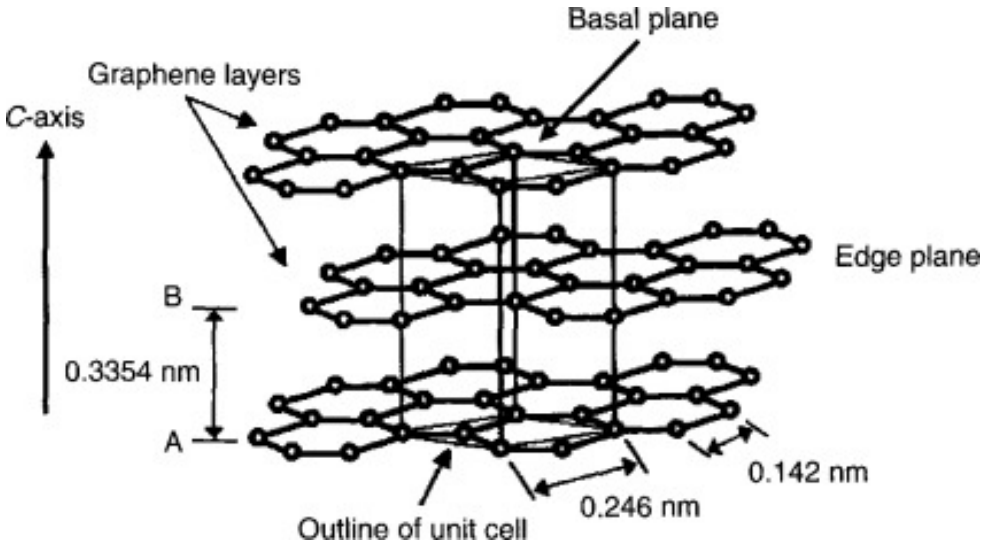

Figure 3-6. Three graphene layers atop one another (Marsh and Rodriguez-Reinoso, 2006a).

The carbon atoms are uniformly separated by 0.142 nm, and each layer is separated by 0.335 nm. Thus, primary chemical bonding only exists within each carbon layer and not between layers. Instead, the layers are merely held together by van der Waals forces (Marsh and Rodriguez-Reinoso, 2006a). The fact that no primary bonding exists between graphene sheets permits graphite to develop porosity (Marsh and Rodriguez-Reinoso, 2006b).

The layers form crystallites that are described as turbostratic crystallites (Sontheimer et al., 1988b). The crystallites are oriented in different directions and are cross-linked to one another at the ends of the

crystallites as shown in Figure 3-7. The variability in the orientation of the crystallites is important because the voids between crystallites form micropores (Sontheimer et al., 1988b).

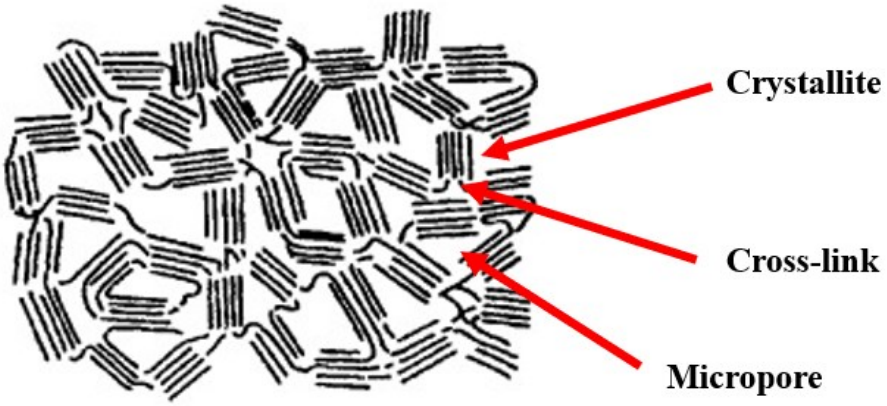

Figure 3-7. Two-dimensional crystallite formation of AC (adapted from Franklin, 1951 and Sontheimer et al., 1988b).

The anisotropic nature of the crystallite formation leaves carbon at the edges of graphitic planes highly available for reaction with chemicals and adsorbates alike (Faust and Aly, 1987c). It is at these edges where surface functional groups are formed during the activation process. While physical adsorption is more common for the removal of potable water contaminants, these surface functional groups impact the electrostatic attraction and hydrophobicity of the AC (Sontheimer et al., 1988b).

3.1.4.2 Surface Function Groups

While the porosity and, ultimately, specific surface area is what sets AC apart from other adsorbents, surface functional groups can have an impact on the diffusion and adsorption of some contaminants (Sontheimer et al., 1988b). The most common surface functional groups present on ACs are oxygen and hydrogen-containing groups (e.g., carboxylic, hydroxyl, carbonyl, etc.) as shown in Figure 3-8. Approximately 5% to 20% of an ACs weight can be made up of non-carbon atoms coming from surface functional groups (Sontheimer et al., 1988b). These surface functional groups can originate from the AC precursor material but are more frequently introduced by the activating agent. The groups tend to form at

the highly reactive edges of graphite crystallites which are approximately 20% more reactive than the internally bound carbon atoms (Sontheimer et al., 1988b).

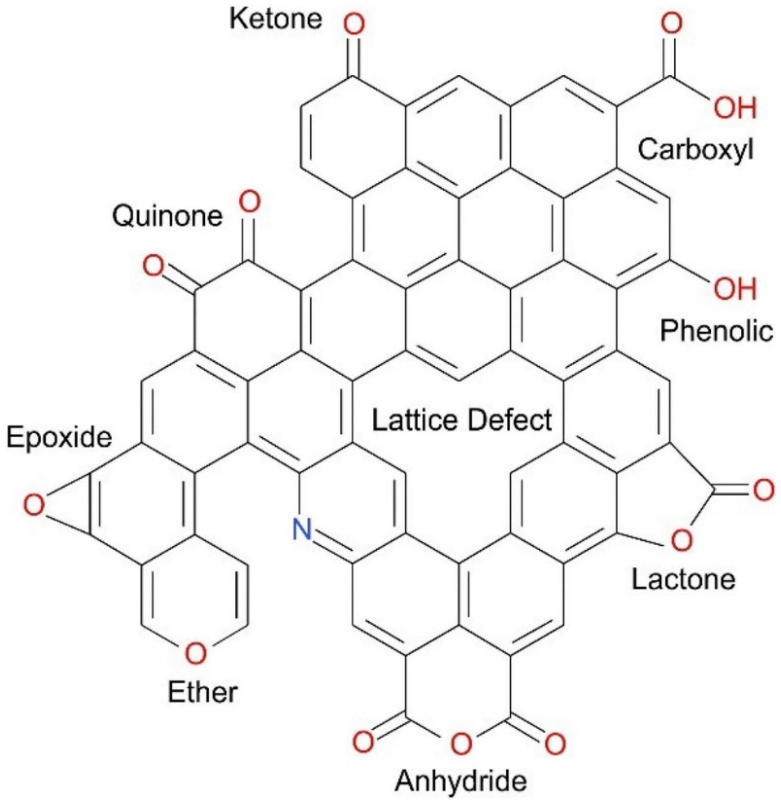

Figure 3-8. Potential surface functional groups on AC (Casimero et al., 2020).

Surface functional groups impact the surface charge of AC and thus impact the electrostatic interaction between the adsorbate and AC. Positively charged heavy metal ions, such as Pb(II) and Cu(II), are typically attracted to the negatively charged surface of AC. The effectiveness of adsorption is amplified by surface functional groups in some cases since they allow for ion exchange, surface complexation and/or precipitation due to interactions between surface functional groups and positively charged metal ions (Yang et al., 2019).

The high porosity, surface area and surface functionalization of AC are developed during the activation process and these properties are highly dependent on the AC manufacturing process employed.

3.2 Activated Carbon Production

ACs are produced by subjecting organic raw material to thermal processing in the absence of air. There are two main activation methods employed in the production of AC, they are PA and CA. The respective methodologies and reaction mechanisms are discussed within this section.

3.2.1 Physical Activation for Activated Carbon Production

PA involves the aggressive reaction between a carbonaceous precursor (e.g. coal, graphite, etc.) and a gaseous (or vapour) oxidative activating agent. PA agents most often include carbon dioxide and steam (Marsh and Rodriguez-Reinoso, 2006c; Sontheimer et al., 1988b). In all cases, the precursor is re-sized for either producing PAC or GAC. Moreover, the smaller sizes provide greater surface area for reaction with the gaseous activating agent resulting in increased reactivity. Typically, the precursor (if not coal) is first carbonized (pyrolyzed) to increase its carbon content prior to physical activation. A schematic of the PA process is simplified and illustrated in Figure 3-9.

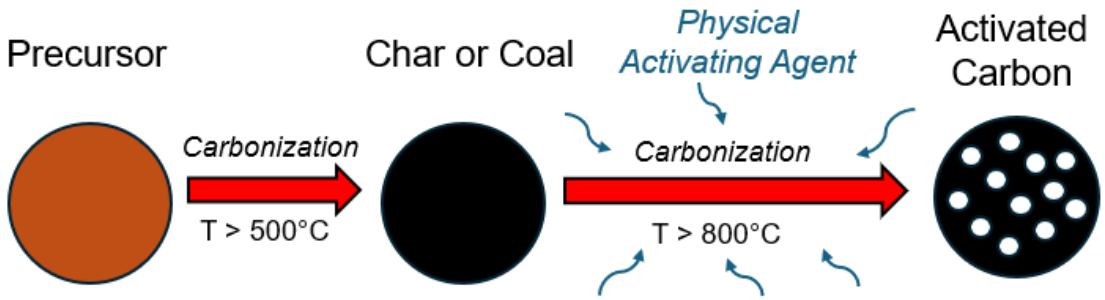

Figure 3-9. Simplified physical activation process.

Marsh and Rodriguez-Reinoso (2006c) produced the most comprehensive summary of the PA processes. Their work guides the following discussion and is elaborated upon using other literature.

Two sets of primary reactions occur between the activating agent (i.e., steam or carbon dioxide) and the precursor. The first is between the activating agent itself and the precursor. The reaction between the precursor and the activating agent produces gaseous products leaving pores in their place. However, at atmospheric pressure, the reaction at the exterior of the precursor particle dominates over reactions within

the precursor particle resulting in negligible porosity development. Thus, increasing the atmospheric pressure is critical to porosity development by PA. In a simplistic manner, the reaction between carbon dioxide and steam with the carbonaceous precursor can be explained by the following stoichiometric equations:

The reaction between carbonaceous precursor and carbon dioxide activating agent:

$$C + CO_2 = 2CO \quad 3\text{-}1$$

The reaction between carbonaceous precursor and steam activating agent:

$$C + H_2O = CO + H_2 \quad 3\text{-}2$$

At greater temperatures (>600 °C) a second set of reactions takes place between molecular oxygen (sourced from carbon dioxide or steam) and the precursor. At such temperatures, molecular oxygen reacts with the carbonaceous precursor in a combustion reaction. These reactions are more simply explained by considering free carbon, C_f, (a carbon atom unbonded with surface complexes of the precursor) and the gaseous products of these reactions vary depending on the temperature at which they take place. For example:

The dominant reaction at temperatures from 600 °C to approximately 900 °C is the release of carbon dioxide as shown in the stoichiometric equation below:

$$C_f + O_2 = CO_2 \quad 3\text{-}3$$

Beyond temperatures of 900 °C, carbon monoxide is the dominant gaseous product released, it is produced through the stoichiometric equation below:

$$2C_f + O_2 = 2CO \quad 3\text{-}4$$

These two mechanisms are primarily responsible for porosity development in PA ACs, but differences exist in the porosity characteristics of resulting ACs. Rodriguez-Reinoso et al. (1995) aimed to

identify the differences in porosity development due to carbon dioxide and steam activation of carbonized olive stones.

The carbon dioxide ACs experienced a gradual increase in both micro- and mesoporosity due to the widening of existing pores in the char. Carbon dioxide activation facilitated new micropore development and increased the diameter of existing micro- and mesopores, increasing the pore volume. The latter effect became more pronounced at holding times longer than 30 minutes at 825 °C (Marsh and Rodriguez-Reinoso, 2006c). On the other hand, steam activation induced pore widening after less than 20 minutes of holding time at a temperature of 750 °C (75 °C lower than carbon dioxide activation). The intense impact of pore widening by steam activation resulted in ACs with less microporosity than carbon dioxide-activated ACs (Marsh and Rodriguez-Reinoso, 2006c).

One limitation of this study was the fact that these chars originated from organic material (i.e., olive stones) (Marsh and Rodriguez-Reinoso, 2006c). Nonetheless, a study carried out by Zhu et al. (2012) in the years shortly following reinforced these identified differences between the activating agents when activating anthracite. Zhu et al. (2012) found that anthracite steam ACs produced at temperatures of 850 °C had 36% less micropore surface area than their carbon dioxide AC counterparts (Zhu et al., 2012).

Physical activation has a much higher energy requirement than chemical activation due to the multiple heating steps and higher temperature requirement by comparison (Neme et al., 2022). These factors alone make chemical activation much more attractive for the present application. The chemical activation process is described in the following section.

3.2.2 Chemical Activation for Activated Carbon Production

CA is most often used for activating carbonaceous precursors of lignocellulosic nature such as wood and plant matter (Sontheimer et al., 1988b). In contrast to PA, where the precursor is first made into charcoal (by carbonizing in an inert atmosphere) and then activated by the PA agent, CA typically involves only a single carbonization step. The precursor is typically re-sized to facilitate saturation with the CA agent.

The two fundamental steps involved in CA are:

1) Impregnation of the precursor material with a CA agent, and

2) Carbonization of the impregnated precursor.

In the impregnation step, the precursor is soaked with an activating agent (an aqueous reagent) to facilitate contact and chemical reactions between the precursor and the activating agent. The time allowed for impregnation is typically between 4 hours (Yakout and El-Deen, 2016) and 24 hours (Diao et al., 2002). The second step involves carbonization (pyrolysis) of the impregnated precursor. A schematic showing the simplified CA process is shown in Figure 3-10.

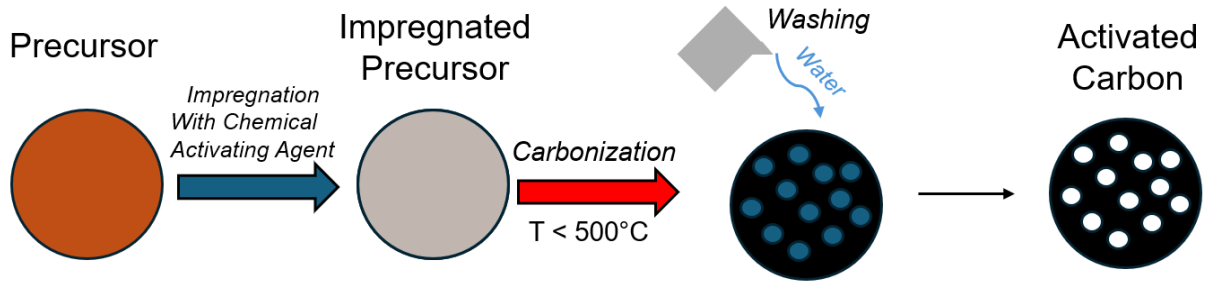

Figure 3-10. Simplified chemical activation process.

It is during the carbonization step when most of the porosity develops because of the changes to the precursor properties induced by the activating agent. The two most common CA agents are phosphoric acid and zinc chloride (Sontheimer et al., 1988b; Marsh and Rodriguez-Reinoso, 2006d). These activating agents are effective because they facilitate severe dehydration of the precursor at temperatures as low as 180 °C for phosphoric acid (Dobele et al., 1999) and 200 °C for zinc chloride (Amarasekara and Ebede, 2009). In either case, the damage to the precursor by the activating agent in the impregnation stage and at temperatures below 200°C during the carbonization stage leads to mesoporosity development and increased surface area.

Contrarily, microporosity characteristics of zinc chloride and phosphoric acid ACs differ. During the carbonization process, the carbon structure of the precursor begins to contract and restructure into

graphitic sheets. When impregnated with a CA agent, this contraction is restricted to a degree by the impregnated activating agent. Upon washing, the activating agent is removed from the AC leaving micropores behind (Molina-Sabio and Rodriguez-Reinoso, 2004).

During the impregnation process, the internal structure of the lignocellulosic biomass gradually swells as the precursor saturates (Marsh and Rodriguez-Reinoso, 2006d). The swelling allows further penetration of the activating agent into the lignocellulosic structure for reaction. Reactions which take place include dehydration and cleavage of glycosidic linkages in cellulose by zinc chloride as illustrated in Figure 3-11 (Amarasekara and Ebede, 2009). The second step in the figure shows how hydrated zinc chloride hydrolyzes the glycosidic linkage between glucose monomers in cellulose, leaving D-glucose as a product. Once subject to temperatures above 200 °C during the carbonization stage, the D-glucose dehydrates and produces various volatile products (e.g., furfural, water, etc.).

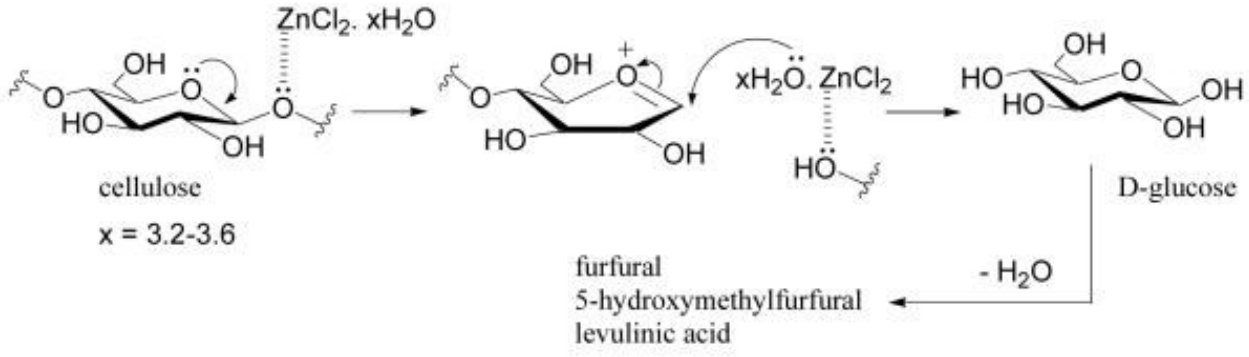

Figure 3-11. Degradation mechanism of cellulose by zinc chloride into D-glucose (Amarasekara and Ebede, 2009).

These depolymerizing reactions drastically reduce the average molecular weight of lignin, hemicellulose and cellulose. These lower molecular weight forms of the biopolymers have significantly lower thermal stability and volatilize during the carbonization stage, leaving pores behind.

To illustrate this idea, consider the case of pure cellulose. Dobele et al. (1999) compared the pyrolysis of dry cellulose and cellulose impregnated by phosphoric acid. Dry cellulose began volatilizing

significantly at approximately 240°C. Meanwhile, 20% of phosphoric acid-impregnated cellulose (cellulose to acid weight ratio of 1:5) volatilized at 200 °C. The premature volatilization brought on by the acid-catalyzed hydrolysis and depolymerization of lignocellulosic components is credited with increased pore volume and mesoporosity development in CA ACs (Molina-Sabio et al., 1995).

While the mechanisms of mesopore development are relatively similar for both zinc chloride and phosphoric acid, the micropore distributions differ between zinc chloride and phosphoric acid ACs. To explain these differences, Molina-Sabio and Rodriguez-Reinoso (2004) activated olive and peach stones using zinc chloride (at 500°C) and phosphoric acid (at 450°C) with varying impregnation ratios. The differences in micropore diameters formed were attributed to the molecular diameters of the respective activating agents. When impregnation ratios exceeded 0.4 g Zn/g precursor, mesopore development was dominant over micropore development due to aggressive dehydration and degradation of the precursor material. The increased degradation due to higher impregnation ratios resulted in greater volatilization of carbon components, leading to larger pores (e.g., meso- and macropores). In experiments where the impregnation ratios were lower than 0.3 g Zn/g precursor, the volume of zinc chloride solution impregnated into the precursor was equivalent to the micropore volume, indicating the micropores formed by the precursor collapsing around the impregnated zinc chloride (Molina-Sabio and Rodriguez-Reinoso, 2004). This microporosity was relatively uniform in these cases since the molecular diameter of the various zinc complexes are similar in size (Maeda et al., 1996).

On the other hand, phosphoric acid impregnation ratios greater than 0.3 g P/g precursor cause greater macro- and mesopore development (Molina-Sabio and Rodriguez-Reinoso, 2004). At lower impregnation ratios when the phosphoric acid does not damage the precursor material as significantly, the produced microporosity is much more heterogeneous when compared to zinc chloride microporosity. This is due to the contraction of the material around the diversely sized polyphosphates (e.g., P_4O_{10}, $H_4P_2O_5$, $H_{13}P_{11}O_{34}$, etc.) which exist at the final carbonization temperature (450°C). Thus, phosphoric acid ACs typically possess much more heterogeneous microporosity even at greater impregnation ratios due to the

variability in molecular weight and size of polyphosphates (Molina-Sabio and Rodriguez-Reinoso, 2004). Moreover, phosphoric acid forms phosphate esters with cellulose at temperatures between 250°C and 450°C as shown in Figure 3-12 (Marsh and Rodriguez-Reinoso, 2006d). These esters form stable cross-links which have greater thermal stability, often facilitating micropore formation since they do not volatilize at greater temperatures.

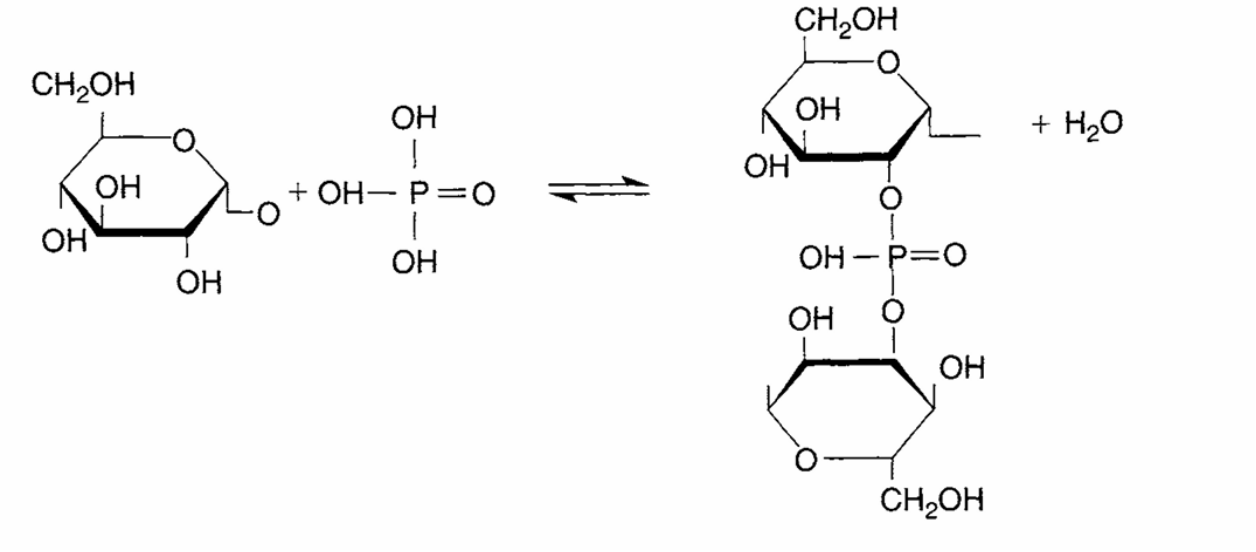

Figure 3-12. Phosphate ester formation on cellulose size chain during phosphoric acid activation at temperatures < 450°C (Marsh and Rodriguez-Reinoso, 2006d).

Between the two common chemical activating agents (phosphoric acid and zinc chloride), phosphoric acid has recently prevailed as the preferred activating agent due to the considerable environmental drawbacks of zinc chloride activation (Neme et al., 2022; Yakout et al., 2016; Foo and Lee, 2010). Further supporting the selection of phosphoric acid is its low cost compared to zinc chloride. At the time of the study, the cost per volume of zinc chloride (0.1M) is five times more than phosphoric acid (85% w/v) (Sigma-Aldrich, 2025a, Sigma-Aldrich, 2025b). Thus, phosphoric acid activation was the method employed in the present study. Phosphoric acid activation is most used for the activation of lignocellulosic biomass. Thus, a discussion on the use of lignocellulosic materials to produce AC is presented in the following section.

3.2.3 Lignocellulosic Materials for the Production of Activated Carbon

The phosphoric acid activation process parameters are most-often altered and optimized for specific precursor materials. In fact, many of the patents associated with AC materials surround the specifics of the activation method employed (Sontheimer et al., 1988b). Several studies have optimized the activation parameters (temperature, phosphoric acid concentration, impregnation ratio, etc.) for different lignocellulosic precursors, including softwoods like pinewood, as shown in Table 3-1 for select studies.

Table 3-1. Surface areas of phosphoric acid activated carbons from various lignocellulosic precursors.

Precursor	**Impregnation Ratio (wt. acid to dry precursor)**	**Pyrolysis Conditions**	**Specific Surface Area (m^2/g)**	**Pore Volume (cm^3/g)**	**Reference**
Pinewood sawdust	1:1	800°C for 15 minutes	1079	0.53	Gao et al., 2017
Coconut shell	1:1	600°C for 120 minutes	479	-	Chin et al., 2018
Palm shell	1.75:1	475°C for 75 minutes	2000	1.2	Lim et al., 2015
Paulownia wood	4:1	400°C for 60 minutes	2806	1.75	Yorgun and Yildiz, 2015
Cashew nutshell	1.7:1	600°C for 120 minutes	1514	1.147	Geczo et al., 2020
Olive stone	3.2:1	500°C for 120 minutes	1218	0.6	Yakout and El-Deen, 2016
Corn cob	1:1	400°C for 60 minutes	2071	1.13	Sych et al., 2012
Rice husk residue	2.5:1	500°C for 60 minutes	1365	0.6	Luo et al., 2018
Tomato plant	2:1	500°C for 40 minutes	748	-	Boundzanga et al., 2022
Poplar wood	2:1	500°C for 40 minutes	1321	-	Boundzanga et al., 2022

The differences in the optimal phosphoric acid activation parameters and resulting pore properties of the ACs are due to the differences in the physical and chemical nature of the raw lignocellulosic precursors. Such differences include variability in the material's chemical structure, microstructure and macroscopic properties. These differences have motivated extensive reviews such as those carried out by Zhang et al. (2024) and Danish and Ahmad (2018). Their findings broadly suggest that the cellular structure of wood provides produced ACs with advantages for the diffusion of a diverse range of contaminants into the resulting AC pore structure. This observation has historically led to wood being recognized as a strong AC precursor for the removal of dyes (Wu and Tseng, 2006), heavy metals (Karthikeyan et al., 2005) and organic contaminants (De Oliveira Sampa et al., 2004).

In Canada, the most used wood material is Spruce-Pine-Fir (S-P-F) which encompasses a range of spruce woods (White, Engleman, Red, etc.), pine woods (Jack, Lodgepole) and fir woods (Balsam, Alpine) commonly grown in Canada (Canadian Wood Council, 2024). The most common of these woods is *Picea glauca*, otherwise known as White spruce or Canadian spruce because of its abundance at a range of elevations (610 m 1520 m) from west to east across Canada as shown in Figure 3-13 (Nienstaedt and Zasada, 1990).

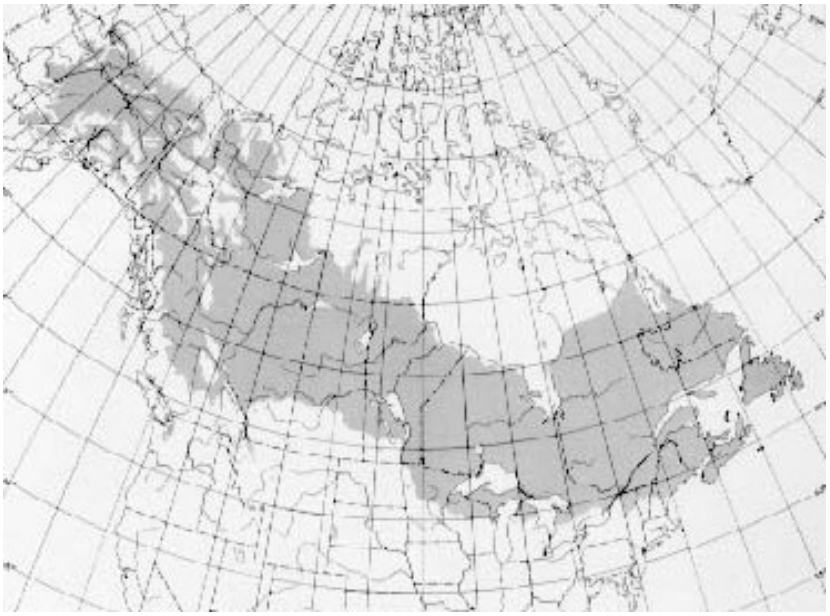

Figure 3-13. Map showing growth range of native white spruce in Canada (Nienstaedt and Zasada, 1990).

Wood waste made up 21% of all solid waste generated in remote First Nations communities in Canada in 2016 (Wang et al., 2023). This wood waste is predominantly generated from white spruce wooden pallets used to ship food and other goods to these remote regions. The high cost associated with shipping the waste wood from Canada's north for re-use as wood pallets or other value-added products results in them accumulating onsite and being burned in most cases (Wang et al., 2023). These facts make white spruce wood a highly suitable candidate for the sustainable production of AC in northern and remote communities of Canada.

As far as the author is aware, the optimal phosphoric acid activation parameters for white spruce wood have not been determined to date. Thus, a clear understanding of the macroscopic features, microstructure and chemical structures of wood is critical for the present study. These characteristics of wood are introduced in the following section.

3.2.4 Wood Characteristics

Wood is one of the oldest materials used by humans for construction, fuel or the making of tools and instruments. The knowledge of wood chemistry is perhaps best documented in a book by Fengel and Wegener (1984). The information documented in this book guides the following discussion to form an understanding of wood.

3.2.4.1 Anatomy of Wood

The macrostructure of wood is characterized by cellular tissue which forms to transfer nutrients throughout the tree or shrub. Observable differences exist between hardwoods and softwoods. However, the present discussion will focus on the properties of softwood since white spruce wood is a softwood species. Softwoods are made up of 90% to 95% tracheids (Fengel and Wegener, 1984b). Tracheids are a type of wood cell characterized by their long and slender shape. The thracheid lumena grow in the longitudinal direction (i.e., up the tree) while parenchyma (ray cells) grow in the radial direction and transfer nutrients radially as illustrated in Figure 3-14. As the tree ages, the older (heartwood) tracheid cell walls grow thicker, and the lumen diameter narrows. Thus, the sapwood tracheid lumena are predominantly

responsible for the transfer of water and nutrients throughout the tree and the heartwood tracheid lumena are responsible for strength and stability (Fengel and Wegener, 1984a).

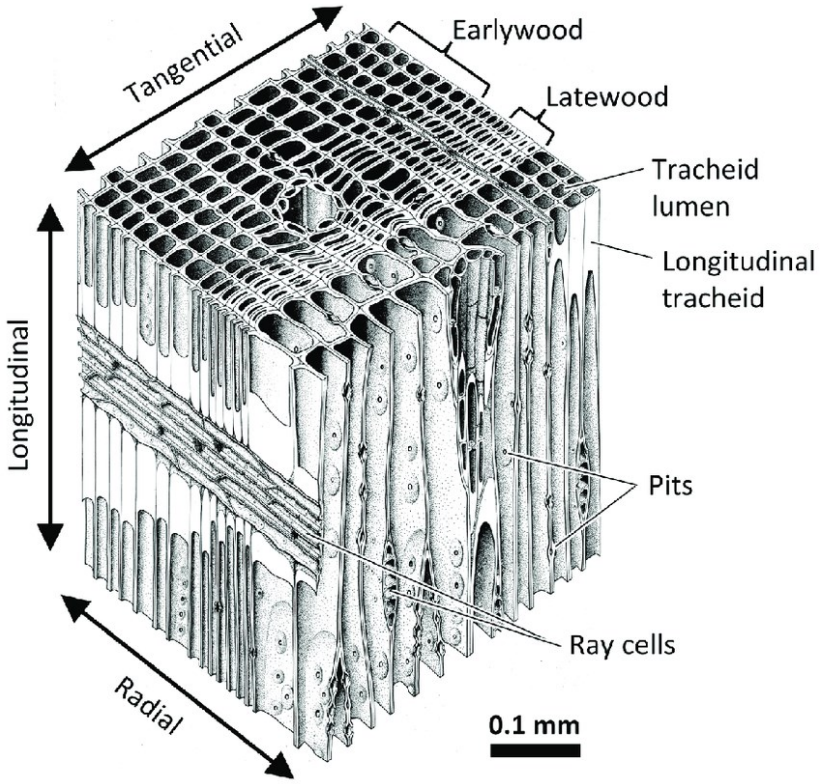

Figure 3-14. Anatomy of softwood cellular structure (Arzola-Villegas et al., 2023).

With a fundamental understanding of the growth structure of wood, taking a closer look, the structure of the cell wall is described in the following section.

3.2.4.2 Wood Cell Wall

The wood cell wall is made up of five components which are best revealed upon isolation of the wood's cellulose (the structural component of the wood) (Fengel and Wegener, 1984a). Generally, the structure of the cell wall is modeled as shown in Figure 3-15. The middle lamella (ML) exists between tracheids and joins the cells together to form the wood tissue. The ML is primarily lignin but also contains pectins (Ansell, 2015). The primary wall (P) and secondary walls (S1, S2) are mostly made up of cellulose microfibrils with varying orientations. The cellulose in the primary wall is thinly layered in a disordered manner allowing for the growth of the cell. The fibrils in the secondary wall 1 (S1) are slightly sloped and

become steeper in the secondary wall 2 (S2). Parenchyma cells have an additional secondary wall referred to as secondary wall 3 (S3). The final layer is sometimes confused with the secondary wall 3 but is actually a tertiary wall (correctly referred to as T, but is S3 as shown in Figure 3-15), which consists of gently sloped fibrils. However, there is a high degree of hemicellulose and lignin in this layer (Fengel and Wegener, 1984a).

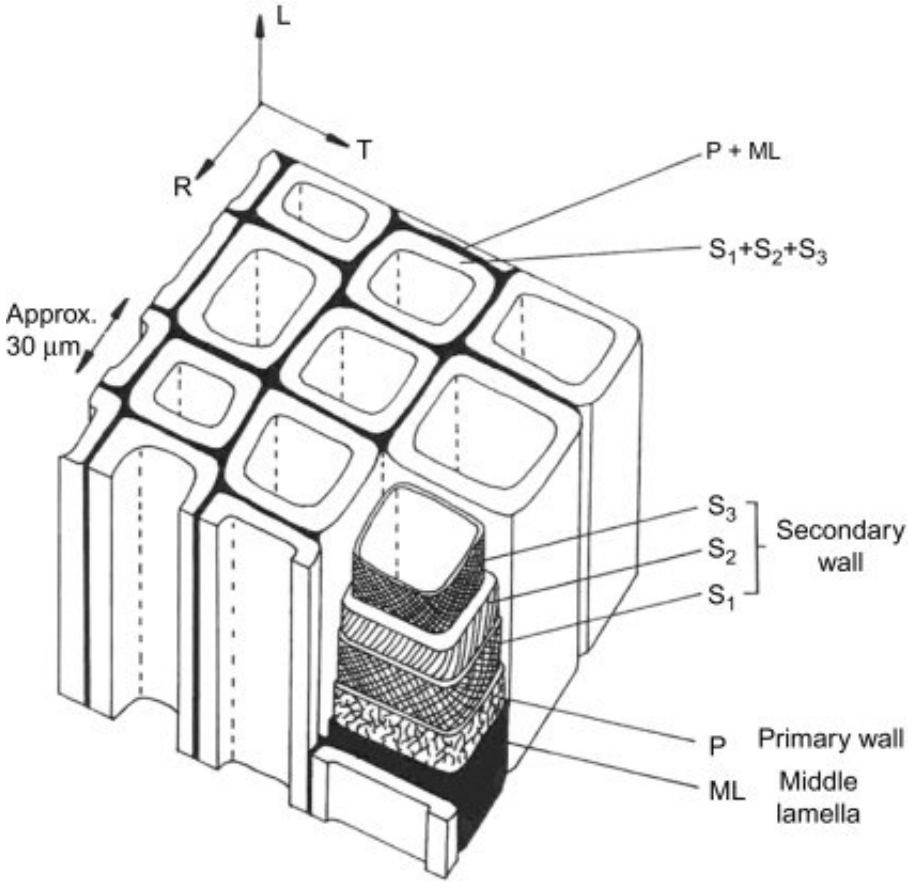

Figure 3-15. Tracheid cell wall structure of softwoods (Ansell, 2015).

Wood, in general, is made up of three fundamental biopolymers (cellulose, hemicellulose and lignin) which each contribute to the chemical and physical properties of wood. The following section takes an even closer look at the chemical composition of wood.

3.2.4.3 Chemical Composition

Each of the lignocellulosic biopolymers have different chemical compositions which contribute to their many physical and chemical properties. In woods, cellulose forms fibrils which make up the cell wall while hemicellulose and lignin support and insulate cellulose as shown in Figure 3-16.

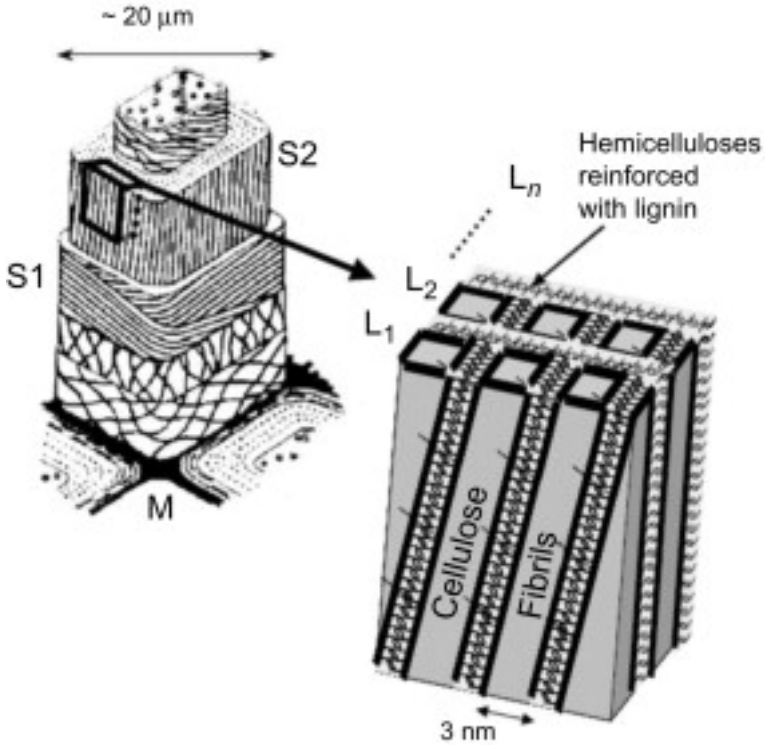

Figure 3-16. Arrangement of cellulose, hemicellulose and lignin in wood cell wall (Ansell, 2015).

The specifics of these three biopolymers are described in the following sections.

3.2.4.3.1 Cellulose

Cellulose is the most abundant biopolymer in nature. It has been estimated that approximately 40% of all carbon from organic matter exists within cellulose (Fengel and Wegener, 1984c). The molecular structure of cellulose is described by the linkage between D-glucopyranose rings which form anhydroglucopyranose (otherwise known as a cellobiose unit) as shown in brackets in Figure 3-17. These units are connected by β-(1→4) glycosidic linkages which are formed by the removal of a singular water molecule between the hydroxylic groups at C1 and C4, respectively.

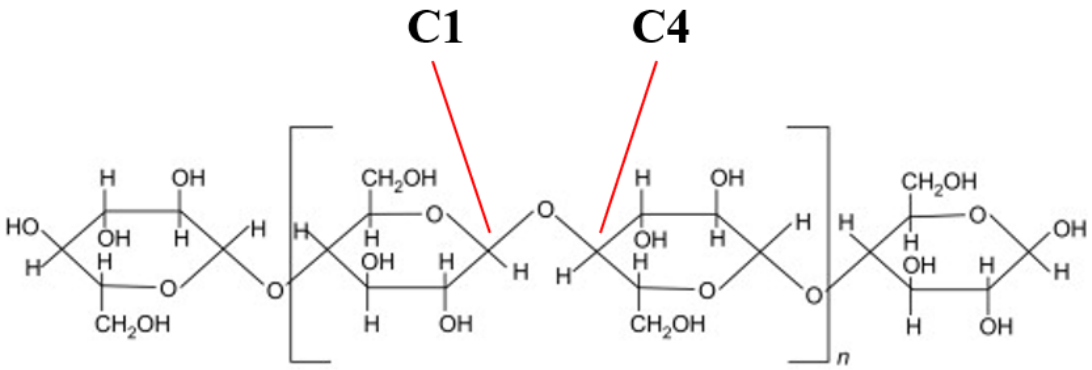

Figure 3-17. Cellulose molecule consisting of D-glucopyranose rings (adapted from Ansell, 2015).

The length of the cellulose chain, quantified by the so-called degree of polymerization (DP) (i.e., the number of glucose molecules within a cellulose chain), is directly proportional to the molecular weight of the cellulose molecule. The DP is typically between 7000 and 15,000 on average within individual plants and varies due to the nature of formation of cellulose in plants (Fengel and Wegener, 1984c).

The D-glucopyranose rings form in the same plane due to the properties of the glycosidic linkage, the pyranose ring itself, and the hydroxyl groups on either end of the chain (at the C1 and C4, respectively). These hydroxyl groups are most responsible for the physical and chemical behaviour of cellulose (Fengel and Wegener, 1984c). Specifically with respect to the supramolecular structure of cellulose in biomass, the hydrogen at the end of the hydroxyl group forms hydrogen bonds with the lone electron pair of adjacent oxygen. This phenomenon occurs in one of two ways in cellulose: intermolecular linkages or intramolecular linkages. Intramolecular linkages occur between adjacent glucose units within an existing cellulose chain. Whereas intermolecular linkages occur between hydroxyl groups of adjacent cellulose chains as shown in Figure 3-18.

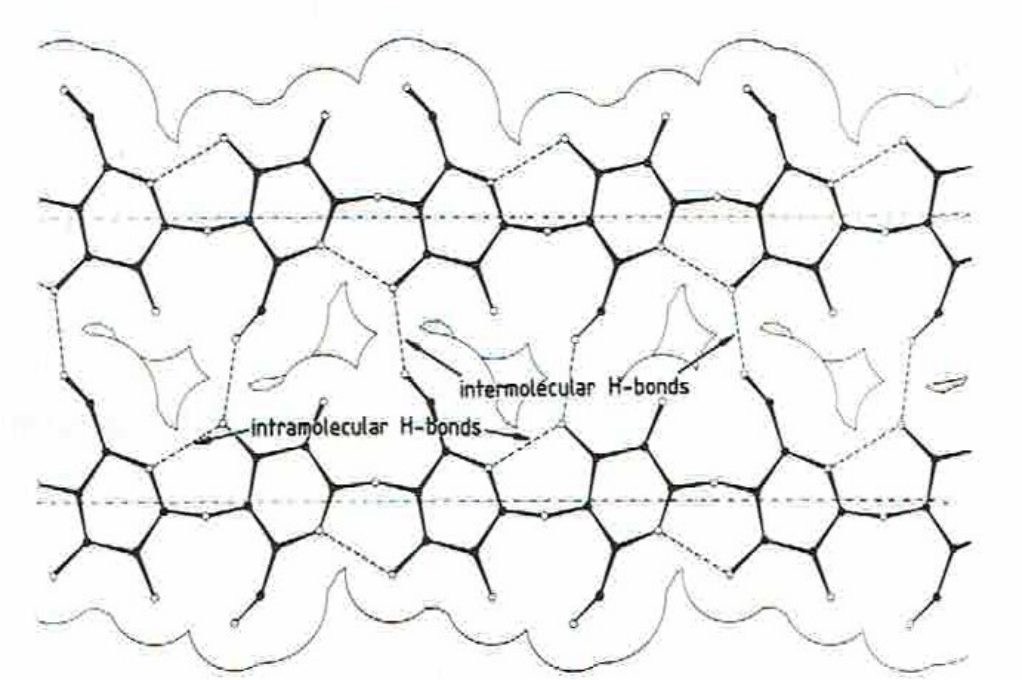

Figure 3-18. Inter- and intramolecular hydrogen bonding shown in the 002 plane (Fengel and Wegener, 1984c).

The intermolecular linkages are responsible for the three-dimensional structure of cellulose shown in Figure 3-19.

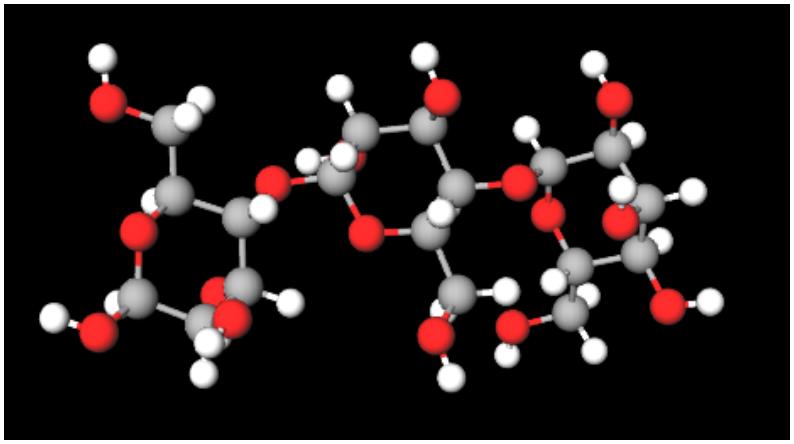

Figure 3-19. 3-Dimensional structure of cellulose molecule with a degree of polymerization equal to three (American Chemical Society, 2022).

Cellulose ultimately forms fibrils which make up the cells and ultimately the tissue of wood. Exposed fibrils can be seen through scanning electron microscope imaging as shown in Figure 3-20 for white spruce wood.

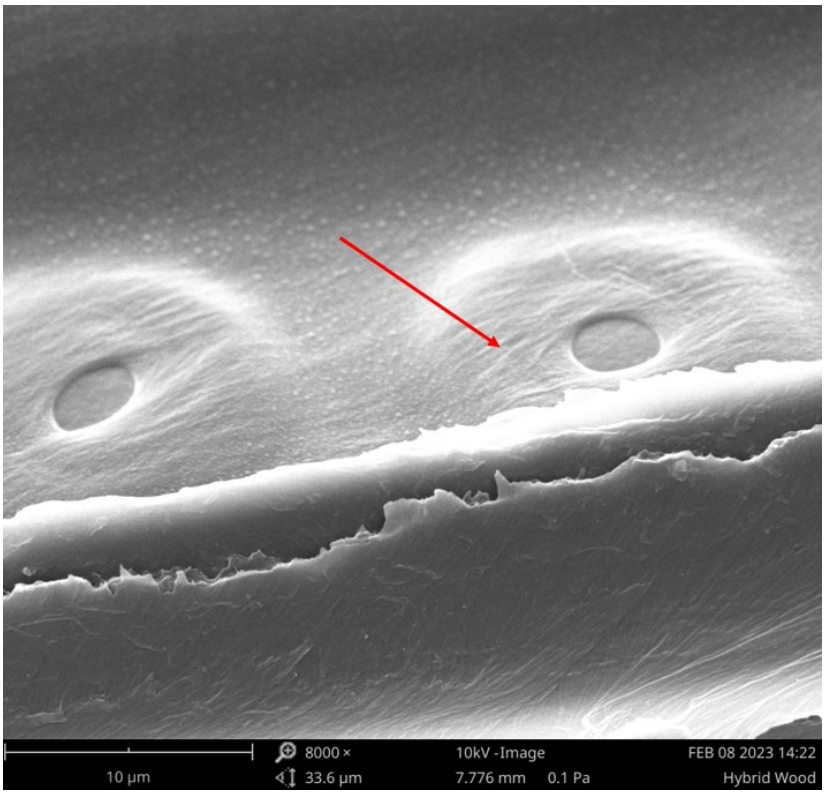

Figure 3-20. Scanning Electron Micrograph of white spruce wood showing exposed cellulose microfibrils.

The intermolecular hydrogen bonding between cellulose chains (chain folding) causes cellulose to be crystalline in some regions (i.e., a uniform and consistent, repeated structure). Thus, cellulose is a semi-crystalline material with amorphous regions (with free hydroxyl groups) that coexist with crystalline regions (with a high proportion of hydroxyl groups bonded to another cellulose chain). Note that in nature, cellulose crystals are referred to as cellulose I and the present discussion is limited to this cellulose polymorph as it is the most relevant.

The crystalline regions (crystallites) vary in size throughout a wood and define its microstructure. Differences in microstructure have a significant impact on how trees thrive in nature and how they may react during phosphoric acid activation. Free hydroxyl groups in cellulose (i.e., those which are not

intermolecularly bonded) are reactive and in nature water-OH forms hydrogen bonds with these free hydroxyl groups. In other words, wood with a high proportion of crystalline cellulose would be less reactive than wood with a high degree of amorphous (non-crystalline) cellulose. These fundamental ideas are, largely, what define the reactivity and behaviour of cellulose in wood.

3.2.4.3.2 Hemicellulose

Hemicellulose and cellulose have one similarity which is that both monomer units are bound by β-(1→4) glycosidic linkages. However, hemicellulose is made up of a variety of monomers that can exist in various hemicelluloses as shown in Figure 3-21. The DP of hemicellulose is, on average, between 100 and 200 (much lower than cellulose) (Rowell et al., 2012).

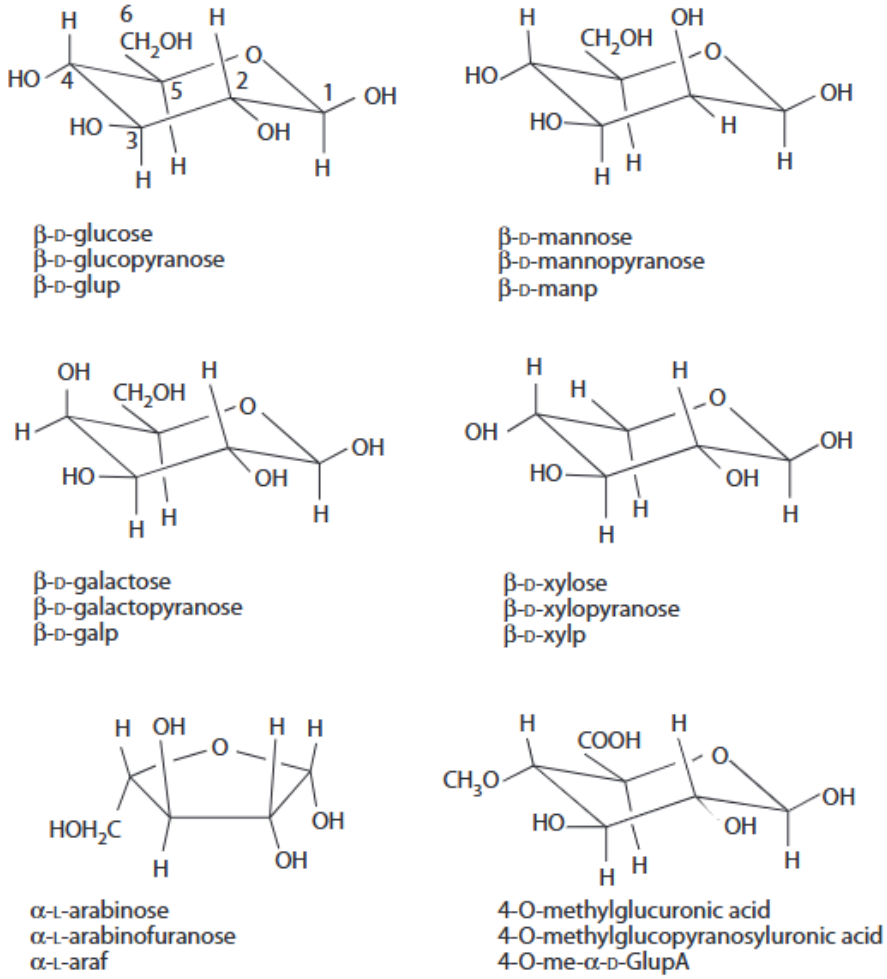

Figure 3-21. Common hemicellulose sugar monomers (Rowell et al., 2012).

Hemicellulose also contains branches emanating from the main chain making it much more reactive than cellulose (Fengel and Wegener, 1984d). This feature makes hemicellulose soluble in alkaline solutions and hydrolysable under acidic conditions (Rowell et al., 2012). Hemicellulose, along with lignin, act to reinforce cellulose fibrils in the secondary cell walls. The hemicellulose-lignin matrix is further reinforced by lignin (Ansell, 2015).

3.2.4.3.3 Lignin

Lignin is the most structurally diverse of the three wood biopolymers. It is mainly comprised of C-O-C and C-C bonds making up aromatic phenylpropane units (Rowell et al., 2012). The main units in lignin are guaiacyl and syringyl units that are represented in varying proportions within softwoods and hardwoods. Softwoods, including white spruce, contain approximately 25% to 35% lignin by mass and most of the softwood lignin is of the guaiacyl variety. While approximately 70% of lignin exists in the cell wall, intertwined with hemicellulose, it exhibits the highest localized density in the middle lamella (Fengel and Wegener, 1984e). The partial chemical structure of softwood lignin is shown in Figure 3-22.

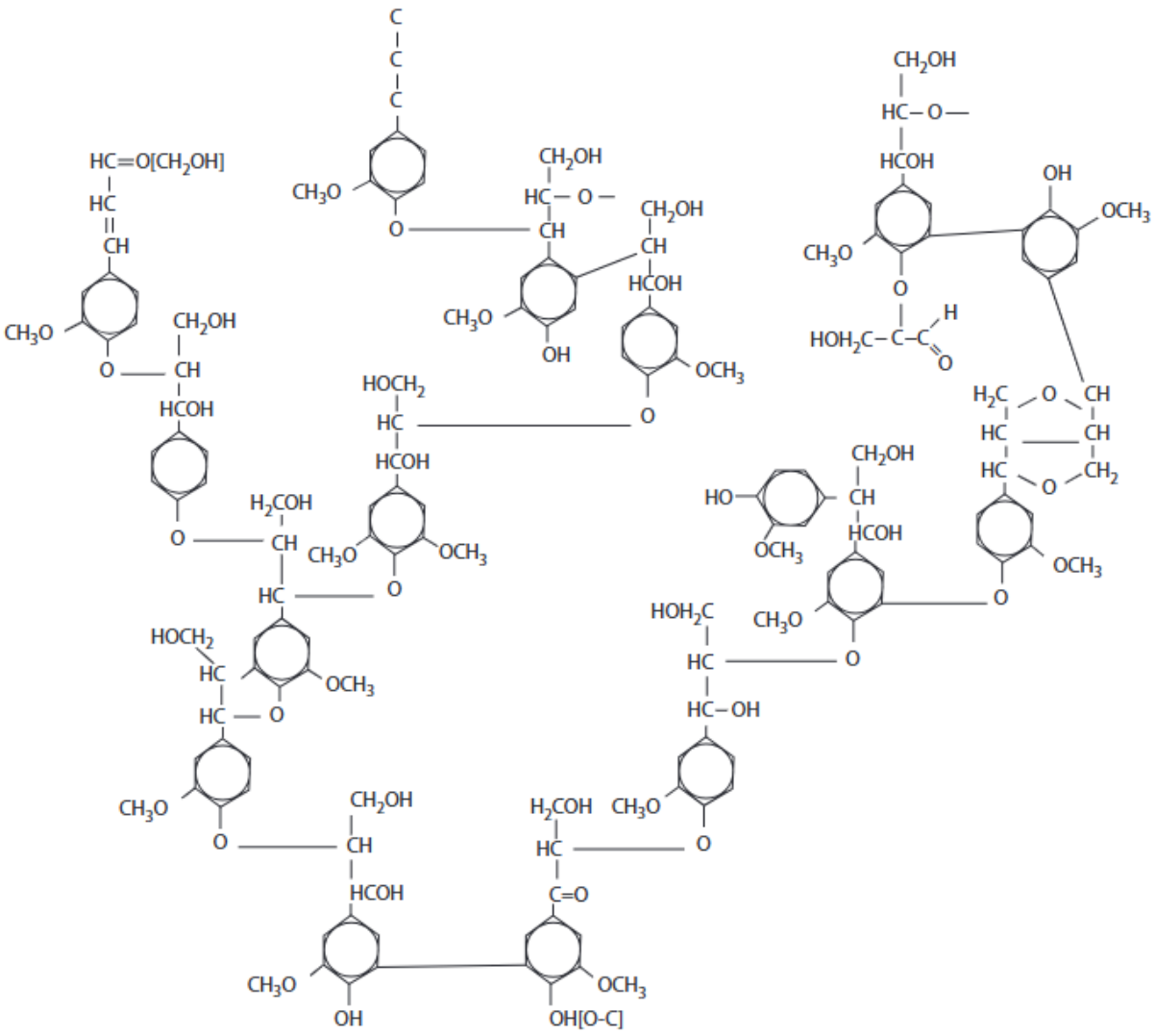

Figure 3-22. Sample structure of part of softwood lignin (Rowell et al., 2012).

Different wood species have different proportions of cellulose, hemicellulose and lignin. In the case of white spruce wood, the proportions are within the ranges of 45% cellulose, 27% lignin, 24-27% hemicellulose and 2-5% extractives (Fengel and Wegener, 1984b). The unique properties of white spruce wood govern the reactions involved in the phosphoric acid activation process which ultimately impact the properties and performance of its produced AC. The impact of these properties is discussed in the following section.

2.5.4 Impact of Wood Properties on Activated Carbon Pore Characteristics

The effectiveness of phosphoric acid activation depends on the macroscopic, crystalline and chemical characteristics of the lignocellulosic precursor. However, the impact these material properties have on the resultant ACs has received limited coverage in the literature. Some researchers have tried to explain the contribution of different proportions of cellulose, hemicellulose and lignin to porosity development of phosphoric acid-prepared ACs (Boundzanga et al., 2022). Similarly, Zuo et al. (2009) attempted to explain the role of crystalline properties of lignocellulosic precursors on porosity development by phosphoric acid activation. The impact of differences in the chemical and crystalline composition of lignocellulosic precursors to phosphoric acid-prepared ACs are discussed in this section.

3.2.4.4 Impact of Wood Chemical Structures on Activated Carbon Porosity

The chemical composition (the nature and proportion of biopolymers in the wood) and crystalline composition (the proportion of crystalline cellulose in the wood) both affect the phosphoric acid activation process. The impact of these two properties on phosphoric acid activation of wood have been researched by Boundzanga et al. (2022) and Zuo et al. (2009), respectively, as discussed in Sections 3.2.4.4.1 and 3.2.4.4.2.

3.2.4.4.1 Chemical Composition

Boundzanga et al. (2022) investigated the contribution of cellulose, hemicellulose and lignin on the pore size distribution and specific surface area of phosphoric acid AC by activating the isolated biopolymers. It was broadly suggested that lignin contributes primarily to microporosity in phosphoric acid ACs. Meanwhile, hemicellulose and cellulose contribute primarily to mesopore development. It was proposed that along with lignin being resistant to thermal decomposition, the phosphoric acid-catalyzed hydrolysis was less effective on lignin decomposition. Both these factors allowed lignin to form linkages with phosphate fractions at the high activation temperatures (>250°C) leading to greater thermal stabilization and ultimately microporosity (Marsh and Rodriguez-Reinoso, 2006d).

On the other hand, cellulose and hemicellulose produced ACs with greater mesoporosity. The phosphoric acid-catalyzed hydrolysis was more impactful on cellulose and hemicellulose than lignin permitting a greater degree of imperfections in their resultant carbon structures (Marsh and Rodriguez-Reinoso, 2006d). This impact may be expected for hemicellulose which innately has a low thermal stability (Fengel and Wegener, 1984h). In the case of cellulose, the cellulose material used in the study was a powder and the potential crystallinity of the cellulose would have been severely compromised (Nelson and Conrad, 1948). Thus, the conclusions made for cellulose are likely only applicable to amorphous cellulose fractions. The impact of varying crystalline properties of lignocellulosic materials is discussed in Section 3.2.4.4.2.

3.2.4.4.2 Crystalline Composition

The impact of the proportion of crystalline cellulose in lignocellulosic biomass on the porosity developed through phosphoric acid activation was investigated by Zuo et al. (2009). Three different biomass precursors were used for the study, each with different degrees of crystallinity (China fir wood, corn cob, cotton stalk). The study also investigated the impact of impregnation time on the crystallinity of the China fir wood and the impact on resultant AC porosity. Their findings suggested that precursors with lower degrees of crystallinity (i.e., a lower ratio of crystalline cellulose to amorphous material) develop greater mesoporosity. This porosity was attributed to the greater impact of phosphoric acid-catalyzed hydrolysis on the more abundant hemicellulose and amorphous cellulose fractions facilitating higher degrees of thermal decomposition leading to mesopore development.

Clearly, the chemical and crystalline structures of the precursor have a significant impact on the resultant properties of the produced ACs (Boundzanga et al., 2022; Zuo et al., 2009). These findings reveal that even after optimizing the many parameters involved in the activation process (e.g., impregnation ratio, carbonization temperature, acid concentration, etc.) the innate properties of the precursor can impose limitations on the potential for porosity and surface area development of produced AC.

It is not certain that the properties of white spruce wood found in remote areas of Canada possesses favourable properties to produce AC. Moreover, the phosphoric acid activation process parameters for

white spruce wood have yet to be optimized, which is a time and resource consuming process. However, the macroscopic, microscopic, chemical and crystalline structures of the wood precursor can be altered by lignocellulosic PTs. These PTs can also bring consistency to the precursor material and remove impurities (which is critical for producing AC for water treatment as described by Sontheimer et al., 1988b), but the impact of PTs on the porosity of produced ACs has not been investigated.

PTs have the potential to:

1. Render unsuitable precursors suitable for AC production by altering their innate properties.
2. Eliminate the need for an extensive chemical activation optimization study by enhancing precursor materials.

The impact of simple PTs on the physical and chemical properties of biomass precursors are introduced and discussed in Section 3.3.

3.3 Woody Biomass Pre-Treatments

PTs are generally described as modifications to the biopolymers in lignocellulosic biomass through depolymerization, bond cleavage and/or deoxygenation (Lee et al., 2024). Most often, PTs primarily decrease the proportion of one or more of the biopolymers (i.e., cellulose, hemicellulose, lignin) in biomass (Lee et al., 2024). This impact, along with the depolymerization and bond cleavage, results in changes to both chemical reactivity and pyrolysis behaviour. Both these factors have the potential to impact the pore properties of the ACs produced. Moreover, PTs have the potential to impact the crystalline nature of lignocellulosic biomass, impacting phosphoric acid reactions in the subsequent chemical activation process.

PTs are categorized by their reaction mechanism. The two main categories of lignocellulosic biomass PTs are physical and chemical. Physical PTs methods, such as grinding, milling or even passing ultrasonic waves through the biomass, impact the physical structure of the biomass. Chemical PTs involve contacting the biomass with solutions such as acids, bases, oxidizing agents or other solvents which partially remove or change the nature of existing biopolymers in the biomass. This section discusses the prevailing

simple and cost-effective physical and chemical PTs and compares them with respect to their suitability for the present application.

3.3.1 Physical Pre-Treatments

The following subsections will discuss select physical PT methods: particle size reduction, torrefaction and ultrasonic PT.

3.3.1.1 Particle Size Reduction

Particle size reduction is a common PT for various applications primarily since it increases external surface area of the lignocellulosic biomass. The increased specific surface area makes the material more amenable to reactions with aqueous solutions, and the smaller size may be required for the end application. While it may be expected that simply changing the particle size of a lignocellulosic biomass would not impact the proportion of the respective biopolymers in the material, the degree of polymerization of all three biopolymers (cellulose, hemicellulose, lignin) is reduced following particle size reduction (Warade et al., 2025). The impact on the degree of polymerization also impacts crystalline cellulose. Bai et al. (2018) showed that with a greater degree of particle re-sizing (i.e., the smaller the particle) the lower the degree of crystallinity (crystallinity index). Kim and Kim (2019) reinforced this finding and added that the mean size of cellulose crystallite also reduced with greater particle size reduction.

3.3.1.2 Torrefaction Pre-Treatment

Although torrefaction is commonly referred to as a thermochemical process, for the purposes of this discussion it is placed under the category of a physical PT because it is carried out in a dry environment (unlike the chemical PTs which take place in aqueous solutions). Torrefaction consists of heating lignocellulosic biomass in an inert environment between temperatures of 200°C and 300°C (Kota et al., 2022). The stages of the torrefaction process are illustrated in Figure 3-23.

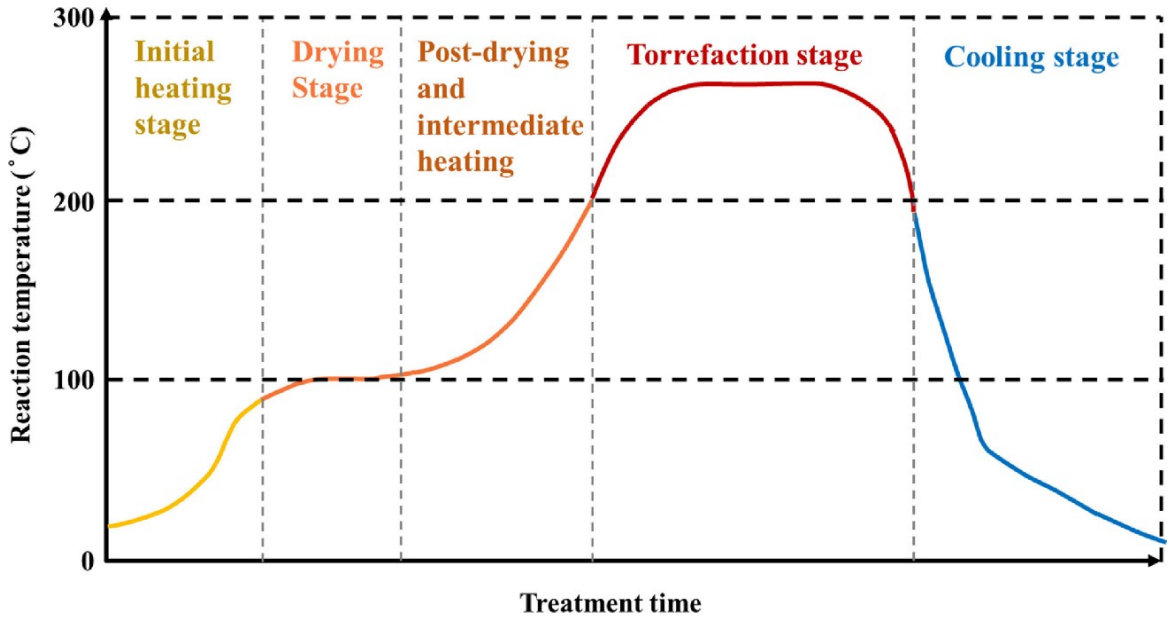

Figure 3-23. Phases of torrefaction pre-treatment (Chen et al., 2021).

Torrefaction PT mostly impacts hemicellulose as it is the least thermally stable of the biopolymers in wood (Fengel and Wegener, 1984h). Dehydroxylation and deacetylation reactions of hemicelluloses dominate the temperature ranges between 200°C and 240°C (Chen et al., 2014). The products of deacetylation include acetic acid which catalyzes further hemicellulose decomposition as well as lignin and cellulose degradation (Collard and Blin, 2014). Beyond temperatures of 240°C, depolymerization of amorphous cellulose, and depolymerization and demothoxylation of lignin occurs without the aid of acetic acid produced from the hemicellulose (Svoboda et al., 2009).

The resultant material (i.e., biochar) has increased hydrophobicity, increased grindability and increased durability (Chen et al., 2021). The overall loss of mass also increases the biomass porosity (Pfriem et al., 2009).

3.3.1.3 Ultrasonic Pre-treatment

Ultrasonic PT consists of immersing the lignocellulosic material in a solution (often distilled water) and subjecting the bath to ultrasonic waves. The ultrasonic waves cause disruptions between the lignocellulosic biopolymers, allowing them to diffuse into the solution (Koutsianitis et al., 2015).

Hemicellulose, lignin and amorphous cellulose are most removed by this PT (Mosier et al., 2005; Barakat et al., 2014). The removal of these amorphous fractions increases the crystallinity index of biomass without having any impact on crystalline cellulose even when carried out under weak basic or acidic conditions (He et al., 2017).

3.3.2 Chemical Pre-Treatments

The following subsections will discuss the select chemical PT methods: hydrothermal, alkaline, and acid hydrolysis PT.

3.3.2.1 Hydrothermal Pre-Treatment

Hydrothermal PT is sometimes referred to as 'physiochemical PT' (Kumar et al., 2010). However, for the simplification of the present discussion, it is herein referred to as a 'chemical PT'. Hydrothermal PT (or "liquid hot water", LHW PT) consists of contacting the lignocellulosic precursor with hot water in a pressure vessel (e.g., autoclave) for times ranging from seconds to several hours (between 150°C and 230°C) (Garrote et al., 1999). The active process is also referred to as 'autohydrolysis' whereby autoionization of water molecules at the elevated temperatures results in an increased concentration of hydronium ions. The hydronium ions catalyze the breaking of heterocyclic ether bonds and acetyl groups in hemicellulose (Garrote et al., 1999; Lu et al., 2016). The decomposition of acetyl groups in particular leads to the formation of acetic acid which further catalyzes hemicellulose degradation, cellulose depolymerization, and lignin depolymerization (Garrote et al., 1999). In fact, the hydronium ions supplied by the autoionization of acetic acid contribute more to the hydrothermal PT than the innate hydronium ions originally in the LHW solution. Rissanen et al. (2014) showed that when hydrothermal PT times exceed 150 minutes, lower molecular mass fractions of hemicellulose, cellulose and/or lignin begin to be released into the bulk solution (i.e., from the lignocellulosic pore matrix). This phenomenon occurs since the 'freed' biopolymers contact the hydronium ions (from the hot water and acetic acid) for a longer period leading to greater depolymerization.

Hydrothermal PT requires relatively low power and equipment requirements while also having a significant impact on the properties of biomass. These advantages have led to a steep increase in hydrothermal PT research, with an increase from 27 articles published in 2001 to over 664 articles published on the topic in 2022 (Yu et al., 2025).

3.3.2.2 Alkaline Pre-Treatment

Alkaline PT consists of using hydroxides, such as sodium, calcium and/or ammonium hydroxide, in solution to contact and modify the biomass (Iroba et al., 2017). The alkaline environment hydrolyzes linkages between lignin and cellulose (Kumar et al., 2010). While the primary lignocellulosic component impacted by alkaline PT is lignin, the fact that it is naturally bound to hemicellulose through phenylpropane cross-links leads to the subsequent solubilization of hemicellulose (Iroba et al., 2017). The hemicellulose is solubilized through saponification of its ester bonds. Thus, alkaline PT ultimately decreases the degree of polymerization of lignin and hemicellulose and removes them from the precursor material. The removal of amorphous lignocellulosic fractions is inevitable during alkaline PT.

The impact on cellulose only becomes more pronounced with increased concentration or contact times. Long contact times (> 48 hours) at relatively low concentrations (e.g., < 3% w/w) cause crystalline cellulose depolymerization and a subsequent decrease in crystallinity index (Woiciechowski et al., 2020; Xue et al., 2013). However, at lower PT times (e.g., 30, 60, 90 minutes) the amorphous regions remain unaffected at similar concentrations (< 3% w/w), and the crystallinity index is increased by the removal of hemicellulose and lignin (Qi et al., 2023). Barman et al. (2020) showed that once concentrations of NaOH solution exceed 20% (w/w) the hydrogen bonds of crystalline cellulose are broken causing a decrease in both crystallinity and crystallinity index of the biomass. Nonetheless, alkaline PT has prevailed as a popular lignocellulosic PT method due to its low energy consumption and effectiveness (Iroba et al., 2017).

3.3.2.3 Acid Hydrolysis

Like alkaline PT, acid hydrolysis PT consists of contacting the biomass precursor with an acidic solution. Acids including sulphuric, hydrochloric, nitric and citric have been evaluated, but sulphuric acid

has prevailed as the most common because it is slightly less corrosive and less costly than the other alternatives (Woiciechowski et al., 2020). Acid hydrolysis decomposes cellulose, hemicellulose and lignin in multi-stage reactions which were best summarized by Lv et al. (2024) as shown in Figure 3-24. In all cases, the hydrolysis of glycosidic linkages occurs to reduce the degree of polymerization of the biopolymers (Fengel and Wegener, 1984f). The depolymerized components are released into solution where they are further decomposed (Woiciechowski et al., 2020). Hemicellulose is first hydrolyzed into xylose and arabinose units which are then further decomposed to furfural, methane acid, levulinic acid and other products. Similarly, cellulose depolymerizes into glucose monomers which are further decomposed in solution. The phenolic nature of lignin leads to its decomposition into various phenols following acid hydrolysis.

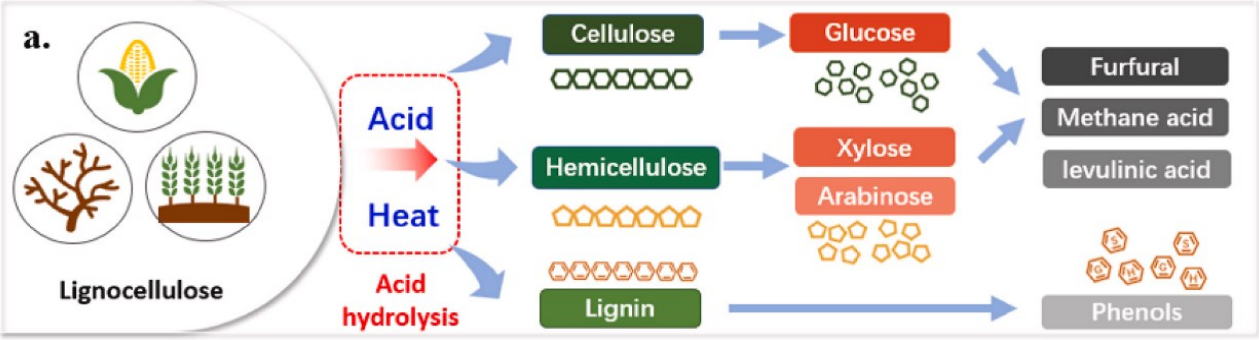

Figure 3-24. Summary of acid hydrolysis of lignocellulosic materials (Lv et al., 2024).

While effective for removing these biopolymers from the wood matrix, acid hydrolysis is not without drawbacks. Firstly, acid hydrolysis is often carried out at temperatures greater than 120°C to improve the kinetics (Santos et al., 2018; Fitria et al., 2019). Additionally, the acid hydrolysis is non-selective for the biopolymers and the degree of removal is dependent on the intensity of the PT (e.g., contact time, concentration, temperature), making the results less predictable when compared to other PTs (Maurya et al., 2015).

3.3.3 Comparison of Pre-Treatment Methods

As discussed, each of the aforementioned PTs have respective impacts on the properties of lignocellulosic biomass. However, the PT methods should be evaluated for their suitability given the present application (using white spruce in remote and resource-limited communities). Table 3-2 presents the advantages and limitations to each of the above-mentioned PTs.

Table 3-2. Comparison of common sustainable and cost-effective pre-treatment methods.

Pre-Treatment	**Advantages**	**Drawbacks**
Particle size reduction	- Simple process. - Relatively low energy consumption.	- Minimal impact on biomass properties other than cellulose crystallinity.
Torrefaction	- Low energy requirement. - No waste generation. - Hemicellulose removal, increased porosity. - Simple process.	- Requirement for inert gas (e.g., nitrogen gas).
Ultrasonic	- No waste generation.	- High energy and capital and maintenance cost requirement.
Hydrothermal	- Low energy consumption and equipment requirements (Yue et al., 2022). - Hemicellulose and lignin removal, increased porosity. - No chemical requirements, corrosion or waste generation (Saha, 2003). - Simple process.	
Alkaline	- Low energy and cost requirement. - Simple process.	- Corrosive chemical waste. - Increased ash content (Woiciechowski et al., 2020). - Requirement to ship chemical.
Acid hydrolysis	- Effective for introducing porosity.	- Corrosive chemical waste. - Temperature and chemical component driving costs higher. - Limited control on what biopolymers are impacted. - Requirement to ship chemicals.

Clearly, some of the PTs have drawbacks which outweigh their advantages for the present application. Particle size reduction is a feasible PT but does not have a significant impact on the chemical properties of the precursor material outside of its crystallinity. Ultrasonic PT is simply unrealistic for remote communities where equipment maintenance and servicing would be costly and challenging. Moreover, acid hydrolysis PT is more costly than the other chemical PT alternatives due to the requirement for elevated temperatures and high concentration of acid, which will have to be transported into these remote communities.

Thus, it may be concluded that for the application of PT of white spruce wood in northern and remote communities of Canada that the following PTs seem the most plausible:

1. Torrefaction PT.
2. Hydrothermal PT.
3. Alkaline PT.

These PT methods have received significant attention in recent years for their sustainability and effectiveness (Mankar et al., 2021; Abolore et al., 2024). Their mechanisms are well defined through the research and various applications for their use have been investigated in the aforementioned review articles by Mankar et al. (2021) and Abolore et al. (2024). However, the impact these PTs have on one single raw material in the same study has yet to be addressed.

3.4 Conclusions and Research Gaps

AC is a highly porous material capable of removing contaminants of increasing concern in remote locations of Canada (e.g., NOM, cyanotoxins, etc.). AC can be produced from carbonaceous precursor materials (most commonly waste materials). However, the specific surface area (and thus, performance) of AC for water treatment applications heavily depends on the physical and chemical properties of the precursor material. As discussed within this chapter, the most sustainable raw material to produce AC in remote and northern Canadian communities is white spruce wood from waste wooden pallets. Given the limited resources available in small and remote northern Canadian communities the most-practical way to

produce AC is by CA using phosphoric acid. However, the optimal phosphoric acid activation parameters for white spruce wood AC have not been studied.

While the impact that PTs have on the characteristics of biomass have been well-researched, the impact these PTs have on the production and characteristics of white spruce wood-based AC have not been studied. Given that for this application, limitations exist in terms of the raw material, it is worthwhile studying the impact of different PT methods. Thus, the present research aims to investigate the effect that simple PTs have on the specific surface area and adsorption capacity of white spruce wood AC prepared by phosphoric acid activation.

Chapter 4 - Materials and Methods

This chapter describes the materials and methods used to conduct the experiments of the present study. The study consisted of the preparation of ACs using white spruce waste material processed by three different PT methods (torrefaction, hydrothermal and alkaline). The porosity and performance evaluation of the resultant ACs (by Nitrogen Gas Adsorption and Iodine Number, respectively) was carried out and the characterization of the PT woods were used to explain the changes in AC porosity and performance. The specifics of the materials (i.e. wood, chemical reagents) and characterization methods (i.e. Thermogravimetric Analysis, Fourier Transform - Infrared Spectrometer, X-Ray Crystallography, etc.) are described to give the reader background on the advantages and limitations of the experimental methodology. A schematic diagram of the experimental procedures implemented in Chapter 4 is also presented and described.

4.1 Materials

4.1.1 Lignocellulosic Precursor

` White spruce (*Picea glauca*) sap wood from Weyerhaeuser (Drayton Valley, AB) was used throughout the experimental campaign. The wood was resized, and samples were prepared according to each part of the study.

4.1.2 Chemicals

Deionized (DI) water was supplied by the Barnstead™ MicroPure™ Water Purification System, Model 50132373 (Thermo-Fisher Scientific, St. Louis, MO, USA). This model uses ultraviolet photo-oxidation, mixed-bed ion exchange and a 0.2 μm filter to produce Type 1 ultrapure water.

All chemicals used for the preparation of reagents or PT mediums were ACS Grade chemicals. The chemicals used throughout the experiments were: sodium hydroxide pellets (>97.0%, LabChem, Zelienople, PA, USA), hydrochloric acid (36.5-38%, VWR Chemicals, Mississauga, ON, CA),

orthophosphoric acid (85%, Fisher Chemical, Ottawa, ON, CA), iodine crystals (>99.99%, BDH Chemicals Limited, Mississauga, ON, CA), sodium thiosulfate penta-hydrate crystals (>99.5%, Macron Fine Chemicals, Mississauga, ON, CA), potassium iodide (>99.0%, Ward's Science, Rochester, NY, USA), potassium iodate (>99.4%, BDH Chemicals Limited, Mississauga, ON, CA), Starch (potato) (100%, Ward's Science, Rochester, NY, USA), and anhydrous sodium carbonate (>99.5%, Fisher Chemical, Ottawa, ON, CA)

Gases used in the experiments included: a) compressed air supplied by the centralized compressed air system in the Colonel By building at the University of Ottawa, ON, CA; b) nitrogen gas (Research Grade, >99.999%, Messer Canada Inc., Ottawa, ON); c) argon gas (Research Grade, >99.99%, Messer Canada Inc., Ottawa, ON); and d) Ultra-High Purity nitrogen gas (Messer Canada Inc., Drummondville, QC).

4.2 Wood Pre-Treatment Methods

4.2.1 Sample Preparation

Three sizes of white spruce wood sample were prepared for respective experiments.

- 15 x 15 x 30 mm wood blocks were prepared for the apparent density experiment by machining white spruce wood as shown in Figure 4-1. The machined blocks were sanded on all sides to remove surface imperfections. The sanded samples were then blown with pressurized air on all sides to remove any remaining sawdust. The blocks were then washed with copious amounts of DI water before being left to dry in a desiccator at ambient temperature.

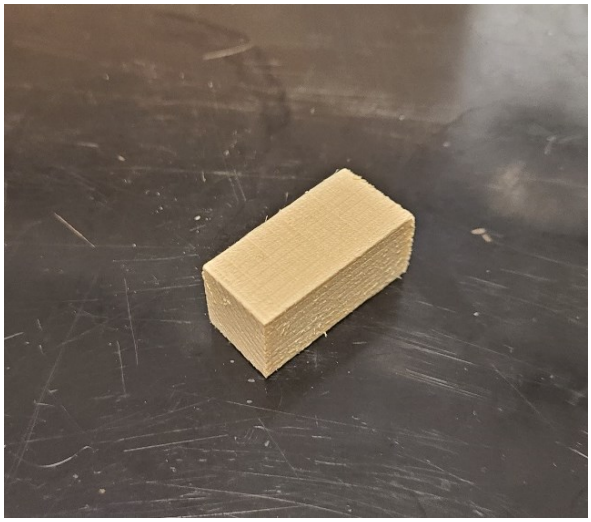

Figure 4-1. 15 x 15 x 30 mm white spruce wood block.

- Wood chips were prepared for producing the ACs by blending 15 x 15 x 30 mm blocks of white spruce wood. The blended wood was captured between a 9.5 mm sieve and 12.7 mm sieve as shown in Figure 4-2. These wood chips were washed by stirring them for 10 minutes in a 2 L beaker filled with DI water. The water was then drained from the beaker and the wood chips were placed in a dry beaker before the drying process.

Figure 4-2. White spruce wood chips with a minimum dimension of 9.5 mm.

- 5 x 5 x 2 mm samples of white spruce were prepared to fit within the pan of the thermogravimetric analyzer (detailed in Section 4.4.2.5.1). The sides of the sample were gently sanded on all sides (example shown in Figure 4-3). The sanded samples were blown with pressured air on all sides to remove loose particles from sanding and washed with copious amounts of DI water. The washed samples were placed in a desiccator to dry at ambient temperature until a constant mass was achieved.

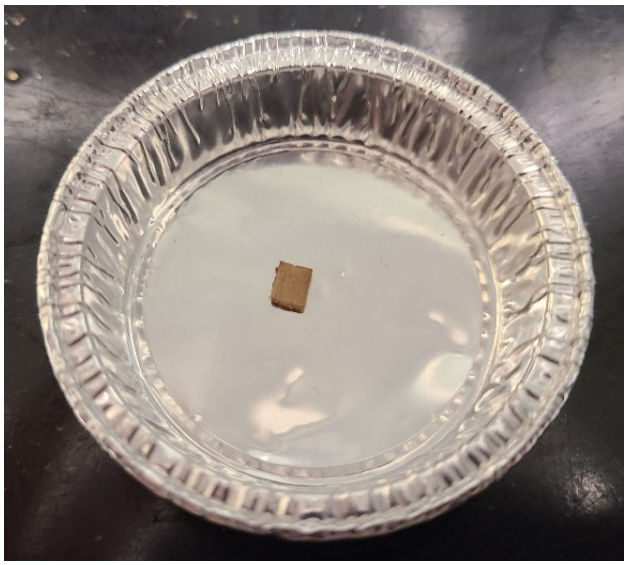

Figure 4-3. 5 x 5 x 2 mm white spruce wood sample after Torrefaction pre-treatment.

Before and after PT, every sample was dried in a convection oven (shown in Figure 4-4) for 24 hours at 103°C ± 2°C.

Figure 4-4. Oven used for drying white spruce wood samples.

Following oven drying, the samples were placed directly into the desiccator (as shown in Figure 4-5) and cooled to ambient temperature.

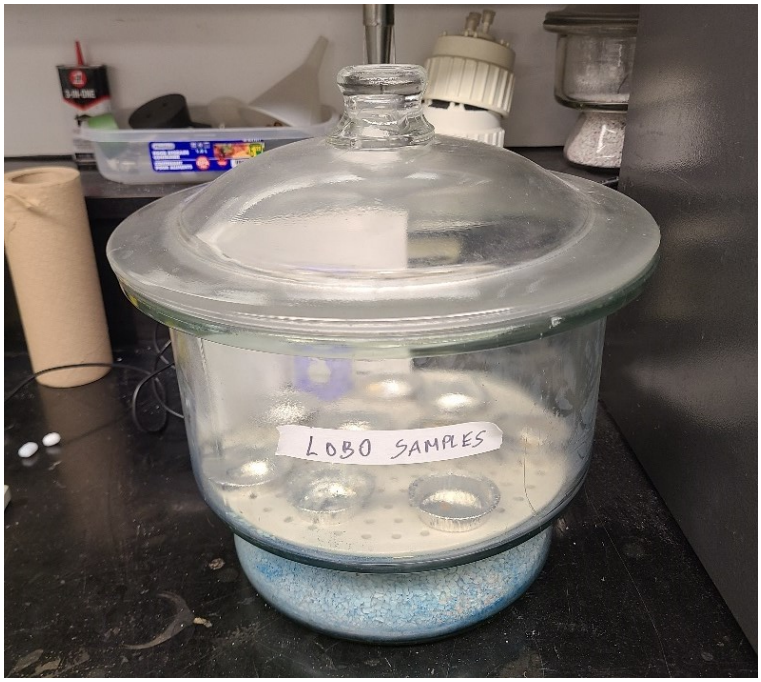

Figure 4-5. Desiccator used for drying samples.

4.2.2 Pre-Treatments

Given the practical context of the research, efforts were made to select PT conditions that consume as little electricity as reasonably possible. As such, preliminary experiments were carried out to determine at which minimum treatment duration HPT and APT would reliably change the apparent density of white spruce wood (used as an indirect indication of porosity development in the wood). The results of these experiments can be found in Appendix A and were used to arrive at the PT durations carried forward in the rest of the study. The conditions studied are described within this subsection.

4.2.2.1 Torrefaction Pre-Treatment

The samples underwent TPT using the Thermolyne™ F6020C-33-60 Atmosphere Controlled Ashing Furnace (ACAF) (Thermo-Fisher Scientific, St. Louis, MO, USA) shown in Figure 4-6. The instrument is capable of three to four air exchanges per minute and is equipped with a chamber for pre-heating influent gases prior to reaching the sample chamber.

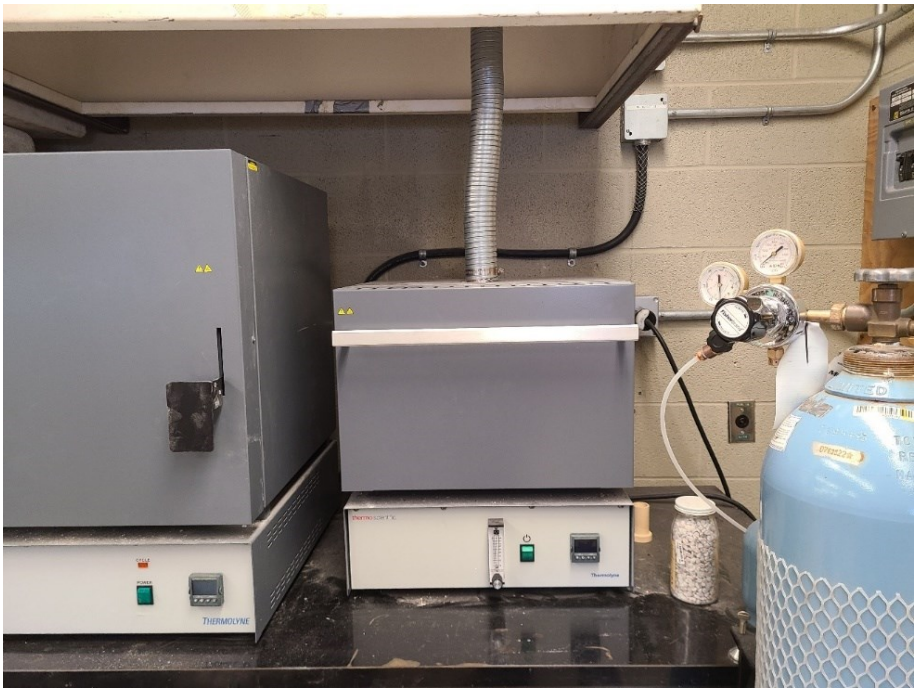

Figure 4-6. Thermolyne™ F6020C-60 Atmosphere Controlled Ashing Furnace.

Clean, dry wood samples were placed in clean, dry, ceramic crucibles as shown in Figure 4-7 for the wood chips (where 13 g ± 1 g of clean, dry wood chips were placed in each crucible).

Figure 4-7. White spruce wood chips in clean, dry, ceramic crucibles.

The filled crucibles were then placed in the chamber of the ACAF as shown in Figure 4-8. The ACAF chamber was purged with argon gas (Messer Canada Inc., Ottawa, ON) at a flowrate of 20 L/minute for three minutes to flush oxygen from the chamber. The flowrate of argon gas was then reduced to 7 L/minute (i.e. one volume exchange every two minutes). The furnace temperature was ramped at a rate of 10°C per minute to a temperature of 220°C and was held at 220°C for two hours. After the two-hour dwelling period, the chamber was allowed to cool to ambient temperature under the same argon flow conditions. The samples were then extracted and placed directly into a desiccator.

Figure 4-8. White spruce wood chips in atmosphere-controlled ashing furnace chamber.

4.2.2.2 Hydrothermal Pre-Treatment

The Hydrothermal PT (HPT) consisted of immersing dry, untreated white spruce wood in boiling (~100°C), DI water for two hours on a hot plate. A weight ratio of approximately 10:1 (water to dry wood) was maintained for all HPTs by keeping a separate beaker of boiling water full at all times to replenish vapourised water losses as shown in Figure 4-9.

Figure 4-9. Hydrothermal pre-treatment apparatus using hot plate.

Following HPT for two hours, the wood was extracted from the solution and placed in a separate, empty beaker. The wood was allowed to cool to ambient temperaratures before being placed in a dessicator to dry for a minimum of 24 hours.

4.2.2.3 Alkaline Pre-Treatment

The Alkaline PT (APT) consisted of immersing the white spruce wood samples in 5% (w/w) solution for a period of two hours at ambient temperature. A weight ratio of approximately 1:2 (dry wood to 100% NaOH) was maintained for all experiments. Samples were immersed in the NaOH solution and stirred using a magnetic stirrer for the complete two hour treatment time as shown in Figure 4-10.

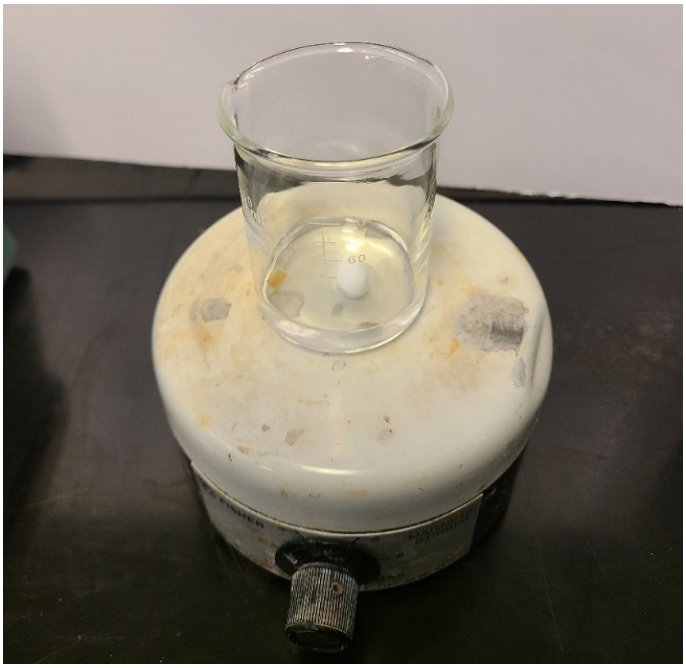

Figure 4-10. Alkaline pre-treatment apparatus for 5 x 5 x 2 mm sample.

Following the two-hour treatment time, the wood was immediately extracted and placed in a DI water bath and stirred with a magnetic stirrer for 30 minutes. The APT white spruce wood was then placed in a desiccator to dry.

4.2.2.3.1 Alkaline Pre-Treatment Washing Procedure

In early phases of the research, charcoal was produced using the APT white spruce wood. Observations of the charcoal revealed that significant sodium from the APT remained as shown in the Scanning Electron Microscope and Energy-Dispersive X-Ray Spectroscope (SEM-EDS) image in Figure 4-11 where the pink represents sodium on the surface of the charcoal. The significant degree of contamination prompted an investigation into a washing procedure for the APT white spruce wood to limit impacts on the properties of AC.

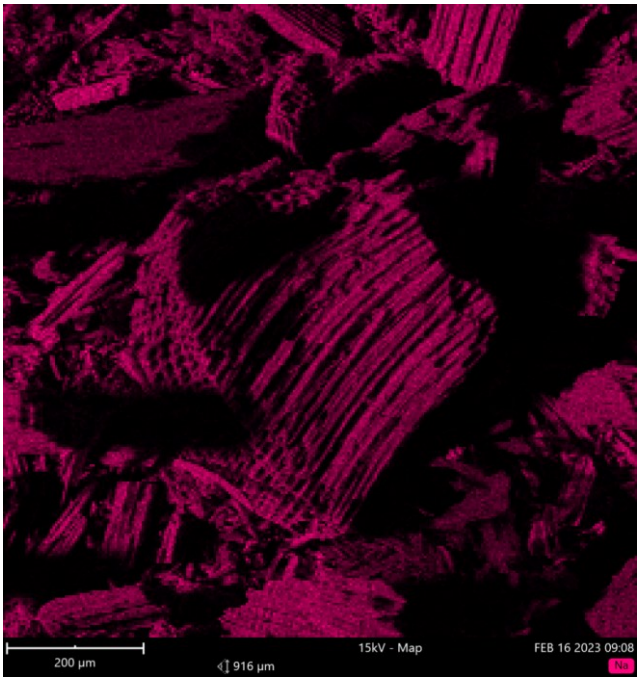

Figure 4-11. SEM-EDS image of Alkaline pre-treated white spruce wood charcoal without washing.

The washing procedure involved two steps. The first step included subjecting the dry, APT wood to vacuum conditions using the Buehler Cast N' Vac, 1000 vacuum chamber (Buehler, Lake Bluff, IL) shown in Figure 4-12.

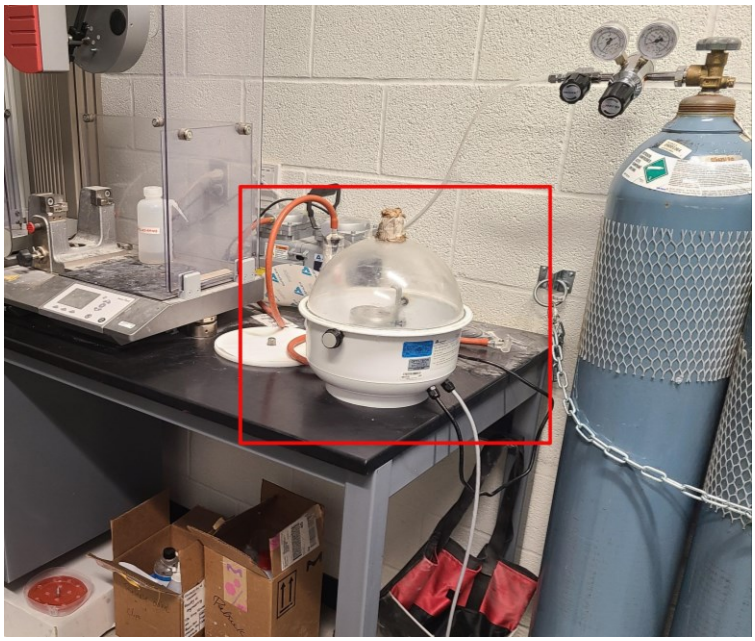

Figure 4-12. Vacuum washing apparatus for Alkaline pre-treatment.

Dry, APT wood was placed in a container within the vacuum chamber and the pores of the wood were evacuated of air by pumping air out of the chamber (to a pressure of -95kPa). Once the pores were evacuated of air, the wood was then immersed in distilled water and allowed to soak for approximately 10 minutes. After the 10-minute soaking time, air was re-introduced to the chamber, pushing water further into the pores of the wood.

The samples were then removed from the container and centrifuged for 10 minutes to pull as much water as reasonably possible from the pores of the wood. The centrifuged samples were returned to the vacuum chamber, and the process was repeated until the supernatant solution was colourless to the eye. The difference in colour between the supernatant after one and two vacuum washing cycles is shown in Figure 4-13.

Figure 4-13. Alkaline pre-treatment supernatant after one (left) and two (right) vacuum washing cycles.

After vacuum washing until a clear supernatant was achieved, the samples were placed in a desiccator and dried until a constant mass was achieved. The dry, vacuum washed APT wood was then placed in a distilled water bath at a mass ratio of 1:50 (dry wood to distilled water) and stirred with a magnetic stirrer for 10 minutes. The initial pH of the bath was measured after 10 minutes of stirring, then the solution was titrated with 5% (w/w) hydrochloric acid (prepared with deionized water) to leach sodium

from the surface and pores of the wood. The bath was carefully titrated until a stable pH of 7 was achieved (i.e., the pH remained constant at 7 for a period of 10 minutes). The wood was then extracted from the bath and copiously washed with DI water. The vacuum-titration washed APT wood was then subject to centrifugation to remove as much water from the pores as reasonably possible. Thereafter, the wood was placed in a desiccator and allowed to dry.

The two step washing procedure effectively reduced the sodium contamination on produced charcoal as shown in Figure 4-14.

Figure 4-14. Charcoal produced from Alkaline pre-treated wood without washing (left), with vacuum washing (center), and with both vacuum and titration washing (right).

4.3 Activated Carbon Preparation Methods

Untreated, TPT, HPT and APT white spruce wood chips were activated in a two-step process consisting of impregnating the chips with phosphoric acid (the activating agent) and heating (carbonization).

The impregnation procedure consisted of soaking the dry wood chips in a 28% (w/v) phosphoric acid solution (prepared with DI water) at an impregnation ratio of 3:2 (100% H_3PO_4 to dry wood) for 24 hours in a fume hood.

After the 24-hour soaking time, the impregnated woods were transferred to clean dry beakers and allowed to air dry for 30 minutes to drain excess acid solution from the surface of the wood.

The wood chips were placed into clean, dry crucibles and transferred to the ACAF. The impregnated wood was then carbonized. The carbonization procedure began by purging the ACAF with argon gas (flowrate of 20 L/minute for three minutes) before heating. The argon gas flowrate was then reduced to 7 L per minute and the temperature of the ACAF increased from ambient temperature to 450°C at a rate of 10°C per minute. After reaching 450°C, the temperature was held at 450°C for two hours. The furnace was then allowed to cool to ambient temperature under the same argon gas flowrate. The cooled AC was then removed from the furnace and ground using a mortar and pestle to powder. The PAC was washed copiously with DI water until a supernatant pH of 6.5 was achieved. The clean PAC was then dried in an oven for 24 hours at 103°C ± 2°C and placed into a desiccator and allowed to cool to ambient temperature. The clean, dry PAC was then further ground with a mortar and pestle and sieved to pass a No. 325 sieve. The No. 325 sieved PAC was placed inside an oven and dried for 24 hours at 103°C ± 2°C before being placed directly into a desiccator and cooling to ambient temperature (minimum of four hours drying in desiccator). A clean, dry container and lid were also placed into the desiccator overnight to dry. The cool, dry AC was transferred to the clean, dry container which was sealed (air-tight) before being transferred for characterization as shown in Figure 4-15 below.

Figure 4-15. Clean, dry, powdered, activated carbon in air-tight container.

4.4 Experimental and Analytical Methodology

The overarching objective of the research was to investigate the impact that accessible and simple wood PTs have on the porosity and adsorption capacity of produced AC. The objective was achieved by first preparing ACs from the PT white spruce wood and characterizing the pore size distribution and adsorption capacity. The impregnation and carbonization procedure were identical across all produced ACs, so the differences in the porosity and performance of the ACs was entirely to do with the respective PTs. Thus, the chemical composition, crystallinity, and macroscopic features of the white spruce wood before and after TPT, HPT and APT were analyzed to explain the changes to pore size distribution and aqueous-phase performance of produced ACs. The overall experimental methodology is illustrated in the schematic diagram shown in Figure 4-16.

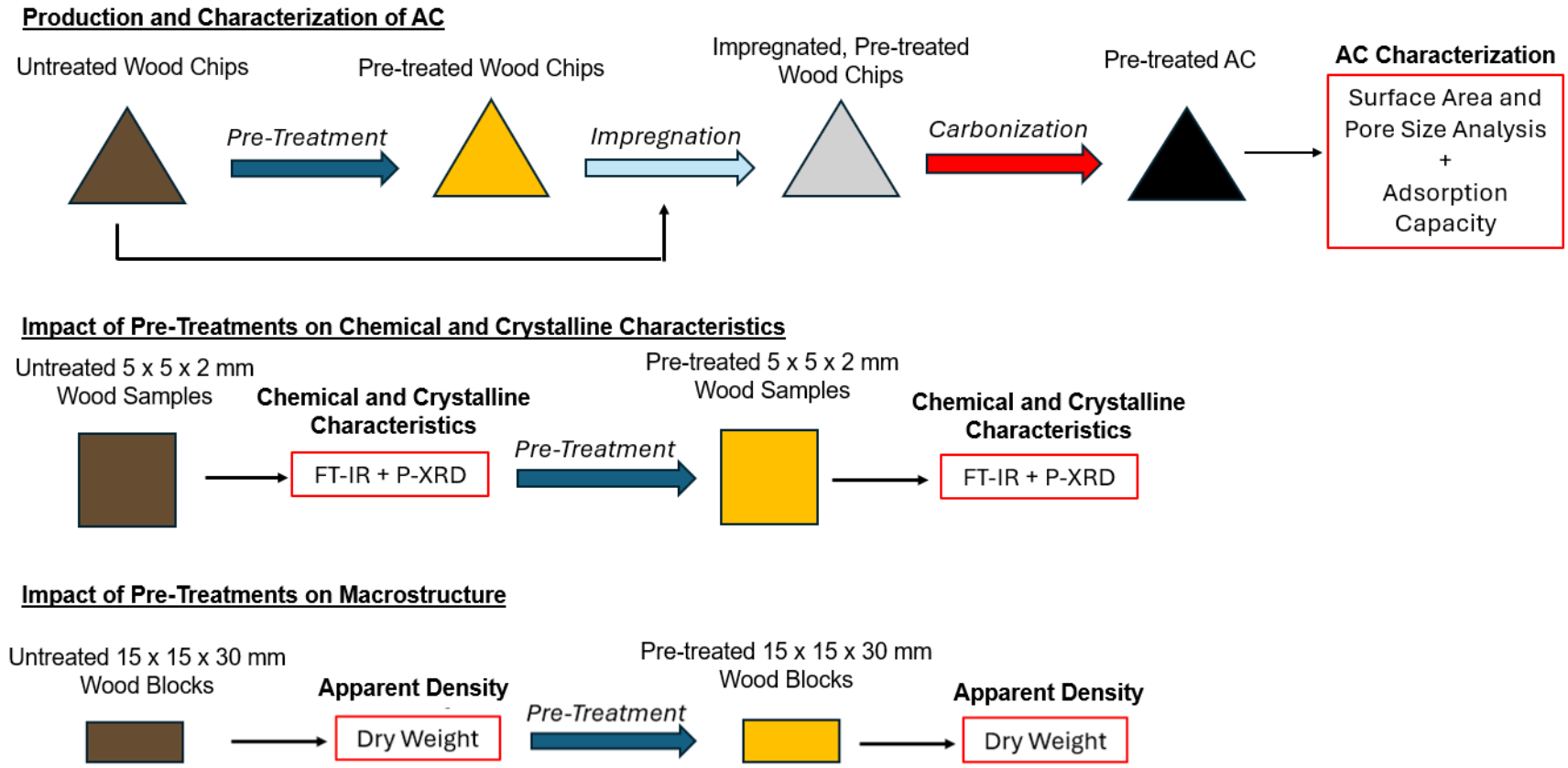

Figure 4-16. Schematic diagram of experimental plan.

The following sections detail the specific experimental and analysis methodologies implemented throughout the study.

4.4.1 Characterization of Activated Carbons

4.4.1.1 Adsorption Capacity Analysis by Iodine Number Test for Activated Carbons

Iodine Numbers (IN) were determined for each activated carbon produced in the study as per ASTM D4607-14 (2021) – *Standard Test Method for Determination of Iodine Number of Activated Carbon* (ASTM, 2021). All reagents were prepared using DI for the IN Test.

The test involves a three-point isotherm where three weights of PACs are divided into three respective narrow-mouthed Erlenmeyer flasks with 0.100 N iodine solution. The IN of an AC is the mass of iodine adsorbed per gram of activated carbon (mg/g) at a residual iodine solution concentration of 0.02 N. The concentration of residual iodine in the isotherm should ideally overlap 0.02 N for the most accurate results. An example of two separate IN Tests carried out on the same AC with two different sets of AC dosages is shown in Figure 4-17.

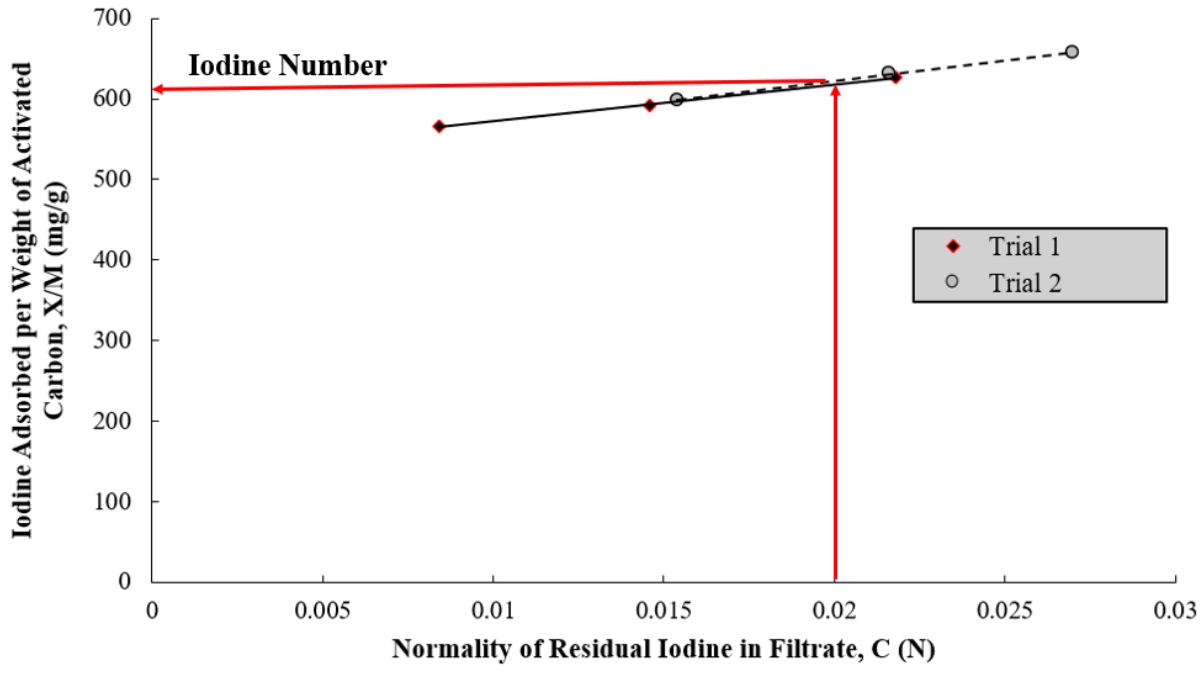

Figure 4-17. IN Isotherm for activated carbon with the Iodine Number highlighted.

Iodine is a small molecule (approximately 0.54 nm diameter) (Zheng et al., 2024) which makes it particularly useful for estimating the BET surface area obtained from nitrogen gas adsorption-desorption isotherms (Sontheimer et al., 1988b). Thus, the IN Test is a logical metric for the aqueous-phase performance evaluation of the produced ACs.

4.4.1.2 Activated Carbon Surface Area and Pore Size Analysis by Nitrogen Adsorption Test

Clean, dry, PAC which passed the No. 325 sieve was also analyzed by nitrogen gas adsorption-desorption isotherms using the Micromeritrics – ASAP 2020 (Norcross, GA, USA). The isotherms were carried out at 77K, and the chamber was equilibrated for ten seconds at each pressure increment. The results accurately indicated the Brunauer-Emmett-Teller (BET) Surface Area, micropore surface area, total pore volume, micropore volume, and average pore diameter of ACs produced from Untreated, TPT, HPT and APT white spruce wood. The tests were carried out at a temperature of 77 K (-196°C) and the pressure was equilibrated for ten seconds at each pressure interval.

The pore measurement range of the analyzer is between 0.35 nm and 500 nm. These bounds mean that the instrument was limited to measuring pore diameters between 0.35 nm to 2 nm within the micropore range and pore diameters between 50 nm and 500 nm within the macropore range.

4.4.2 Characterization of Pre-Treated Woods

4.4.2.1 Powder – X-Ray Diffraction of Wood Samples

The changes to crystalline properties of the white spruce due to each PT was revealed by powder X-Ray Diffraction (P-XRD) using the Bruker D8 Endeavor instrument (Bruker, Karlsruhe, DE), equipped with the LynxEye XE-T detector shown in Figure 4-18 below. Electrons from the K-shell of copper were used, specifically Cu Kα. The wavelength of Cu Kα radiation is 0.154 nm.

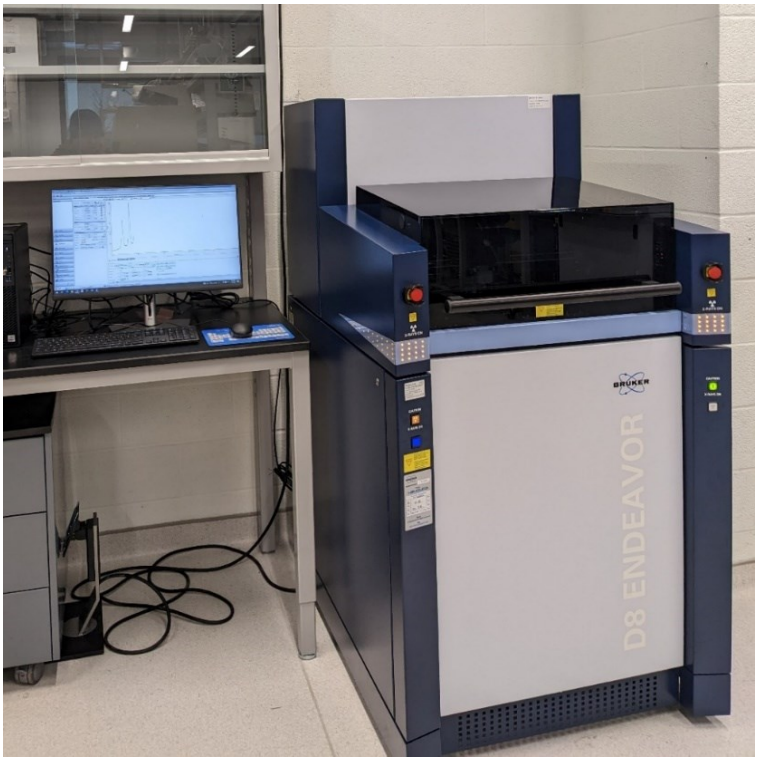

Figure 4-18. Bruker D8 Endeavor instrument.

The P-XRD spectrum spanning from a 2θ (exit angle) of 10° to 60° were obtained for the 5 x 5 x 2 mm white spruce wood samples before and after TPT, HPT and APT. The spectra were used to calculate the changes to the mean size of cellulose crystallites (τ) and the Crystallinity Index (CrI) of 5 x 5 x 2 mm samples by each PT.

4.4.2.1.1 Mean Size of Cellulose Crystallites in Wood Samples

The Mean Size of Cellulose Crystallites (τ) was calculated using the Scherrer Equation. Scherrer (1918) proposed the method to calculate the mean size of crystallites using collected XRD data. The calculation includes the full width at half maximum (FWHM) as a primary component of the calculation as follows:

$$\tau = \frac{k \cdot \lambda}{\beta \cdot \cos\ \theta_B} \qquad 4\text{-}1$$

Where τ is the mean size of cellulose crystallites, k is a shape factor (0.94 for cellulose), λ is the X-ray wavelength (0.1542 nm), β is the FWHM of the crystalline cellulose peak in the 002 plane, and θ_B is the Bragg angle (the angle of peak intensity of the 002 plane of crystalline cellulose) as shown in Figure 4-19.

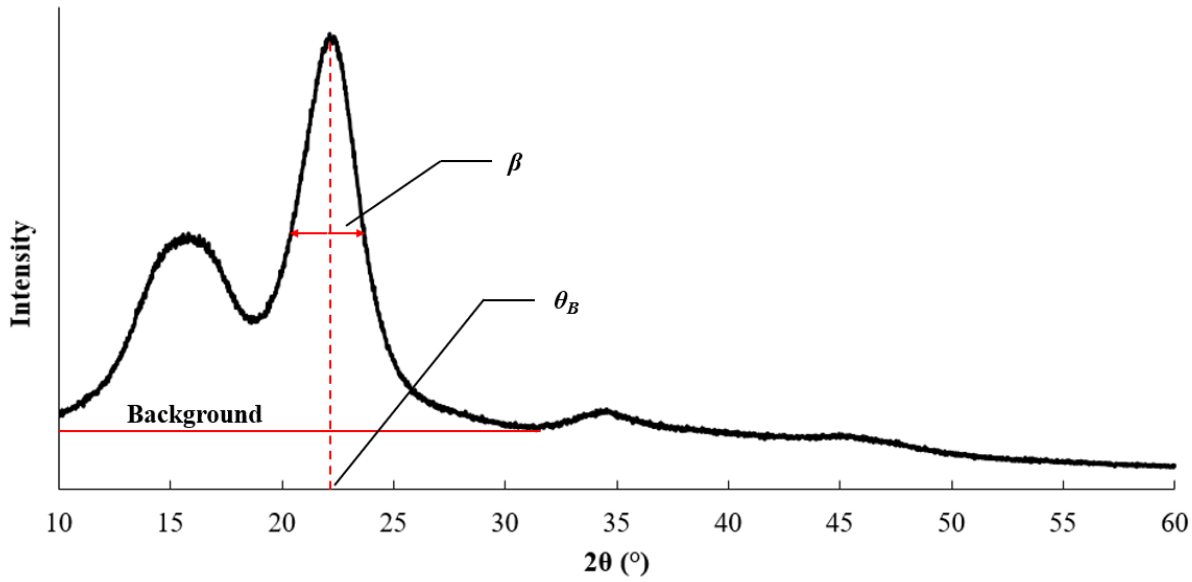

Figure 4-19. Sample X-Ray Diffraction spectrum with Scherrer Equation parameters highlighted.

4.4.2.1.2 Crystallinity Index of Wood Samples

The CrI of a lignocellulosic material is calculated based on a proportionality comparison, or ratio, between the fraction of crystalline and amorphous material within the sample. Leon Segal proposed the following equation to calculate the CrI of a lignocellulosic material using collected XRD data (Segal et al., 1959):

$$CrI = \frac{(I_{002} - I_{am})}{I_{002}} \times 100 \qquad 4\text{-}2$$

Where I_{002} is the intensity at the 002 crystalline cellulose peak and I_{am} is the intensity at approximately 2θ = 18°, representing the intensity of the amorphous components in the wood as shown in Figure 4-20.

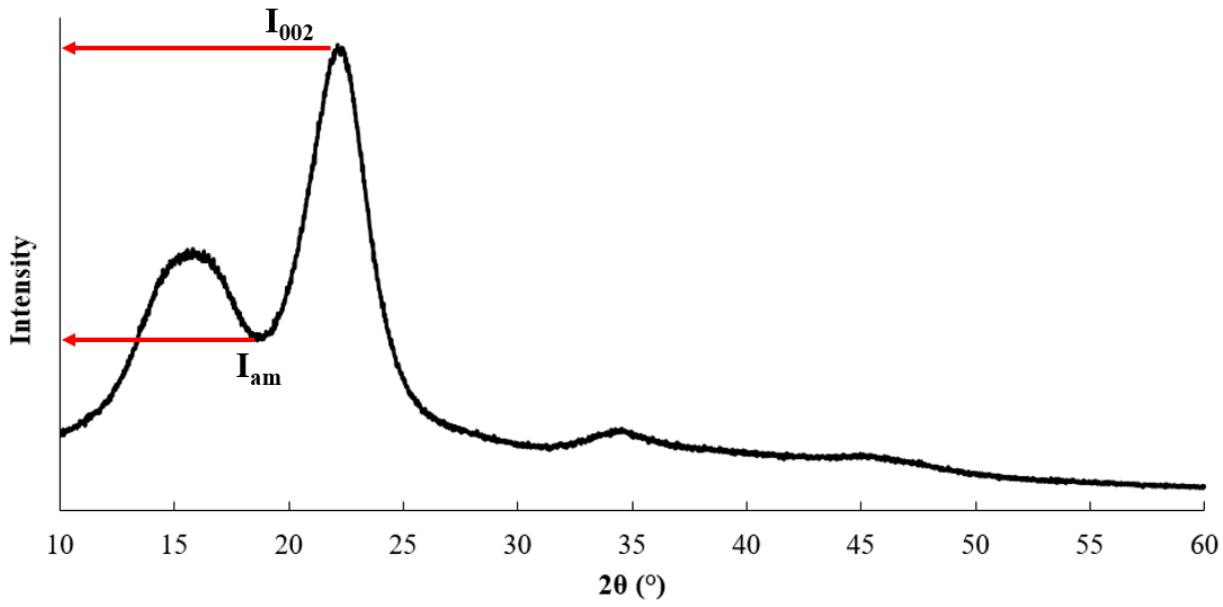

Figure 4-20. Sample X-Ray Diffraction spectrum with Crystallinity Index parameters highlighted.

4.4.2.2 Fourier Transform – Infrared Spectroscopy of Wood Samples

The changes to the chemical composition of white spruce wood were revealed by Fourier Transform – Infrared Spectroscopy (FT-IR) using the Thermo Scientific™ Nicolet™ iS650 FT-IR Spectrometer with the iS650 ATR Module (Thermo-Fisher Scientific, St. Louis, MO, USA) as shown in Figure 4-21.

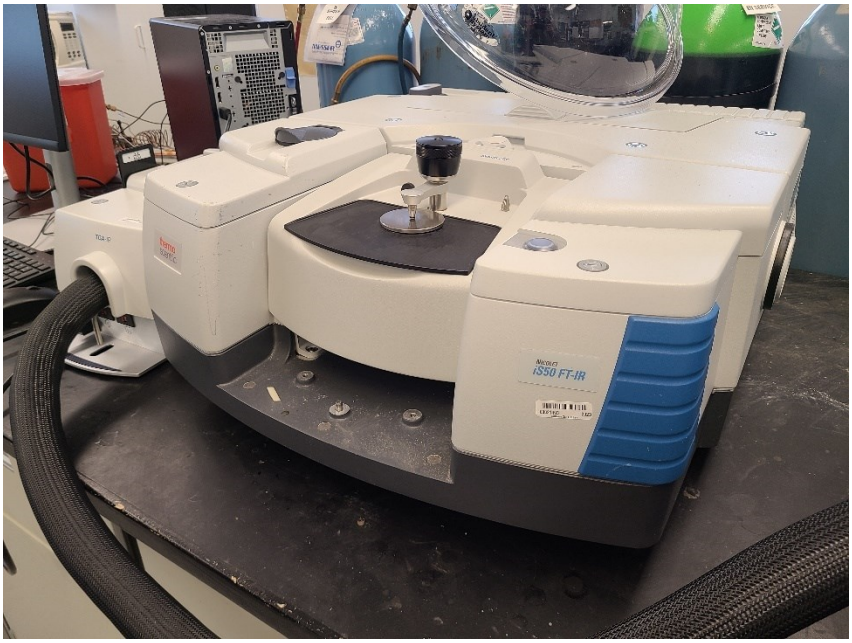

Figure 4-21. Thermo Scientific™ Nicolet™ iS650 FT-IR Spectrometer equipped with the ATR Module.

The FT-IR spectrum of dry 5 x 5 x 2 mm samples was measured before and after TPT, HPT and APT. The average of 64 scans between 4000 cm^{-1} and 400 cm^{-1} at a resolution of 4 cm^{-1} was used to compile the spectra for each sample. The crystal was cleaned with alcohol before each separate measurement as per the methods described in the iS50 ATR Module User Guide (Thermo-Fisher Scientific, 2021).

4.4.2.3 Apparent Density of Wood Blocks

The standard 15 x 15 x 30 mm white spruce wood blocks were prepared to evaluate the change in apparent density due to each PT. The identical volume of the wood blocks (6.75 cm^3) meant that the change in dry weight of the blocks following each PT was an indirect indicator of porosity development in the wood blocks due to PTs. Ten 15 x 15 x 30 mm white spruce wood blocks were prepared for each PT. Each dry sample was massed before and after undergoing TPT, HPT or APT. The apparent density of the dry wood blocks was calculated using the following equation:

$$\rho_{dry} = \frac{m_{dry}}{6.75\ cm^3} \times 100\% \qquad 4\text{-}3$$

The change in apparent density of each individual sample due to each PT was calculated using the following equation:

$$d_i = \frac{\rho_{dry,after\ pre-treatment} - \rho_{dry,before\ pre-treatment}}{\rho_{dry,before\ pre-treatment}} \times 100\% \quad 4\text{-}4$$

where $\rho_{dry,before\ pre-treatment}$ is the apparent density of a dry sample before PT, g; and $\rho_{dry,after\ pre-treatment}$ is the dry mass a sample after PT, g.

The Paired t-Test Analysis (Berthouex and Brown, 2002) was used to statistically verify the significance of the change in apparent density (and thus, porosity development) induced by the PTs. The average of differences (d_{AVE}) was calculated as follows:

$$d_{AVE} = \frac{\sum d_i}{N} \quad 4\text{-}5$$

Where d_i represents the difference between a sample's apparent density before and after PT and N is the number of paired observations (i.e., 10 paired blocks per PT). The sample variance of differences (σ^2) was calculated as:

$$\sigma^2 = \frac{\sum(d_i - d_{AVE})}{N-1} \quad 4\text{-}6$$

The sample standard deviation of the differences (σ) was used to calculate the standard error of the average differences (s_d):

$$s_d = \frac{\sigma}{\sqrt{N}} \quad 4\text{-}7$$

The confidence intervals or limits (CI) were calculated as follows:

$$CI = d_{AVE} \pm s_d \cdot t_{N-1,1-\alpha} \quad 4\text{-}8$$

Where t is the value from the t-distribution that depends on the significance level (α) and the degrees of freedom (N -1). In the case of the present study, ten samples were used, and the 95% confidence interval

was used. Thus, $t_{9,0.025} = 2.262$ was used to calculate the confidence limits for the wood apparent density experiment.

4.4.2.4 Identifying Differences in Activated Carbon Pore Development Mechanisms

The changes to the chemical composition, crystallinity, and macroscopic structure of white spruce wood due to the PTs were analyzed using the methodologies presented in the previous sections. The impact these changes had on the AC properties were revealed by analyzing the gaseous products produced during the carbonization step of phosphoric acid activation.

4.4.2.5 Carbonization of Phosphoric Acid Impregnated Wood and Analysis of Produced Off-Gases

To further analyze the differences in pore development mechanisms during the activation process due to the PTs, the 5 x 5 x 2 mm samples were impregnated with phosphoric acid and carbonized using the same activation procedure used to prepare the ACs (effectively simulating the activation process). The off-gases produced during the carbonization process were accurately analyzed to help explain the differences in mechanisms of porosity development due to the PTs as shown in Figure 4-22.

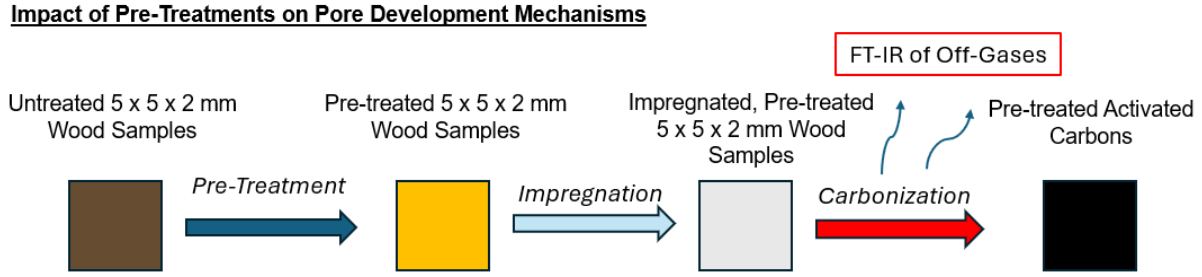

Figure 4-22. Schematic diagram showing the analysis of off-gases produced during the carbonization step of the phosphoric acid activation of pre-treated samples.

The PT 5 x 5 x 2 mm samples were impregnated with phosphoric acid using the same methodology described in Section 4.3 as shown in Figure 4-23.

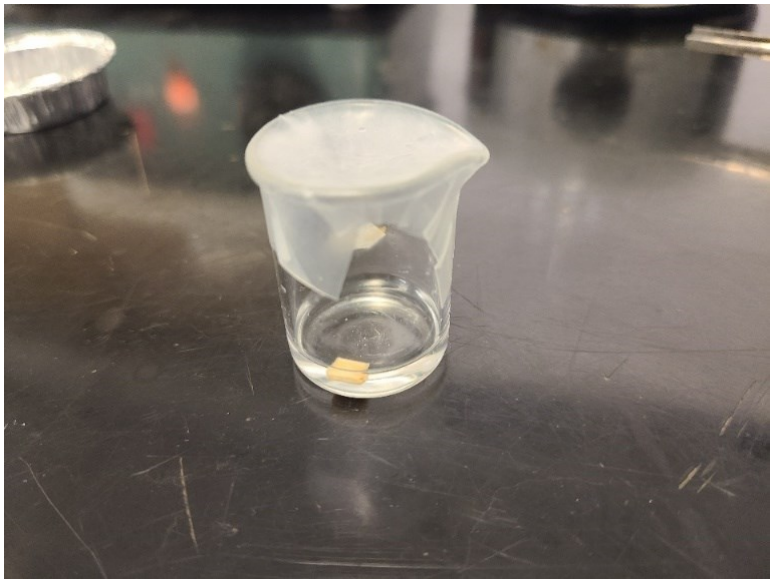

Figure 4-23. Chemical impregnation of 5 x 5 x 2 mm sample.

4.4.2.5.1 Thermogravimetric Analysis

Thermogravimetric analysis (TGA) (i.e., change in sample weight with respect to temperature) was carried out on the phosphoric acid-impregnated Untreated, TPT, HPT and APT 5 x 5 x 2 mm white spruce wood samples using the TA Instruments Discovery SDT650 Simultaneous Thermal Analyzer (TA Instruments, New Castle, DE) shown in Figure 4-24.

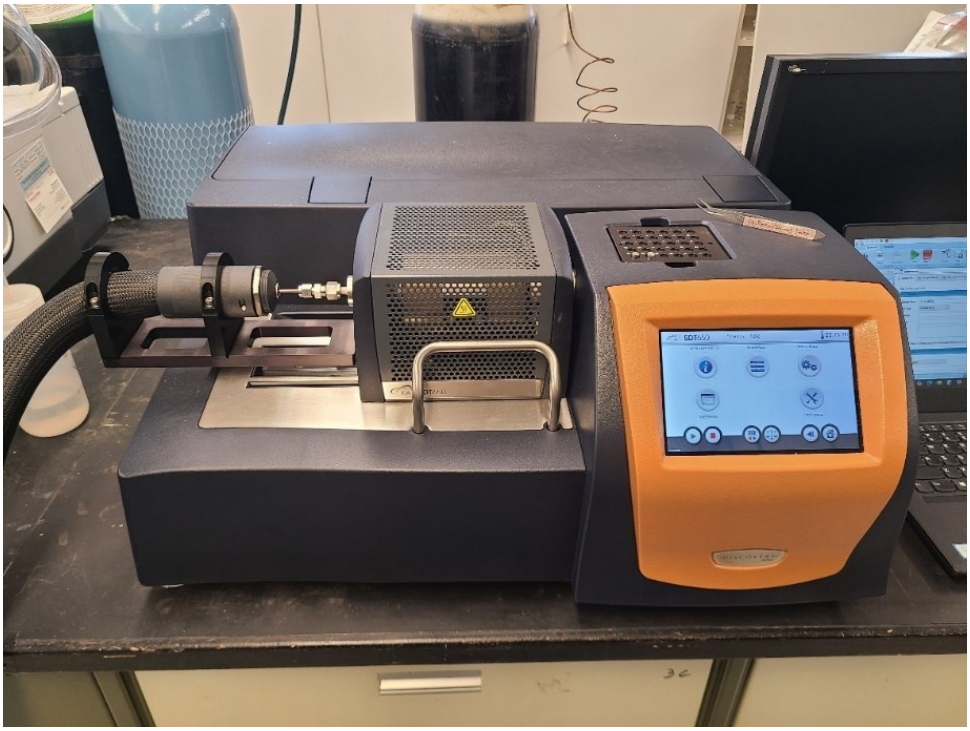

Figure 4-24. TA Instruments Discovery SDT 650.

Individual, clean, dry 5 x 5 x 2 mm Untreated or PT samples were placed into a clean, dry, 90 uL alumina pan which was transferred directly into the instrument chamber as shown in Figure 4-25.

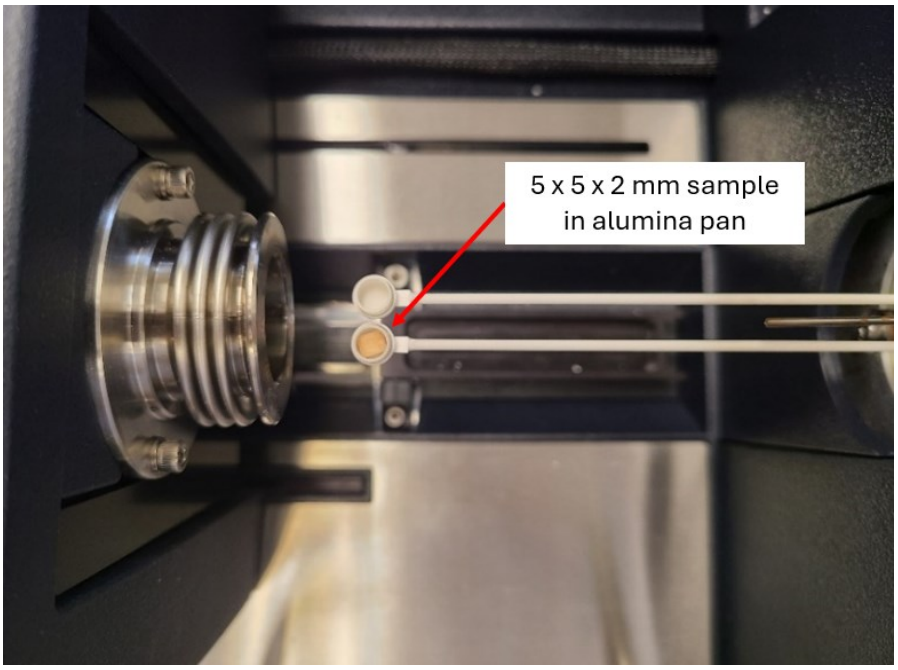

Figure 4-25. 5 x 5 x 2 mm phosphoric acid impregnated sample prepared for thermogravimetric analysis.

After sealing the chamber, nitrogen gas (Research Grade, >99.999%, Messer Canada Inc., Ottawa, ON) was flushed into the chamber at a rate of 50 mL per minute for five minutes at ambient temperature to provide an inert atmosphere. The carbonization protocol was exactly as used to prepare the ACs in Section 4.3 as follows: The temperature was increased from ambient temperature at a rate of 10°C per minute to 450°C where the temperature was held for two hours (under 50 mL per minute nitrogen flow). After the two-hour holding time, the chamber was cooled to ambient temperature under the 50 mL per minute nitrogen flow. An example of a sample post-carbonization via the TGA is shown in Figure 4-26.

Figure 4-26. Activated carbon produced from carbonization in the thermogravimetric analyzer.

4.4.2.5.2 Differential Thermogravimetric Analysis

The derivative of the TGA yielded the Differential Thermogravimetric Analysis (DTG) curve was calculated as the first derivative of the sample weight (%) with respect to the sample temperature (°C).

4.4.2.6 FT-IR of Off-Gases Produced During Carbonization of Dry and Impregnated Wood

Throughout the carbonization process, produced off-gases were fed directly into a Thermo-Fisher™, Nicolet™ iS50 FT-IR Spectrometer (Thermo-Fisher Scientific, St. Louis, MO, USA) shown in

Figure 4-27. The detection vessel was heated to a temperature of 200°C and equilibrated as much as reasonably possible with nitrogen gas prior to the start of the carbonization procedure.

Figure 4-27. Thermo Fisher Scientific Nicolet™ iS50 FT-IR Spectrometer.

Resolution of the FT-IR instrument was set to 4 cm^{-1}, and the breadth of wavelength measurements was 4000 cm^{-1} to 500 cm^{-1}. The integrated OMNIC software developed a 3-D surface describing the off-gassing behaviour during the thermal degradation of phosphoric acid impregnated samples. The FT-IR spectrum at certain instances throughout the carbonization procedure were used to identify degradation mechanisms and ultimately changes to the route of porosity development in AC due to each PT.

Chapter 5 - Sustainable Pre-Treatments for White Spruce Wood-based Activated Carbon: Impact on Porosity and Aqueous-Phase Adsorption

Authors: Kieran Lobo, Mohammad Reza Foruzanmehr, Roberto M. Narbaitz

5.1 Abstract

White spruce wood pallets used for the transportation of goods to remote Northern Canadian communities represent a considerable solid waste management challenge. These communities also experience challenges in producing potable water. A potential solution is to use waste white spruce wood pallets to produce activated carbon (AC) for water treatment. The novelty of this study is that it focused on the impact simple wood pre-treatments (PTs), namely Torrefaction (HPT), Hydrothermal (HPT) and Alkaline (APT), have on the porosity and adsorption capacity of the AC produced by phosphoric acid activation using one single raw material. All three of the PTs significantly increased the surface area and iodine adsorption capacity (Iodine Number, IN) of the resulting ACs. The improved properties of the ACs produced were attributed to the structural modifications that the PT methods applied to the chemical composition, crystallinity and macroscopic characteristics of the wood feedstock. These modifications paved the way for the activation process through increased porosity of white spruce wood, facilitating the diffusion of the phosphoric acid activating agent into the macrostructure of the wood, and altering cellulose crystallite size to govern the pore development mechanisms as supported by the analysis of the gaseous products during the carbonization step of the activation process. The HPT AC showed the greatest increase in specific surface area (increase of 75%) and IN (increase of 80%). The changes introduced by TPT, HPT and APT opened doors for reductions in chemical requirements and shipping frequency to produce high performing AC in remote communities.

5.2 Introduction

Historically, activated carbon (AC) has been widely used in potable water treatment to remove dissolved organic compounds, including taste and odour-causing compounds, harmful pesticides, and

herbicides (Sontheimer et al., 1988a; Crittenden et al., 2012; Chowdhury et al., 2013). Its high specific surface area and vast pore size distribution give AC a high adsorption capacity and affinity for a wide array of contaminants (Sontheimer et al., 1988a). In recent years, AC has emerged as a leading technology for removing per- and poly-fluoroalkyl substances (PFAS) from potable water. The introduction of legislation requiring PFAS removal from potable water is expected to cost the United States approximately $3.8 billion per year in upgrades (Black and Veatch and AWWA, 2023). The high mobility of short-chain PFAS raises concerns for water quality globally (Ateia et al., 2019). Beyond these recent applications, AC has been widely used in municipal-scale potable water treatment, particularly for taste and odour removal. It also plays a role in removing natural organic matter (NOM) to limit the formation of toxic disinfection byproducts (DBPs) in finished water (Crittenden et al., 2012). Northern Canadian waters, particularly those influenced by muskeg and decaying vegetation, exhibit high concentrations of NOM (Decker and Long, 1992). This challenge has become increasingly significant in recent years, as climate change has led to rising NOM levels across Canada's North (Anderson et al., 2023), further highlighting the usefulness of ACs for effective water treatment. Climate change has also led to increased frequency of algal and cyanobacterial blooms, resulting in more taste and odour events and the possible release of cyanobacterial toxins in raw water sources (Gobler, 2020; USEPA, 2025). These issues have plagued communities of Canada's North (Barrera, 2019) and AC has the potential to play a critical role in their management.

While northern and remote communities in Canada face present and emerging water treatment challenges, they also encounter difficulties in constructing and maintaining treatment infrastructure (Flanagan, 2021). The low population of these communities (frequently far fewer than 5,000 people) often means that the economic resources and labour force are insufficient for on-site construction and maintenance of treatment infrastructure (Government of Canada, 2025b). Due to the remoteness and poor land transportation infrastructure, equipment and workers often require to be flown in, significantly increasing project costs and durations (Arctic Council, 2009; Brigham, 2007; Flanagan, 2021). Consequently, there are currently 33 active long-term (over 12 months) drinking water advisories in remote

Canadian First Nations communities (Government of Canada, 2025a). However, First Nations are not the only communities affected. A recent article revealed there are 113 long-term drinking water advisories in Newfoundland alone (The Canadian Press, 2025). A comprehensive study by the David Suzuki Foundation (2017) concluded that funding alone cannot sustainably solve these drinking water issues.

One sustainable long-term solution is to manufacture water treatment materials and/or equipment onsite. This approach eliminates the need for shipping, effectively reducing costs and lead times. Most goods transported into remote northern communities are shipped on white spruce wooden pallets, which often become waste materials in these regions. A 2016 study found that 21% of all solid waste generated in Canadian First Nations communities was wood based (Wang et al., 2023). Manufacturing AC from these pallets is a potentially sustainable solution that can positively impact the environment, health and economy of these communities by 1) eliminating waste material, 2) creating a value-added product that could improve potable water quality in communities, and 3) possibly generating local employment opportunities. AC is an attractive material for these applications because it can be used in either granular (GAC) or powdered (PAC) form. PAC can often be integrated into existing treatment processes, reducing the cost and time needed to improve treatment performance, further emphasizing the potential utility of AC in remote locations (Davoodbeygi et al., 2023; Ruhl et al., 2014). However, economic and technical constraints in these locations necessitate the development of cost-effective and simplified methodologies for producing high-performance AC. Among the two main methods of producing AC (physical and chemical), chemical activation is simpler and is carried out at much lower temperatures, consuming less energy (Jiao et a., 2025), making it more feasible for use in northern and remote communities. Among common chemical activating agents, phosphoric acid is considered the most environmentally sustainable and versatile (El Qada et al., 2008; Kumar and Jena, 2016; Oginni et al., 2019).

The two most desirable properties in an effective AC precursor are consistent quality and low impurities (Sontheimer et al., 1988b). Lignocellulosic Pre-Treatments (PTs) alter the fundamental characteristics of biomass, resulting in more consistent quality and the removal of impurities. These PTs

impact the fundamental crystalline, chemical and macroscopic characteristics of the precursor, all of which can impact activation efficiency, AC porosity and performance. However, the impact of PTs on the porosity and performance of wood-based ACs has yet to be studied. This gap poses a significant barrier to sustainable water treatment solutions in northern and remote communities.

The present work aims to investigate the impact of low-cost, sustainable PTs on the porosity and aqueous-phase performance of white spruce wood-based AC produced via H_3PO_4 activation. To achieve this primary objective, three simple PTs were investigated: torrefaction (TPT), hydrothermal (HPT) and alkaline (APT). These PTs have been studied on numerous raw materials, but their impacts on the same raw material have not been compared directly within a single study, making this study novel. ACs were prepared from the three PT white spruce woods, and their porosity and adsorption capacities were quantified. Subsequently, changes in the chemical structure, macroscopic properties and microstructure of white spruce wood induced by the PTs were analyzed to explain the variations in pore characteristics and performance of the ACs.

5.3 Materials and Methods

This section presents the materials used, the PT methodologies, the AC preparation method and the material characterization approaches utilized. For a more detailed description of the materials and methods refer to the lead author's thesis (Lobo, 2025).

5.3.1 Materials

White spruce (*picea glauca*) wood was obtained from Weyerhaeuser (Drayton Valley, AB). Three sized samples were prepared for different tests.

5.3.2 Sample Resizing

The characterization methods required different sized samples as described below.

For the preparation of ACs, wood chips were prepared by blending. The wood chips were captured between a 9.5 mm sieve and 12.7 mm (i.e., maximum dimension 12.7 x 12.7 mm) and washed in a beaker

by stirring in distilled water for 10 minutes. The clean wood chips were allowed to air-dry before being placed in a convection oven for 24 hours at 103°C ± 2°C. Following oven drying, the samples were placed into a desiccator and cooled to ambient temperature.

For evaluating changes to the apparent density due to the PTs, uniformly sized wood blocks were prepared. White spruce wood was machined to 15 × 15 × 30 mm blocks. All sides of the samples were sanded to minimize surface imperfections. The blocks were then washed copiously with distilled water and air dried before being placed in a convection oven for 24 hours at 103°C ± 2°C. The wood blocks were then placed into a desiccator and cooled to ambient temperature.

For analyzing the changes to chemical and crystalline characteristics of the wood, samples of 5 × 5 × 2 mm size were prepared. All sides of these samples were carefully sanded to remove surface imperfections. The samples were then washed with distilled water and placed in a convection oven to dry at 103°C ± 2°C for 24 hours before being placed in a desiccator to cool to ambient temperature.

5.3.3 Pre-Treatment Processes

5.3.3.1 Torrefaction Pre-Treatment

TPT was carried out by heating the white spruce wood samples in a controlled atmosphere furnace (CAF) (Thermolyne™ 6020C-33-60, Thermo-Fisher Scientific, St. Louis, MO, USA) under an argon gas (>99.99%, Messer Canada Inc., Ottawa, ON) flow rate of 7 L per minute. The temperature increased from ambient temperature to 220°C at a rate of 10°C per minute and held for two hours. After the two-hour holding time, the chamber was allowed to cool to ambient temperature under the same argon gas flow rate before being placed in a desiccator.

5.3.3.2 Hydrothermal Pre-Treatment

HPT consisted of immersing the dry sample in boiling distilled water for two hours. A weight ratio of approximately 10:1 (water to dry wood) was maintained throughout the two-hour treatment period. After two hours, the wood was extracted from the solution and allowed to cool to ambient temperature in an

empty, dry beaker. Once air dry and cool, the sample was placed in a convection oven to dry at 103°C ± 2°C for 24 hours before being placed in a desiccator to cool to ambient temperature.

5.3.3.3 Alkaline Pre-Treatment

APT consisted of immersing the sample in 5% (w/w) NaOH solution prepared from distilled water and NaOH pellets (>97.0%, LabChem, Zelienople, PA, USA). The samples were stirred in the solution for two hours at ambient temperature. A weight ratio of approximately 1:2 (dry wood to 100% NaOH) was used. During the two-hour period, the solution was constantly stirred using a magnetic mixer. Following the two-hour immersion period, the sample was immediately extracted and placed in a distilled water bath and stirred for 30 minutes. The wood was then removed from the bath and allowed to air-dry before being placed in a convection oven to dry at 103°C ± 2°C for 24 hours before being placed in a desiccator to cool to ambient temperature.

5.3.4 Preparation of Activated Carbon

ACs were produced from Untreated, TPT, HPT and APT wood chips via a two-step process. The first step consisted of impregnating the sample with phosphoric acid, and the second step involved the carbonization (pyrolysis) of the impregnated wood.

The impregnation procedure involved soaking the dry wood chips in 28% (w/v) phosphoric acid (85%, Fisher Chemical, Ottawa, ON) solution at an impregnation ratio of 3:2 (100% phosphoric acid to dry wood) for 24 hours in a fume hood. After the 24-hour impregnation period, the wood was extracted from the solution and allowed to air-dry for 30 minutes before the carbonization step.

The surface-dry, impregnated wood chips were carbonized in the CAF under an argon gas (>99.99%, Messer Canada Inc., Ottawa, ON) flow rate of 7 L per minute. The sample temperature increased from ambient to 450°C at a rate of 10°C per minute and was held at 450°C for two hours. After the holding time, the AC was cooled to ambient temperature under the same argon gas flow rate. The cooled AC was then ground to a powder using a mortar and pestle and washed copiously with distilled water until a

supernatant pH of 6.5 was achieved. The clean PAC was then dried in an oven for 24 hours at 103°C before being placed in a desiccator and allowed to cool to ambient temperature. The clean, dry PAC was then further ground with a mortar and pestle to pass through a No. 325 US sieve. The 325-sieved AC was, again, placed in the oven to dry for 24 hours before returning to the desiccator to cool to ambient temperature.

5.3.5 Characterization of Activated Carbons

The characteristics of the produced ACs were determined by two methods. The first method (Iodine Number Test) quantified the iodine adsorption capacity of the produced ACs in an aqueous environment. The second method (Nitrogen Adsorption Test) revealed differences in specific surface areas, pore volumes and pore size distribution of the ACs. The specifics of the two tests are described within this section.

5.3.5.1 Aqueous-Phase Adsorption Capacity by Iodine Number of Activated Carbons

The aqueous-phase performance of the ACs produced in this study was quantified in terms of their adsorption capacity for iodine; otherwise known as the Iodine Number (IN). The IN was determined as per ASTM D4607-14 (2021) – *Standard Test Method for Determination of Iodine Number of Activated Carbon* (ASTM, 2021).

5.3.5.2 Surface Area and Pore Size Analysis by Nitrogen Adsorption Tests

The Brunauer-Emmett-Teller (BET) Surface Area, micropore surface area, total pore volume, micropore volume and average pore diameter of the PACs (No. 325 sieved) produced were determined by nitrogen gas adsorption-desorption isotherm (ASAP 2020, Micrometrics, Norcross, GA, USA).

5.3.6 Methods of Characterizing the Impact of Pre-Treatments on Wood Properties

The impact that PTs had on the crystalline structure and composition, chemical composition, and apparent density of white spruce wood were analyzed using Powder X-Ray Diffraction (P-XRD), Fourier Transform – Infrared Spectroscopy (FT-IR), and apparent density measurements, respectively. A paired approach was employed wherein the analyses were carried out on individual samples before and after each

PT. The specifics of the P-XRD, FT-IR and apparent density analyses are described in the following sections.

5.3.6.1 Powder X-Ray Diffraction

The P-XRD spectrum was measured for each 5 × 5 × 2 mm sample before and after PT using the D8 Endeavour XRD system equipped with a LinxEye XE-T detector (Bruker, Karlsruhe, DE). A Cu K-α beam was used for all measurements. The span of the spectra was between exit angles (2θ) of 10° and 60°. The spectra were used to calculate two parameters used to characterize the crystallites in the samples, described next.

5.3.6.1.1 Calculation of Mean Size of Cellulose Crystallites in Wood Samples

The Scherrer Equation (Scherrer, 1918) was used to calculate the mean size of cellulose crystallites in 5 × 5 × 2 mm white spruce wood samples before and after each PT. The calculation includes the full width at half maximum (FWHM) as a primary component of the calculation as follows:

$$\tau = \frac{k \cdot \lambda}{\beta \cdot \cos\ \theta_B} \qquad 5\text{-}1$$

where τ is the mean size of cellulose crystallites, nm; k is a shape factor (0.94 for cellulose); λ is the X-ray wavelength (0.1542 nm); β is the FWHM of the crystalline cellulose peak in the 002 plane; and θ_B is the Bragg angle (the angle of peak intensity of the 002 plane of crystalline cellulose). β was taken as the width of the peak at half the intensity of the 002 plane θ_β peak subtracting the intensity of the background.

5.3.6.1.2 Calculation of Crystallinity Index of Wood Samples

The Segal Crystallinity Index, CrI, was used to calculate the proportion of crystalline cellulose in the 5 × 5 × 2 mm white spruce wood samples before and after each PT (Segal et al., 1959). The calculation was made using the following equation:

$$CrI = \frac{(I_{002} - I_{am})}{I_{002}} \times 100 \qquad 5\text{-}2$$

where I_{002} is the intensity at the 002 crystalline cellulose peak; and I_{am} is the intensity at approximately 2θ = 18°, representing the intensity of the amorphous components in the wood.

5.3.6.2 Fourier Transform – Infrared Spectroscopy

The FT-IR spectra of the 5 × 5 × 2 mm samples were collected before and after each PT using the Nicolet™ iS650 FT-IR Spectrometer (Thermo Fisher Scientific, St. Louis, MO, USA). The spectra were measured between 4000 cm^{-1} and 400 cm^{-1} (average of 64 scans) at a resolution of 4 cm^{-1}. The spectrophotometer's attenuated total reflectance (ATR) crystal was cleaned with alcohol before each sample measurement as per the methods described in the iS50 ATR Module User Guide (Thermo Scientific, 2021).

5.3.6.3 Change in Apparent Density of Wood Blocks as an Indirect Indicator of Porosity Development in Wood

The percentage change in the apparent density wooden samples was used as an indirect indicator of porosity development in the wood. Ten 15 × 15 × 30 mm white spruce wood blocks were prepared for each of TPT, HPT and APT (i.e., 30 blocks total). The apparent volume of the blocks was 6.75 cm^3 so, the apparent density of the dry wood blocks was calculated as:

$$\rho_{dry} = \frac{m_{dry}}{6.75\ cm^3} \times 100\% \qquad 5\text{-}3$$

Where ρ_{dry} (g/cm^3) is the apparent density of the wood block and m_{dry} (g) is the measured dry mass of the wood block.

Each dry block was massed before and after PT. The difference in apparent density of the wood blocks (d_i) was thus:

$$d_i = \frac{\rho_{dry,after\ pre-treatment} - \rho_{dry,before\ pre-treatment}}{\rho_{dry,before\ pre-treatment}} \times 100\% \quad 5\text{-}4$$

where $\rho_{dry,before\ pre-treatment}$ is the apparent density of a dry sample before PT, g; and $\rho_{dry,after\ pre-treatment}$ is the dry mass a sample after PT, g.

5.3.6.3.1 Statistical Analysis for Change in Apparent Density of Wood Blocks

The Paired t-Test Analysis was used to statistically verify that the change in apparent density induced by the PTs was significant (Berthouex and Brown, 2002). The average of differences (d_{AVE}) was calculated as follows:

$$d_{AVE} = \frac{\sum d_i}{N} \quad 5\text{-}5$$

where N is the number of paired observations (i.e., 10 paired samples). The sample variance of differences (σ^2) was calculated as:

$$\sigma^2 = \frac{\sum(d_i - d_{AVE})}{N-1} \quad 5\text{-}6$$

The sample standard deviation of the differences (σ) was used to calculate the standard error of the average differences (S_d):

$$S_d = \frac{\sigma}{\sqrt{N}} \quad 5\text{-}7$$

The confidence intervals or limits (CI) were calculated as follows:

$$CI = d_{AVE} \pm s_d \cdot t_{N-1,1-\alpha} \quad 5\text{-}8$$

where t is the value from the t-distribution that depends on the significance level (α) and the degrees of freedom (N -1). In the case of the present study, ten samples were used, and the 95% confidence interval was used. Thus, $t_{9,0.025} = 2.262$ was used to calculate the confidence limits for the change in apparent density experiment.

5.3.7 Gaseous Carbonization Products from Phosphoric Acid Impregnated Wood

The thermal degradation behaviour and off-gases produced during the carbonization step of activation were investigated by thermogravimetric analysis (TGA) paired with FT-IR (herein referred to as TGA-FTIR). The methods used for this experiment are described in the following subsection.

5.3.7.1 Thermogravimetric Analysis Paired with Fourier Transform – Infrared Spectroscopy

Untreated and PT 5 x 5 x 2 mm white spruce wood samples were impregnated with phosphoric acid under identical conditions used for preparing the ACs (described in Section 5.3.4). Following impregnation, the samples were allowed to dry for 30 minutes before being placed in a TGA analyzer (TA Instruments SDT650, New Castle, DE). This carbonization protocol was also identical to that described in Section 5.3.4 used for producing the ACs and consisted of heating the samples from ambient temperature to 450°C at a rate of 10°C per minute under a nitrogen gas (>99.999%, Messer Canada Inc., Ottawa, ON) flow rate of 50 mL per minute. Once the sample temperature reached 450°C, the temperature was held constant for two hours. Differential Thermogravimetric Analysis (DTG) was calculated by the analyzer as the first derivative of the sample weight (%) with respect to the sample temperature (°C).

The off-gases generated throughout the carbonization process were analyzed in-line using the Nicolet™ iS650 FT-IR Spectrometer (Thermo Fisher Scientific, St. Louis, MO, USA). The FT-IR resolution of the instrument was set to 4 cm^{-1}, and the breadth of wavelength measurements was 4000 cm^{-1} to 500 cm^{-1}.

5.4 Results and Discussion

This section presents and discusses the results of the experiments in two parts. The first part characterizes the aqueous-phase adsorption performance and pore size distribution of the produced ACs. The second part compares the crystalline, chemical and macroscopic characteristics of Untreated and PT wood samples.

5.4.1 Characterization of Produced Activated Carbons

This section presents and discusses the adsorption capacity of iodine, as determined by the IN Test, and the pore size distribution of the produced ACs.

5.4.1.1 Aqueous Phase Adsorption Capacity of Activated Carbons

The IN is frequently used in the field of water treatment as an indicator of the activity of ACs (Ganjoo et al., 2023). Thus, the IN was used to compare the aqueous phase performance potential of the white spruce wood-based ACs. Table 5-1 shows that TPT, HPT and APT resulted in 54%, 80% and 42% increases in the IN of produced ACs, respectively.

Table 5-1: Iodine Number of activated carbons prepared from Untreated and Pre-Treated white spruce wood.

Pre-Treatment	Iodine Number (mg/g)	Percent Increase in Iodine Number (%)
Untreated	620	-
TPT	957	54
HPT	1113	80
APT	880	42

The IN number of Filtrasorb® 400 (F-400), one of the most-popular commercially produced water treatment ACs, is 1000 mg/g at a minimum (Calgon Carbon Corporation, 2024). Thus, the PTs increased the IN to competitive levels with even the most common and frequently used AC on the market. When compared to a popular commercially produced softwood, phosphoric acid-prepared AC (Acticarbone® by Chemviron) which has a minimum IN of 1150 mg/g, HPT AC remains competitive (Calgon Carbon Corporation, 2017). Overall, TPT, HPT and APT ACs show promise in their ability to compete or exceed adsorption capacities of some of the most popular commercially produced ACs on the market.

The adsorption capacity of AC for different adsorbate molecules in a water treatment setting highly depends on the pore size distribution (i.e., the proportions of differently sized pores) of the AC. These results are presented and discussed in the following section.

5.4.1.2 Pore Size Distribution and Surface Area of Activated Carbons

The PTs had varying effects on the pore development and pore size distribution of produced ACs. Table 5-2 presents the key pore properties of ACs produced from Untreated, TPT, HPT and APT white spruce wood as determined by the Nitrogen Gas Adsorption Test.

Table 5-2. Porosity characterization by nitrogen gas adsorption-desorption isotherm of activated carbons produced from Untreated and Pre-Treated white spruce wood.

Sample	**Specific Surface Area (BET)**	**Increase in Specific Surface Area (BET)**	**Surface Area (meso- and macropores, > 2 nm dia.)**	**Percent Meso- and Macropore Area**	**Surface Area (micropores, < 2nm dia.)**	**Percent Micropore Area**	**Pore Diameter (average[1])**	**Pore Volume (total)**
	(m^2/g)	***(%)***	***(m^2/g)***	***(%)***	***(m^2/g)***	***(%)***	***(nm)***	***(cm^3/g)***
Untreated	679	-	333	49	346	51	4.80	0.39
TPT	1002	47.6	698	70	304	30	4.33	0.51
HPT	1189	75.1	1052	88	137	12	5.10	0.80
APT	1029	51.5	789	77	240	23	4.51	0.57

[1] Barret-Joyner-Halenda pore diameter (4V/A).

The BET surface areas of the ACs increased by 75.1%, 51.5% and 47.6% due to HPT, APT and TPT, respectively, when compared to the Untreated sample. The increase in surface area of the ACs due to PTs presumably contributed to their increased INs. The relatively small molecular size of iodine (~0.54 nm diameter) (Zheng et al., 2024) allows it to adsorb onto a broad range of pore sizes, including micropores. Thus, the IN of an AC is often highly correlated with its BET surface area (Sontheimer et al., 1988b). The correlation between the INs and BET surface areas of the ACs produced in the present study is relatively strong ($R^2 = 0.9533$) as shown in Figure 5-1. The strong correlation indicates that the PTs woods not only produced AC with increased specific surface areas, but also that the surface area is largely accessible to aqueous adsorbates.

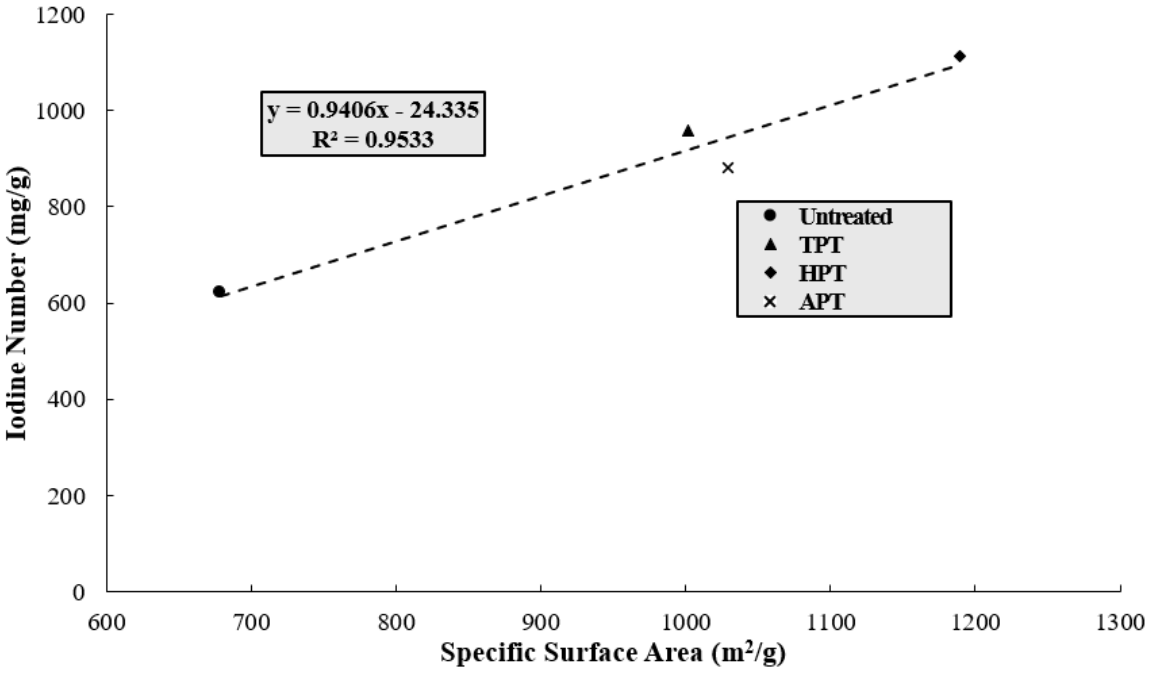

Figure 5-1. Correlation between specific surface areas and Iodine Numbers of produced activated carbons.

Overall, the PTs resulted in a decrease in the micropore surface area and increase in the total surface area. Thus, the increase in total surface area was due to meso- and macropore development (i.e., pores greater than 2 nm diameter), which was enhanced by the three PTs. The average pore size was approximately 5 nm for all the ACs, suggesting that characteristics of the raw material (whether Untreated

or PT) had a significant impact on the size of pores developed. Given the average pore diameters were on the lower end of the mesopore range (i.e., diameter between 2 nm and 50 nm), the increase in proportion of mesoporosity was presumably due to the three PTs facilitating the enlargement of micropores or the creation of new pores in the lower diameter mesopore range. The enhanced mesopore development by phosphoric acid activation is typically attributed to micropore widening (Jiao et al., 2025). This pore development mechanism was most pronounced for the HPT sample, which exhibited an increased average pore diameter (from 4.80 nm for Untreated AC to 5.10 nm for HPT AC) as well as the greatest increase in pore volume (105% increase compared to Untreated AC). TPT and APT ACs had lower average pore diameters (4.33 nm and 4.51 nm, respectively) than the Untreated AC (4.80 nm). Accordingly, these PTs presumably facilitated the enlargement of micropores differently.

Mesoporous ACs have increased adsorption capacity of relatively large sized contaminants such as colour-causing compounds (Ganjoo et al., 2023), cyanotoxins (Pivokonsky et al., 2021) and NOM (Gong et al., 2020). Wood-based ACs are commonly used for such applications due to their innate macro- and mesoporous structure of wood (Sontheimer et al., 1988b) and it is evident that this favourable feature of wood was emphasized by the PTs.

The only difference in the preparation of all the ACs produced was the PT of the white spruce wood feedstock. Thus, the differences in the resultant properties and performance of the ACs were entirely related to the impact of the PTs on the properties of the white spruce wood. Section 5.4.2 details the changes to the crystalline properties, chemical composition, and macroscopic properties of white spruce wood resulting from each PT. Ultimately, the changes to the feedstock properties are used to explain how these alterations influence pore development in the ACs leading to higher adsorption capacities.

5.4.2 Characterization of Pre-Treated White Spruce Wood

The PTs had clear impacts on the crystalline, chemical and macroscopic structures of the white spruce wood precursor. These changes are analyzed and discussed sequentially within this section.

5.4.2.1 Impact of Pre-Treatments on the Crystalline Structure of Wood

Changes to the crystalline structure of the white spruce wood due to each PT were identified and compared using P-XRD spectra of samples before and after PT. The changes to the mean size of cellulose crystallites and the crystalline composition of wood samples, and how these characteristics presumably contribute to pore development in the produced ACs are discussed within this section.

5.4.2.1.1 Change to Mean Size of Cellulose Crystallites in Wood

The change of Scherrer's mean size of cellulose crystallites, calculated using P-XRD spectra for white spruce wood before and after each PT, was used to assess the impact of PTs on the wood's cellulosic microstructure (Table 5-3).

Table 5-3. Change in mean cellulose crystallite size of white spruce wood due to Pre-Treatments.

Pre-Treatment	**Change in Mean Cellulose Crystallite Size, τ (%)**
TPT	-2.07
HPT	+1.58
APT	+10.07

The growth of mean cellulose crystallite size following APT was the most pronounced when compared to the other PTs. This finding is consistent with other works where an increase in cellulose crystallite size is generally more pronounced in biomass subject to APT (Wan et al., 2010; Sarko and Muggli, 1974) than HPT (Parades et al., 2008; Li et al., 2017). In the case of APT and HPT, the increase in cellulose crystallite size occurs due to the removal of amorphous material, which allows chain folding to occur in amorphous and/or quasi-crystalline cellulose regions, resulting in the growth of the cellulose crystallites (Wan et al., 2010; Sarko and Muggli, 1974; Paredes et al., 2008; Li et al., 2017). Comparatively, TPT reduced the mean cellulose crystallite size (-2.07%), presumably by degrading cellulose during the thermal process (Ni et al., 2025). The depolymerization of crystalline cellulose at pyrolysis temperatures below 300°C is associated with the decomposition of O-acetyl groups in hemicellulose resulting in the

formation of acetic acid, which attacks crystalline cellulose, making it susceptible to thermolysis at reduced temperatures (Fengel and Wegener, 1984c; Lourenço et al., 2020).

The impact of these changes in the mean size of cellulose crystallites on the resultant pore properties of the AC may be explained by two mechanisms. The first involves the widening of existing pores or creation of new pores during the activation process and may be explained by the grain boundary diffusion theory. The theory states that the diffusion coefficient at a grain boundary (i.e., at the surface of the cellulose crystallite) is high, and in contrast, is exceedingly low inside the crystal (Young and Funderlic, 1973). Using the framework of the grain boundary diffusion theory, it is hypothesized that phosphoric acid reactions with wood biopolymers were magnified at the surface of crystallites where amorphous regions exist. These amorphous chains at the surface of cellulose crystallites are susceptible to acid-catalyzed hydrolysis into low molecular weight sugars which tend to volatilize leaving pores in their place during carbonization (Morales-delaRosa et al., 2014). The second mechanism involves the shifting of cellulose crystallites during the carbonization process where they eventually stabilize by way of inter-crystallite phosphate ester (cross-link) formation. The cross-linked crystallites are thermally stable and become turbostratic crystallites during carbonization, representing the walls of pores (Jagtoyen and Derbyshire, 1993; Chen et al., 2012; Kim et al., 2022). These two pore development mechanisms occur simultaneously but it is hypothesized that the changes to the mean crystallite size causes shifts in the dominant activating reaction mechanisms.

The smaller crystallites of the TPT sample facilitated the formation of the smallest pores when compared to the other PTs (as evidenced by the highest proportion of micropore surface area and lowest average pore diameter of the PT ACs). The increased surface area at the grain boundary (due to the smaller crystallites) presumably facilitated the acid catalyzed-hydrolysis of biopolymers leading to an increased AC pore volume and surface area (Chen et al., 2015). Meanwhile, the tendency of the TPT sample to form smaller pores is proposed to be caused by the smaller crystallites forming stable inter-crystalline cross-links during the carbonization process (as illustrated by the leftmost diagram in Figure **5-2**). These cross-links stabilize and inhibit cellulose volatilization and the stabilization of a much more microporous AC structure

in TPT AC when compared to HPT and APT ACs (Jagtoyen and Derbyshire, 1993). On the other hand, APT presumably had the opposite effect. The larger crystallites of APT and HPT exhibit less uniform reaction and decomposition behaviour which tend to result in the formation of non-uniform pore sizes in the meso- and even macroporous range (Prieto et al., 2024). The increased crystallite size of the APT sample is proposed to have led to slightly larger pores when cross-links were formed during the carbonization process (as illustrated by the rightmost diagram in Figure **5-2**).

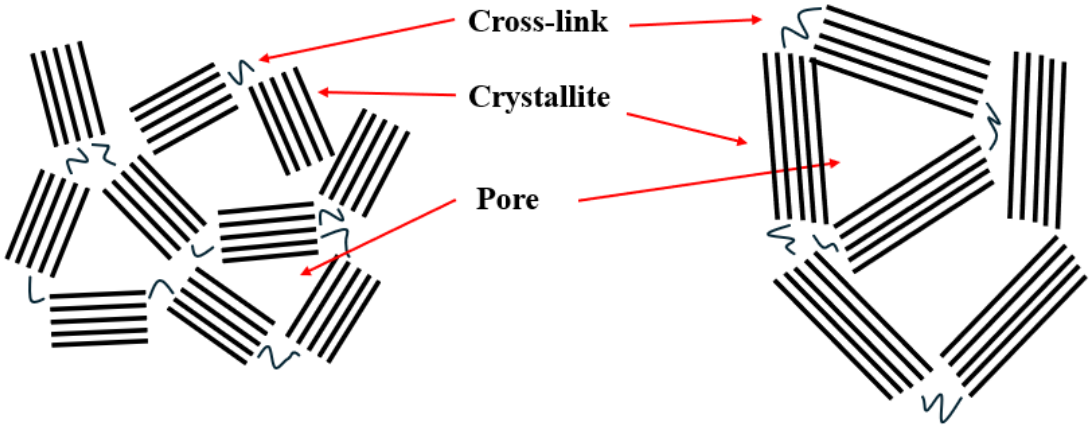

Figure 5-2. Hypothesized impact of smaller crystallites (left) versus larger crystallites (right) on pore development in wood-based activated carbon.

HPT presumably provided the most favourable conditions for the formation of larger pores when compared to TPT and APT ACs. It is proposed that the larger pores of HPT AC were caused by a slight shift of reaction preference to acid-catalyzed hydrolysis and volatilization leading to a higher degree of pore widening instead of cross-link formation. Compared to APT, HPT caused a smaller increase in crystallite size, which presumably enhanced acid-catalyzed hydrolysis of the reactive amorphous regions, leading to the formation of larger pores. When compared to the TPT sample, HPT had larger crystallites, and these larger crystallites presumably tended to form slightly larger pores during carbonization (as illustrated by the rightmost diagram in Figure **5-2**). The combination of these two factors lead to HPT AC exhibiting the

highest adsorption capacity, specific surface area, average pore diameter and pore volume; notably, HPT AC also exhibited the lowest microporosity of the ACs.

The aforementioned ideas are supported by the FT-IR spectra of the off-gases produced (at the temperature of peak thermal degradation) during the TGA test of the phosphoric acid impregnated samples (Figure 5-3). Both TPT and APT, released less methane and methanol (products of cellulose thermal degradation) (Yang et al., 2007; Lv et al., 2015), suggesting that thermally stable cross-links were formed between cellulose crystallites (Marsh and Rodriguez-Reinoso, 2006; Jagtoyen and Derbyshire, 1993). On the other hand, the greater release of methane and methanol during the carbonization step of HPT activation suggests that a greater degree of cellulose volatilization occurred, leading to more mesopore formation.

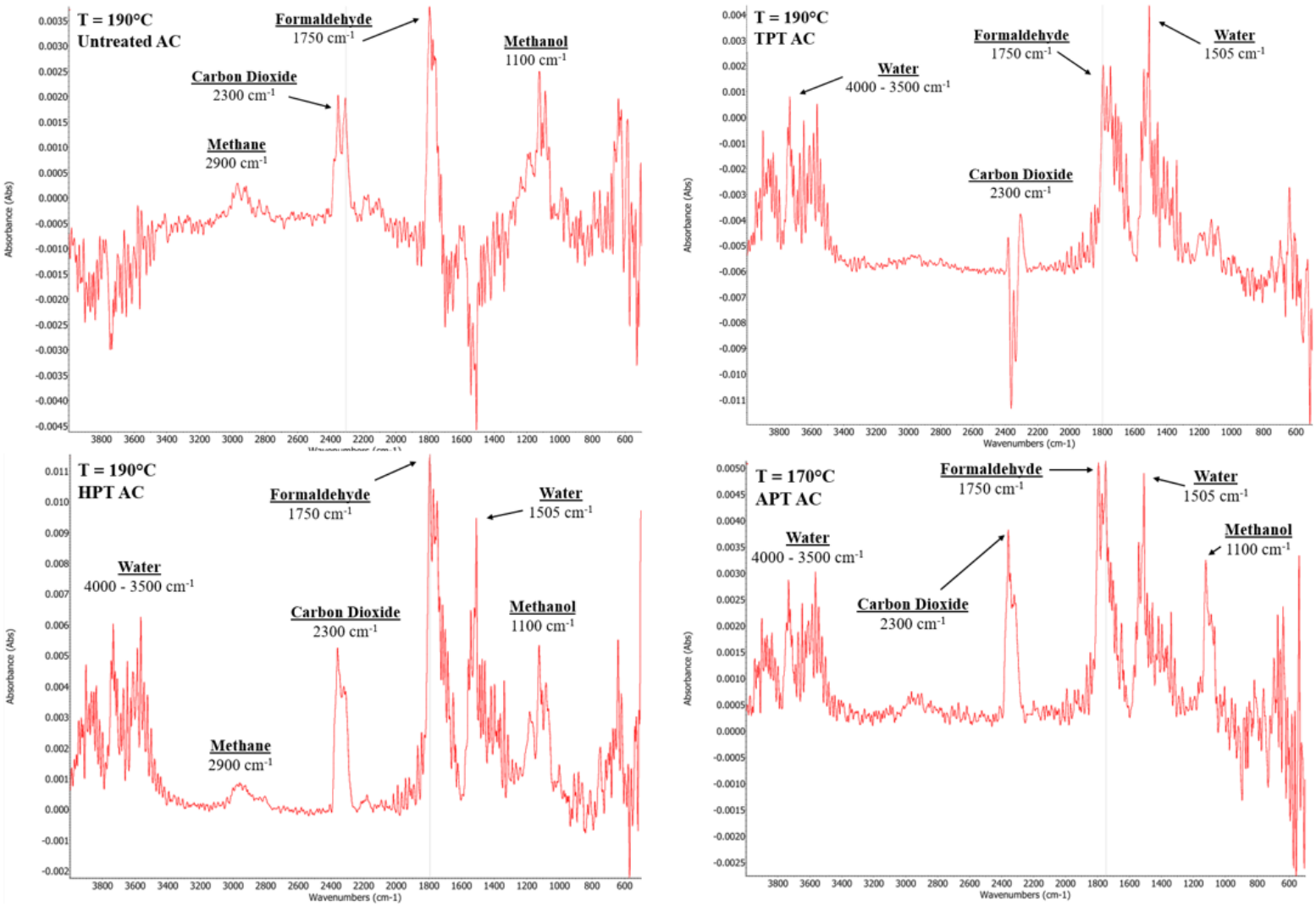

Figure 5-3. Fourier Transform – Infrared Spectroscopy of off-gases produced during the thermogravimetric analysis of the H_3PO_4 impregnated samples.

5.4.2.1.2 Impact of Pre-Treatments on Crystallinity Index

The Segal CrI indicates the proportion of crystalline cellulose to amorphous content in wood. Thus, a sample with a high CrI has a greater proportion of crystalline cellulose relative to amorphous material than a sample with a lower CrI. The changes to the CrI white spruce wood due to the PTs are presented in Table 5-4.

Table 5-4. Change in CrI of white spruce wood due to Pre-Treatments.

Pre-Treatment	**Change in CrI (%)**
TPT	+3.67
HPT	+5.45
APT	+5.32

The PTs all caused an increase in the CrI of the white spruce wood samples. This increase is commonly observed for lignocellulosic materials subject to TPT (Chang et al., 2012; Lu and Gu, 2022), HPT (Peleaz-Samaniego et al., 2013), and APT (Qi et al., 2023; Jeoh et al., 2007).

Higher CrI have been attributed to an increased preference for acid-catalyzed hydrolysis of amorphous fractions (Chen et al., 2015) which would presumably lead to formation of widening of pores (Jagtoyen and Derbyshire, 1993). The comparatively low increase in CrI due to TPT suggests that reactions between crystalline cellulose in TPT wood were preferred more than in HPT and APT (Chen et al., 2015). This idea, in combination with the fact that TPT had the smallest crystallites presumably indicates that cross-link formation was preferred in the TPT sample and the smaller crystallites are proposed to form smaller pores when compared to HPT and APT (which had larger crystallites). On the other hand, HPT and APT samples exhibited a similar impact on the CrI of the samples (+5.45% and +5.32%, respectively). The magnified increase in proportion of crystalline cellulose in these samples presumably shifted the preference of phosphoric acid to react with amorphous biopolymers in the wood (Chen et al., 2015) which consistently contribute to meso- and macropore formation in phosphoric acid activated ACs (Boundzanga et al., 2022; Suo et al., 2009). However, the reaction sites at the surface of crystalline cellulose were more limited for

the APT sample than HPT sample due to the greater impact on crystallite growth (+10.01% versus +1.58%, respectively). Thus, HPT likely experienced more acid-catalyzed hydrolysis of amorphous cellulose than the APT sample, interrupting crystalline regions, resulting in the formation of larger pores. Ultimately, this difference explains why HPT AC had the largest average pore size and more mesoporosity when compared to the APT AC. This conclusion is supported by the off-gases produced during the carbonization step (i.e. TGA-FTIR of the phosphoric acid impregnated samples) which shows that HPT released the highest proportion of gases (Figure 5-3) demonstrating the elevated impact of acid-catalyzed hydrolysis on the sample's biopolymers.

While it is apparent that the removal of amorphous material from the samples caused an increase in the CrI of the white spruce wood, the nature of the removed amorphous material has not been analyzed. These details are discussed in the following section to further explain differences in pore development mechanisms in the produced ACs.

5.4.2.2 Impact of Pre-Treatments on the Chemical Composition of Wood

Characteristic FT-IR spectra peaks for cellulose, hemicellulose and lignin were identified for Untreated white spruce wood. Qualitative changes to the FT-IR spectra of PT woods spectra revealed alterations in their chemical compositions, as shown in Figure 5-4.

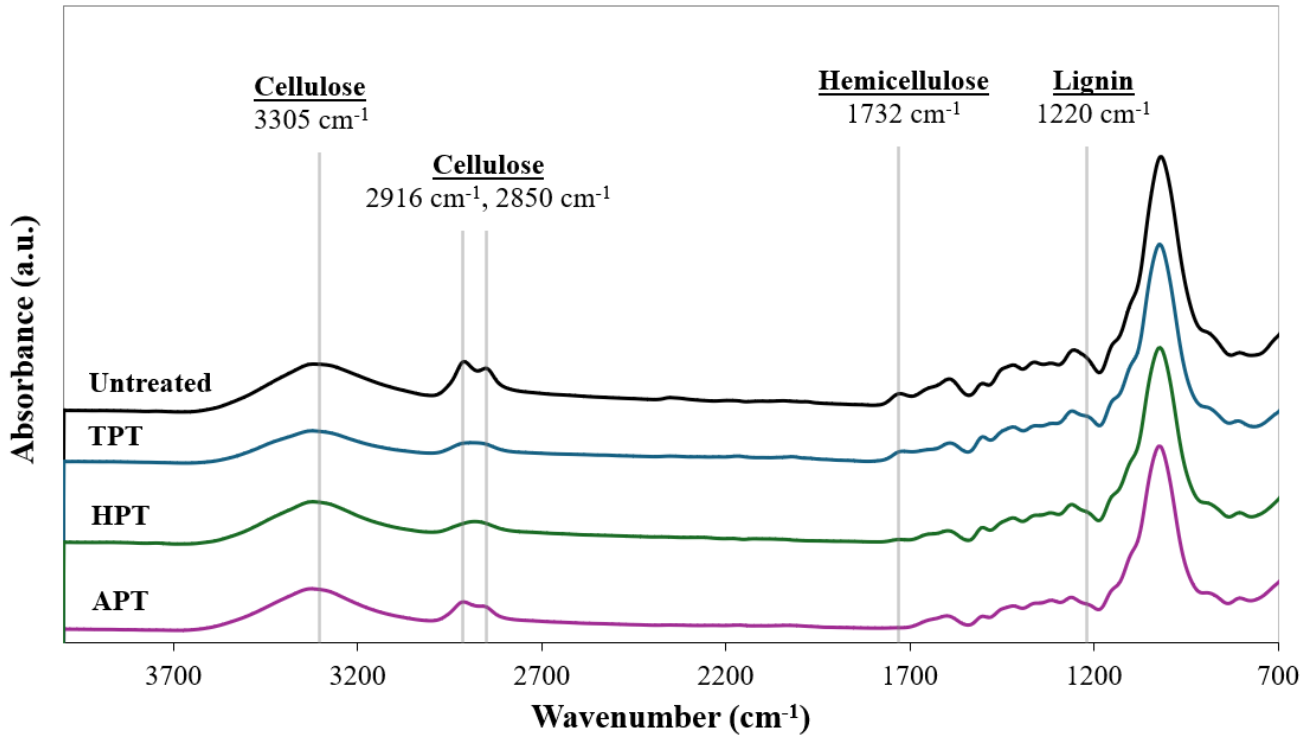

Figure 5-4. FT-IR spectra of Untreated and Pre-Treated white spruce wood.

As the individual spectra are normalized relative to the height of the largest peak, which differ from sample to sample, the comparison of peak heights among the samples is rather qualitative in nature. The FT-IR spectrum for TPT wood showed that hemicellulose and cellulose were impacted to varying degrees. Hemicellulose is the least thermally stable biopolymer in wood (Fengel and Wegener, 1984c), so a reduced intensity of C=O bonds in hemicellulose (at 1732 cm^{-1}) due to TPT (a thermal process) was expected and is reported in other studies (Özgenç et al., 2017). Both the slightly reduced intensity of the cellulose peaks at 2916 cm^{-1} and 2850 cm^{-1} (C-H stretching groups), indicate that cellulose fractions were also removed by TPT (Sharma et al., 2020) which may explain the reduced mean size of cellulose crystallite sizes (discussed in Section 5.4.2.1.1). The removal of cellulose due to TPT at similar temperatures (i.e., between 200°C and 300°C) is less common but still reported (Ibrahim et al., 2013; Niu et al., 2019) and is attributed to acetic acid (from hemicellulose decomposition) attacking cellulose (as described in Section 5.4.2.1.1). The fact that hemicellulose was presumably degraded during TPT supports the idea that this mechanism occurred.

The presumed removal of both hemicellulose and cellulose implies that lignin existed in greater proportion within TPT wood than in Untreated wood. Thus, the potentially increased interaction between lignin and phosphoric acid likely allowed for enhanced cleavage of lignin aryl ether bonds to promote pore widening during the carbonization step (Zuo et al., 2009). This idea is supported by the fact that carbon dioxide and formaldehyde (lignin decomposition products) (Lv et al., 2015) were the predominant gaseous products released at the temperature of peak thermal degradation of the carbonization stage of TPT activation as shown in Figure 5-3.

HPT also removed hemicellulose, as evidenced by the flattening of the peak at 1732 cm^{-1} (Chen et al., 2010). Galactoglucomannan hemicellulose is highly water soluble, making it susceptible to removal by HPT (Fengel and Wegener, 1984a). While HPT increased cellulose crystallite size, the intensity of C-H stretching groups in cellulose (2916 cm^{-1} and 2850 cm^{-1}) exhibited a decreased intensity (Sharma et al., 2020). The lack of impact on crystalline cellulose degradation (as evidenced by the growth in cellulose crystallites in Section 5.4.2.1.1) when compared to TPT may have to do with the fact that acetic acid produced from the decomposition of O-acetyl groups in hemicellulose was diluted in the HPT solution, limiting its ability to attack glycosidic linkages in cellulose. The fact that HPT primarily removed hemicellulose implies that phosphoric acid had greater access to remaining cellulose and lignin. The enhanced access to these biopolymers due to HPT likely increased acid-catalyzed hydrolysis of these components leading to the greatest increase in pore volume and specific surface area of all the ACs of the study. The proposed impact of the observed changes in the FT-IR spectra of gases produced during the activation process aligns with Figure 5-3, which shows that the highest absorption of carbon dioxide (a product of lignin decomposition) and formaldehyde (product of lignin and/or cellulose decomposition) was observed during the carbonization step of HPT activation (Lv et al., 2015).

APT removed hemicellulose as evidenced by the flattening of the 1732 cm^{-1} peak (Sharma et al., 2020; Chen et al., 2010). The flattening of the hemicellulos peak is generally associated with the cleavage of lignin aryl ether bonds (Barman et al., 2020) which leads to the subsequent separation and

depolymerization of hemicellulose (Kim et al., 2016). However, the change in the lignin peak was relatively insignificant for the APT sample of the present study. In contrast to TPT and HPT, the peaks at 2916 cm^{-1} and 2850 cm^{-1} remained pronounced following APT. This observation may have to do with the fact that glycosidic linkages in cellulose are relatively insulated from alkaline attack by lignin and hemicellulose in the wood cell wall (Fengel and Wegener, 1984b) and show resistance to cleavage by NaOH at solution concentrations lower than 7% (w/w) (Iroba et al., 2017) which explains why the 5% (w/w) NaOH solution used in the present study had limited impact on cellulose removal. Overall, the removal of hemicellulose facilitated greater acid-catalyzed hydrolysis of the remaining biopolymers. Figure 5-3 shows that carbon dioxide and formaldehyde were the predominant gaseous products released at the temperature of peak thermal degradation. These two gases are consistent with the volatilization of lignin (Lv et al., 2015) which may be the main component that volatilized at this temperature considering the low proportion of methane and methanol released (from cellulose). The volatilization of lignin at these temperatures presumably contributed to pore widening and increased pore volume and specific surface area of APT AC when compared to Untreated and TPT ACs.

The removal of these chemical components (primarily hemicellulose) from the wood also has a potential impact on the apparent density of the wood. The changes to the apparent density of wood samples were used as an indirect indicator of porosity development in the wood by the PTs as discussed in the following section.

5.4.2.3 Impact of Pre-Treatments on Wood Macroscopic Structure

The apparent density of wood blocks (15 × 15 × 30 mm) were reduced to a statistically significant degree following all PTs as shown in Figure 5-5 (with respective 95% confidence limits).

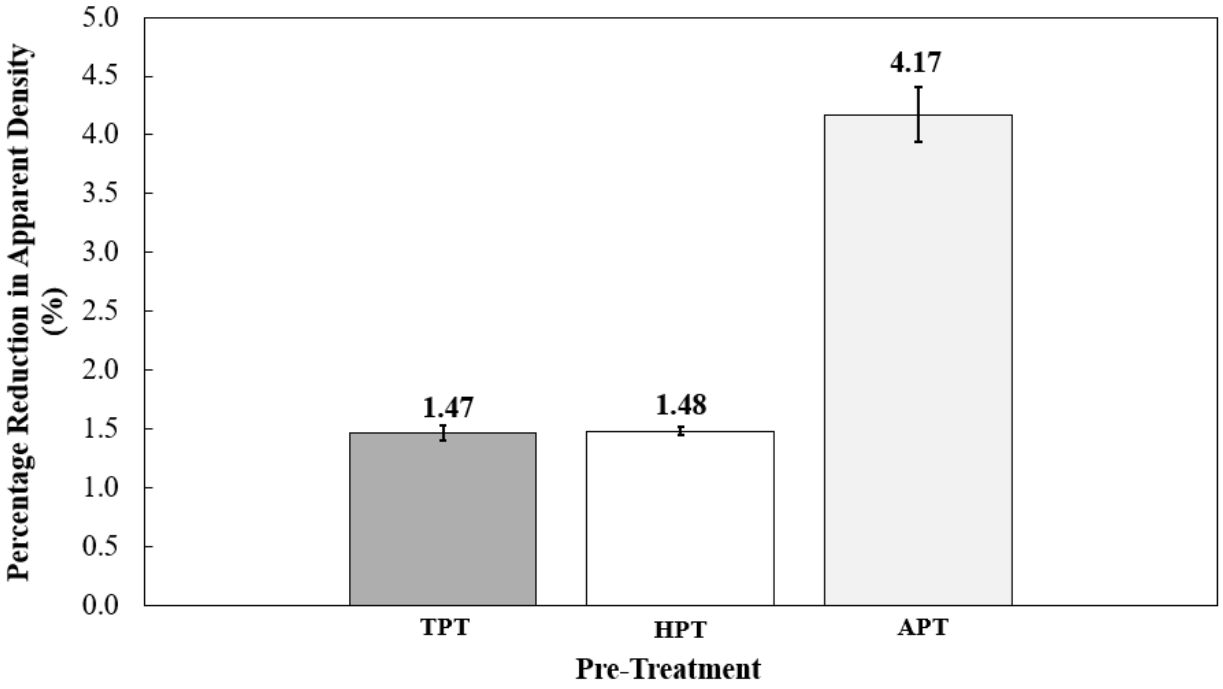

Figure 5-5. Percentage decrease in apparent density of wood blocks due to Pre-Treatments.

The reduced apparent density of the samples indirectly indicates that the PTs increased internal porosity of the wood. The increased porosity presumably permitted phosphoric acid more efficient permeation into the pores of the wood, enhancing reactions with the biopolymers in the wood, contributing to the increased development of porosity in the produced ACs. This idea was supported by the DTG curve which shows much greater weight losses between temperatures of 50°C and 110°C for the impregnated PT samples compared to the Untreated samples (Figure 5-6).

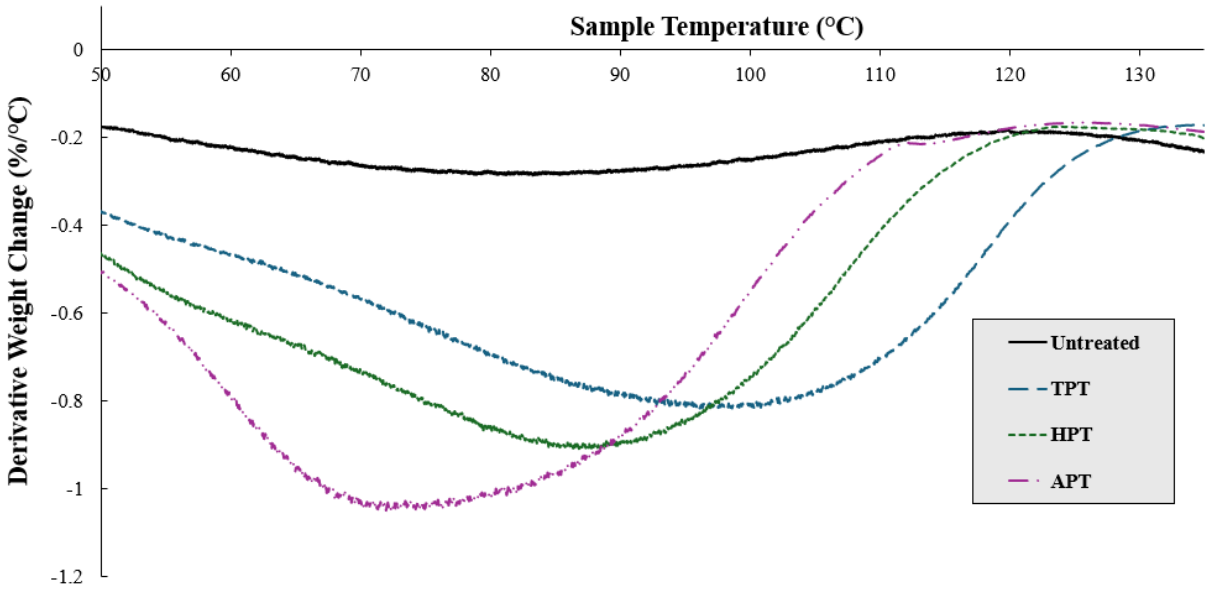

Figure 5-6. Differential thermogravimetric analysis of impregnated Untreated and Pre-Treated white spruce wood.

The mass loss within this temperature range during the carbonization of phosphoric acid-impregnated wood is attributed to the evaporation of water, mainly sourced from the impregnated phosphoric acid itself (Bedoui et al., 2021). Thus, uptake of phosphoric acid by the PT wood samples was increased, magnifying the impact of the changes to the crystalline and chemical properties of the wood on the activation process. The impregnation ratio (mass of acid solution to mass of dry wood sample) was constant for all samples. Therefore, the drastic increase in evaporated water from the PT samples suggests that a significant proportion of phosphoric acid used for the Untreated sample did not heavily contribute to the activation process. This observation suggests that the PT samples may require less phosphoric acid for effective activation. This advantage would not only result in significant cost savings but also provides a logistical advantage by reducing the frequency of required consumables shipments, highlighting the potential suitability of PTs for producing AC in northern and remote communities. However, this conclusion needs to be experimentally verified.

Clearly, the changes to the crystalline, chemical and macroscopic properties of the wood induced by the PTs had varying impacts on the impregnation and carbonization steps of the activation process. Ultimately, these changes resulted in enhanced pore widening leading to increased mesoporosity, specific surface area and aqueous-phase adsorption capacity of the ACs.

5.5 Conclusions

The impacts of TPT, HPT and APT on the characteristics of a single raw material (white spruce wood) were studied for the first time. The three PTs helped produce ACs with much higher specific surface area and IN than that produced from the Untreated wood. HPT proved to be the most effective, producing AC with surface area and IN comparable to the most popular commercial AC used for water treatment. The pore size distribution of the PT ACs potentially makes them suitable for the removal of taste and odour-causing compounds, cyanotoxins and NOM in potable water treatment; all of which are of increasing concern in northern water of Canada.

The PTs impacted pore widening and formation to different degrees during the carbonization step of the activation process which magnified the positive pore properties of wood-based ACs. The improved surface area, adsorption capacity and pore volume were facilitated by the changes PTs induced to the crystalline, chemical and macroscopic properties of the white spruce wood precursor. All PTs removed amorphous biopolymers (primarily hemicellulose) from the white spruce wood feedstock. The removal of these compounds decreased the apparent density of the wood which presumably facilitated increased penetration of phosphoric acid into the wood's macrostructure. The removal of these compounds also increased the CrI of white spruce wood leading to phosphoric acid's preference for reaction with amorphous biopolymers, increasing the degree of pore widening and formation. However, the nature of the crystalline cellulose was altered in different manners by each PT, and this characteristic had the greatest impact on the dominant pore development mechanism in the ACs. Smaller cellulose crystallites in TPT promoted micropore development by forming stable inter-crystalline cross-links that inhibited volatilization. In contrast, APT led to larger crystallites, resulting in slightly larger pores due to different cross-linking

behavior during carbonization. The slightly larger crystallites of the HPT sample promoted the development of larger pores by shifting the dominant reaction mechanisms toward acid-catalyzed hydrolysis and volatilization while forming larger pores during cross-link formation. Its smaller crystallites compared to APT enhanced the breakdown of amorphous regions, further contributing to pore widening. As a result, HPT AC displayed the highest adsorption capacity, surface area, pore diameter, and pore volume, while exhibiting the lowest microporosity among the samples. Analysis of the produced gaseous products during the carbonization step supported the conclusion that variations in crystallite size directly influenced the dominant reaction mechanisms shaping the final pore structure of the ACs.

The findings also revealed that PTs may have the potential to reduce the chemical activating agent requirements for producing high performance ACs. These findings further emphasize the suitability of PT waste wood pallets as a raw material to produce AC for water treatment in northern and remote communities by potentially lowering both cost requirements and material shipping frequency.

5.6 References

Anderson, L. E., DeMont, I., Dunnington, D. D., Bjorndahl, P., Redden, D. J., Brophy, M. J., & Gagnon, G. A. (2023). A review of long-term change in surface water natural organic matter concentration in the northern hemisphere and the implications for drinking water treatment. *Science of The Total Environment, 858*, 159699. https://doi.org/10.1016/j.scitotenv.2022.159699

Arctic Council. (2009). *Arctic Marine Shipping Assessment 2009 Report*. UNT Digital Library. https://digital.library.unt.edu/ark:/67531/metadc949512/m1/4/

ASTM (2021) *D4607-14 Standard Test Method for Determination of Iodine Number of Activated Carbon*. ASTM International, West Conshohocken, PA, USA.

Ateia, M., Maroli, A., Tharayil, N., & Karanfil, T. (2019). The overlooked short- and ultrashort-chain poly- and perfluorinated substances: A review. *Chemosphere, 220*, 866–882. https://doi.org/10.1016/j.chemosphere.2018.12.186

Barman, D. N., Haque, Md. A., Hossain, Md. M., Paul, S. K., & Yun, H. D. (2020). Deconstruction of pine wood (Pinus sylvestris) recalcitrant structure using alkali treatment for enhancing enzymatic saccharification evaluated by Congo red. *Waste and Biomass Valorization, 11(5)*, 1755–1764. https://doi.org/10.1007/s12649-018-00547-z

Barrera, J. (2019). *Attawapiskat declares state of emergency over water quality.* CBC News, Ottawa, Ontario, CA. https://www.cbc.ca/news/indigenous/attawapiskat-water-quality-emergency-1.5204652

Bedoui, A., Souissi-Najar, S., Idris, S. S., Rahman, N. A., & Ouederni, A. (2021). Thermal behaviour of impregnated olive stones with phosphoric acid via TGA-MS. *Chimie, 24(S1)*, 149–162. https://doi.org/10.5802/crchim.118

Berthouex, P. M. & Brown, L. C. (2002). Chapter 17 – Paired t-Test for assessing the average of differences. In *Statistics for Environmental Engineers (2nd ed.),* 147-154. Lewis Publishers, Boca Raton, Florida, USA.

Black and Veatch & AWWA. (2023). *AWWA statement on proposed PFAS drinking water standards*. American Water Works Association. https://www.awwa.org/AWWA-Articles/awwa-statement-on-proposed-pfas-drinking-water-standards/

Boundzanga, H. M., Cagnon, B., Roulet, M., de Persis, S., Vautrin-Ul, C., & Bonnamy, S. (2022). Contributions of hemicellulose, cellulose, and lignin to the mass and the porous characteristics of activated carbons produced from biomass residues by phosphoric acid activation. *Biomass Conversion and Biorefinery, 12(8)*, 3081–3096. https://doi.org/10.1007/s13399-020-00816-9

Brigham, L. W. (2007, October). Thinking about the Arctic's future: scenarios for 2040. *The Futurist, 41(5)*, 27-29,31-34.

Calgon Carbon Corporation (2024). *Filtrasorb® granular activated carbon.* Calgon Carbon Corporation, Coraopolis, Pennsylvania, USA. https://www.calgoncarbon.com/app/uploads/F400-Final.pdf

Calgon Carbon Corporation (2017). *Acticarbone® activated wood carbon*. Calgon Carbon Corporation, Coraopolis, Pennsylvania, USA. https://www.rbon.com/acticarbone/

Chang, S., Zhao, Z., Zheng, A., He, F., Huang, Z., & Li, H. (2012). Characterization of products from torrefaction of sprucewood and bagasse in an auger reactor. *Energy & Fuels, 26(11)*, 7009–7017. https://doi.org/10.1021/ef301048a

Chen, C.-X., Huang, B., Li, T., & Wu, G.-F. (2012). Preparation of phosphoric acid activated carbon from sugarcane bagasse by mechanochemical processing. *BioResources, 7(4)*, 5109–5116. https://doi.org/10.15376/biores.7.4.5109-5116

Chen, H., Ferrari, C., Angiuli, M., Yao, J., Raspi, C., & Bramanti, E. (2010). Qualitative and quantitative analysis of wood samples by Fourier transform infrared spectroscopy and multivariate analysis. *Carbohydrate Polymers, 82(3)*, 772–778. https://doi.org/10.1016/j.carbpol.2010.05.052

Chen, L., Wang, Q., Hirth, K., Baez, C., Agarwal, U. P., & Zhu, J. Y. (2015). Tailoring the yield and characteristics of wood cellulose nanocrystals (CNC) using concentrated acid hydrolysis. *Cellulose, 22(3)*, 1753–1762. https://doi.org/10.1007/s10570-015-0615-1

Chowdhury, Z. K., Summers, R.S., Westerhoff, G.P., Leto, B.J., Nowack, K.O., Corwin, C.J. (2013). Chapter 4 – Activated carbon application approaches. In *Activated Carbon: Solutions for Improving Water Quality,* 31-72. American Water Works Association, Denver, Colorado, USA.

Crittenden, J. C., Trussell, R.R., Hand, D.W., Howe, K.J. & Tchobanoglous, G. (2012). Chapter 15: Adsorption. In *MWH's Water Treatment: Principles and Design. (3rd ed.),* 1117-1263. John Wiley and Sons, Ltd., Hoboken, New Jersey, USA.

David Suzuki Foundation. (2017). *Glass half empty? Year 1 progress toward resolving drinking water advisories in nine First Nations in Ontario.* David Suzuki Foundation, Vancouver, British Columbia, CA. https://davidsuzuki.org/science-learning-centre-article/report-glass-half-empty-year-1-progress-toward-resolving-drinking-water-advisories-nine-first-nations-ontario/

Davoodbeygi, Y., Askari, M., Salehi, E., & Kheirieh, S. (2023). A review on hybrid membrane-adsorption systems for intensified water and wastewater treatment: Process configurations, separation targets, and materials applied. *Journal of Environmental Management, 335*, 117577. https://doi.org/10.1016/j.jenvman.2023.117577

Decker, K. C., & Long, B. W. (1992). Canada's cooperative approach to drinking water regulation. *American Water Works Association, 84(4)*, 120–28, https://doi.org/10.1002/j.1551-8833.1992.tb07337.x.

Dias, J. M., Alvim-Ferraz, M. C. M., Almeida, M. F., Rivera-Utrilla, J., & Sánchez-Polo, M. (2007). Waste materials for activated carbon preparation and its use in aqueous-phase treatment: A review. *Journal of Environmental Management, 85(4)*, 833–846. https://doi.org/10.1016/j.jenvman.2007.07.031

El Qada, E. N., Allen, S. J., & Walker, G. M. (2008). Influence of preparation conditions on the characteristics of activated carbons produced in laboratory and pilot scale systems. *Chemical Engineering Journal, 142(1)*, 1–13. https://doi.org/10.1016/j.cej.2007.11.008

Fan, L. T., Lee, Y.-H., & Beardmore, D. H. (1980). Mechanism of the enzymatic hydrolysis of cellulose: Effects of major structural features of cellulose on enzymatic hydrolysis. *Biotechnology and Bioengineering, 22(1)*, 177–199. https://doi.org/10.1002/bit.260220113

Fengel, D., & Wegener, G. (1984a). Chapter 5 – Polyoses (hemicellulose). In *Wood: Chemistry, Ultrastructure, Reactions*, 106-131. W. de Gruyter, Berlin, DE.

Fengel, D., & Wegener, G. (1984b). Chapter 11 – Reactions in alkaline medium. In *Wood: Chemistry, Ultrastructure, reactions*, 296-318. W. de Gruyter, Berlin, DE.

Fengel, D., & Wegener, G. (1984c). Chapter 12 – Influence of temperature. In *Wood: Chemistry, Ultrastructure, Reactions*, 319-343. W. de Gruyter, Berlin, DE.

Flanagan, C. M. (2021). *Water Security on First Nations Reserves in Ontario: Exploring the Impact of Source Water Protection, Community Location, and Fiscal Capacity*, M.A. McGill University,

Montreal, Quebec, CA. https://www.proquest.com/docview/2652145851/abstract/A2ACB82237E14326PQ/1

Ganjoo, R., Sharma, S., Kumar, A., & Daouda, M. M. A. (2023). Chapter 1 - Activated carbon: Fundamentals, classification, and properties. In *Activated Carbon: Progress and Applications*, 1-22. Royal Society of Chemistry, Piccadilly, London, UK. https://doi.org/10.1039/BK9781839169861-00001

Garrote, G., Domínguez, H., & Parajó, J. C. (1999). Hydrothermal processing of lignocellulosic materials. *Holz Als Roh- Und Werkstoff, 57(3)*, 191–202. https://doi.org/10.1007/s001070050039

Gobler, C. J. (2020). Climate change and harmful algal blooms: Insights and perspective. *Harmful Algae, 91*, 101731. https://doi.org/10.1016/j.hal.2019.101731

Gong, X.-J., Li, Y.-S., Dong, Y.-Q., & Li, W.-G. (2020). Arsenic adsorption by innovative iron/calcium in-situ-impregnated mesoporous activated carbons from low-temperature water and effects of the presence of humic acids. *Chemosphere, 250*, 126275. https://doi.org/10.1016/j.chemosphere.2020.126275

Government of Canada. (2025a). *Drinking water advisories – Causes of boil water advisories*. https://open.canada.ca/data/en/dataset/0492d0f6-9d95-43e2-8db7-80751b18d6fc

Government of Canada. (2025b). *Map of long-term drinking water advisories on public systems on reserves.* https://sac-isc.gc.ca/eng/1620925418298/1620925434679

He, Z., Wang, Z., Qu, L., Qian, J., & Yi, S. (2019). Gaseous decomposition products from wood degradation via thermogravimetric and Fourier transform infrared analysis during thermal modification of beech and pine woods. *BioResources, 14(3)*, 6883–6894. https://doi.org/10.15376/biores.14.3.6883-6894

Ibrahim, R. H. H., Darvell, L. I., Jones, J. M., & Williams, A. (2013). Physicochemical characterization of torrefied biomass. *Journal of Analytical and Applied Pyrolysis, 103*, 21–30. https://doi.org/10.1016/j.jaap.2012.10.004

Iroba, K. L., Soleimani, M., & Tabil, L. G. (2017). Chapter 14 - Compositional and structural modification of lignocellulosic biomass for biofuel production by alkaline treatment. *Biomass Preprocessing and Pretreatments for Production of Biofuels,* 384-412. CRC Press, Boca Raton, Florida, USA.

Jagtoyen, M., & Derbyshire, F. (1993). Some considerations of the origins of porosity in carbons from chemically activated wood. *Carbon, 31(7)*, 1185–1192. https://doi.org/10.1016/0008-6223(93)90071-H

Jeoh, T., Ishizawa, C. I., Davis, M. F., Himmel, M. E., Adney, W. S., & Johnson, D. K. (2007). Cellulase digestibility of pretreated biomass is limited by cellulose accessibility. *Biotechnology and Bioengineering, 98(1),* 112-122. https://doi.org/10.1002/bit.21408

Jiao, H., Guo, X., Shu, F., Zhang, Q., Wu, W., Jin, Y., & Jiang, B. (2025). Structure-property-function relationships of wood-based activated carbon in energy and environment materials. *Separation and Purification Technology, 353*, 128607. https://doi.org/10.1016/j.seppur.2024.128607

Jjagwe, J., Olupot, P. W., Menya, E., & Kalibbala, H. M. (2021). Synthesis and application of granular activated carbon from biomass waste materials for water treatment: A review. *Journal of Bioresources and Bioproducts, 6(4)*, 292–322. https://doi.org/10.1016/j.jobab.2021.03.003

Kim, J.H., Jung, S.C., Lee, H.M., & Kim, B.J. (2022). Comparison of pore structures of cellulose-based activated carbon fibers and their applications for electrode materials. *International Journal of Molecular Sciences, 23(7)*, Article 7. https://doi.org/10.3390/ijms23073680

Kim, J. S., Lee, Y. Y., & Kim, T. H. (2016). A review on alkaline pretreatment technology for bioconversion of lignocellulosic biomass. *Bioresource Technology, 199*, 42–48. https://doi.org/10.1016/j.biortech.2015.08.085

Kim, T. H. (2021). Pretreatment of lignocellulosic biomass. In *Bioprocessing Technologies in Biorefinery for Sustainable Production of Fuels, Chemicals, and Polymers,* 91–110. John Wiley & Sons, Ltd., Hoboken, New Jersey, USA. https://doi.org/10.1002/9781118642047.ch6

Kumar, A., & Jena, H. M. (2016). Preparation and characterization of high surface area activated carbon from Fox nut (Euryale ferox) shell by chemical activation with H3PO4. *Results in Physics, 6*, 651–658. https://doi.org/10.1016/j.rinp.2016.09.012

Li, M., Cao, S., Meng, X., Studer, M., Wyman, C. E., Ragauskas, A. J., & Pu, Y. (2017). The effect of liquid hot water pretreatment on the chemical–structural alteration and the reduced recalcitrance in poplar. *Biotechnology for Biofuels, 10(1)*, 237. https://doi.org/10.1186/s13068-017-0926-6

Liu, H., Cheng, C., & Wu, H. (2021). Sustainable utilization of wetland biomass for activated carbon production: A review on recent advances in modification and activation methods. *Science of The Total Environment, 790*, 148214. https://doi.org/10.1016/j.scitotenv.2021.148214

Lobo, K. (2025). Chapter 4 – Materials and Methods. *Sustainable Pre-Treatments for White Spruce Wood-Based Activated Carbon: Impact on Porosity and Aqueous-Phase Adsorption [Unpublished Master of Applied Science Thesis]*, 58-91. University of Ottawa, Ottawa, Ontario, CA.

Lourenço, A., Araújo, S., Gominho, J., & Evtuguin, D. (2020). Cellulose structural changes during mild torrefaction of eucalyptus wood. *Polymers, 12(12)*, 1–17. https://doi.org/10.3390/polym12122831

Lu, X., & Gu, X. (2022). A review on lignin pyrolysis: Pyrolytic behavior, mechanism, and relevant upgrading for improving process efficiency. *Biotechnology for Biofuels and Bioproducts, 15(1)*, 106. https://doi.org/10.1186/s13068-022-02203-0

Lv, P., Almeida, G., & Perre, P. (2015). TGA-FTIR analysis of torrefaction of lignocellulosic components (cellulose, xylan, lignin) in isothermal conditions over a wide range of time durations. *BioResources 10(3)*, 4239-4251. https://bioresources.cnr.ncsu.edu/

Marsh, H., & Rodríguez-Reinoso, F. (2006). Chapter 6 – Activation processes (Chemical). In *Activated Carbon*, 322-365. Elsevier Science Ltd., Amsterdam, NL. https://doi.org/10.1016/B978-008044463-5/50020-0

Morales-delaRosa, S., Campos-Martin, J. M., & Fierro, J. L. G. (2014). Optimization of the process of chemical hydrolysis of cellulose to glucose. *Cellulose, 21(4)*, 2397–2407. https://doi.org/10.1007/s10570-014-0280-9

Ni, X., Cen, K., Li, X., Cui, D., Liu, M., Zhu, L., & Chen, D. (2025). Cellulose upgradation by torrefaction pretreatment and effect of torrefaction severity on the quality of pyrolysis products. *Industrial Crops and Products, 225*, 120516. https://doi.org/10.1016/j.indcrop.2025.120516

Niu, Y., Lv, Y., Lei, Y., Liu, S., Liang, Y., Wang, D., & Hui, S. (2019). Biomass torrefaction: Properties, applications, challenges, and economy. *Renewable and Sustainable Energy Reviews, 115*, 109395. https://doi.org/10.1016/j.rser.2019.109395

Oginni, O., Singh, K., Oporto, G., Dawson-Andoh, B., McDonald, L., & Sabolsky, E. (2019). Effect of one-step and two-step H3PO4 activation on activated carbon characteristics. *Bioresource Technology Reports, 8*, 100307. https://doi.org/10.1016/j.biteb.2019.100307

Özgenç, Ö., Durmaz, S., Boyaci, I. H., & Eksi-Kocak, H. (2017). Determination of chemical changes in heat-treated wood using ATR-FTIR and FT Raman spectrometry. *Spectrochimica Acta Part A: Molecular and Biomolecular Spectroscopy, 171*, 395–400. https://doi.org/10.1016/j.saa.2016.08.026

Paredes, J. J., Jara, R., Shaler, S. M., & van Heiningen, A. (2008). Influence of hot water extraction on the physical and mechanical behavior of OSB. *Forest Products Journal, 58(12)*.

Pastor-Villegas, J., Pastor-Valle, J. F., Rodríguez, J. M. M., & García, M. G. (2006). Study of commercial wood charcoals for the preparation of carbon adsorbents. *Journal of Analytical and Applied Pyrolysis, 76(1)*, 103–108. https://doi.org/10.1016/j.jaap.2005.08.002

Pelaez-Samaniego, M. R., Yadama, V., Lowell, E., & Espinoza-Herrera, R. (2013). A review of wood thermal pretreatments to improve wood composite properties. *Wood Science and Technology, 47(6)*, 1285–1319. https://doi.org/10.1007/s00226-013-0574-3

Pivokonsky, M., Kopecka, I., Cermakova, L., Fialova, K., Novotna, K., Cajthaml, T., Henderson, R. K., & Pivokonska, L. (2021). Current knowledge in the field of algal organic matter adsorption onto activated carbon in drinking water treatment. *Science of The Total Environment, 799*, 149455. https://doi.org/10.1016/j.scitotenv.2021.149455

Prieto, M.J., Ellis, G., Budarin, V., Morales, E., Naffakh, M., & S. Shuttleworth, P. (2024). Understanding pore size relation in cellulose-derived, nitrogen-doped, hydrothermal carbons for improved supercapacitor performance. *Journal of Materials Chemistry, 12(43)*, 29698–29707. https://doi.org/10.1039/D4TA04477K

Qi, Y., Zhou, Z., Xu, R., Dong, Y., Zhang, Z., & Liu, M. (2023). Effect of NaOH pretreatment on permeability and surface properties of three wood species. *ACS Omega, 8(43)*, 40362–40374. https://doi.org/10.1021/acsomega.3c04745

Rehman, M. M., Zeeshan, M., Shaker, K., & Nawab, Y. (2019). Effect of micro-crystalline cellulose particles on mechanical properties of alkaline treated jute fabric reinforced green epoxy composite. *Cellulose, 26(17)*, 9057–9069. https://doi.org/10.1007/s10570-019-02679-4

Rowell, R. M., Pettersen, R., & Tshabalala, M. A. (2012). Chapter 3 – Cell wall chemistry. In *Cell Wall Chemistry,* 34-70. Taylor & Francis, Oxfordshire, USA. https://www-taylorfrancis-com.proxy.bib.uottawa.ca/reader/download/55e8474f-5952-4c3a-8d36-4180507f1834/chapter/pdf?context=ubx

Ruhl, A. S., Altmann, J., Zietzschmann, F., Meinel, F., Sperlich, A., & Jekel, M. (2014). Integrating micro-pollutant removal by powdered activated carbon into deep bed filtration. *Water, Air, & Soil Pollution, 225(3)*, 1877. https://doi.org/10.1007/s11270-014-1877-1

Sarko, A., & Muggli, R. (1974). Packing analysis of carbohydrates and polysaccharides. III valonia cellulose and cellulose II. *Macromolecules, 7(4)*, 486–494. https://doi.org/10.1021/ma60040a016

Scherrer, P. (1918). Bestimmung der größe und der inneren struktur von kolloidteilchen mittels röntgenstrahlen. *Nachrichten von der Gesellschaft der Wissenschaften zu Göttingen, Mathematisch-Physikalische Klasse, 1918*, 98–100.

Segal, L., Creely, L. L., Martin Jr., A. E., & Conrad, C. M. (1959). An empirical method for estimating the degree of crystallinity of native cellulose using the X-Ray diffractometer. *Textile Research Journal, 29(10),* 786-794. https://doi-org.proxy.bib.uottawa.ca/10.1177/004051755902901003

Sharma, V., Yadav, J., Kumar, R., Tesarova, D., Ekielski, A., & Mishra, P. K. (2020). On the rapid and non-destructive approach for wood identification using ATR-FTIR spectroscopy and chemometric methods. *Vibrational Spectroscopy, 110*, 103097. https://doi.org/10.1016/j.vibspec.2020.103097

Sontheimer, H., Crittenden, J.C., & Summers, R.S. (1988a). Chapter 1: Water treatment through adsorption processes. In *Activated Carbon for Water Treatment (2nd ed.),* 1-49. DVGW-Forschungsstelle, Engler-Bunte-Institut, Universität Karlsruhe, Karlsruhe, DE.

Sontheimer, H., Crittenden, J.C., & Summers, R.S. (1988b). Chapter 2: The production and physical-chemical evaluation of activated carbon. In *Activated Carbon for Water Treatment (2nd ed.),* 51-103. DVGW-Forschungsstelle, Engler-Bunte-Institut, Universität Karlsruhe, Karlsruhe, DE.

The Canadian Press. (2025). *Unsafe tap water is common in Newfoundland. This town just overcame a 1989 boil order.* CTVNews, Toronto, Ontario, CA. https://www.ctvnews.ca/canada/article/unsafe-tap-water-is-common-in-newfoundland-this-town-just-overcame-a-1989-boil-order/

USEPA (2025). *Summary of cyanotoxins treatment in drinking water.* USEPA, Washington, D.C., USA. https://www.epa.gov/ground-water-and-drinking-water/summary-cyanotoxins-treatment-drinking-water

Wan, J., Wang, Y., & Xiao, Q. (2010). Effects of hemicellulose removal on cellulose fiber structure and recycling characteristics of eucalyptus pulp. *Bioresource Technology, 101(12)*, 4577–4583. https://doi.org/10.1016/j.biortech.2010.01.026

Wang, Z., Chen, Z., & An, C. (2023). A review on solid waste management in Canadian First Nations communities: Policy, practices, and challenges. *Cleaner Waste Systems, 4*, 100074. https://doi.org/10.1016/j.clwas.2022.100074

Yang, H., Yan, R., Chen, H., Lee, D. H., & Zheng, C. (2007). Characteristics of hemicellulose, cellulose and lignin pyrolysis. *Fuel, 86(12)*, 1781–1788. https://doi.org/10.1016/j.fuel.2006.12.013

Young, G., & Funderlic, R. E. (1973). On the grain boundary diffusion theory of Fisher and Whipple. *Journal of Applied Physics, 44(11)*, 5151–5154. https://doi.org/10.1063/1.1662107

Zhang, Y., Gao, Y., Zhao, M., Feng, X., Wang, L., Yang, H., Ma, H., & Zhou, J. (2021). Effects of Torrefaction on the Lignin of Apricot Shells and Its Catalytic Conversion to Aromatics. *ACS Omega, 6(39)*, 25742–25748. https://doi.org/10.1021/acsomega.1c04095

Zheng, Z., Lin, Q., Gao, Y., Ji, X., Sessler, J. L., & Wang, H. (2024). Recent advances in iodine adsorption from water. *Coordination Chemistry Reviews, 511*, 215860. https://doi.org/10.1016/j.ccr.2024.215860

Zhuang, X., Wang, W., Song, B., & Yu, Q. (2021). Chapter 4 - Liquid hot water pretreatment for lignocellulosic biomass biorefinery. *Emerging Technologies for Biorefineries, Biofuels, and Value-Added Commodities,* 81–109. Springer International Publishing, Baar, CH. https://doi.org/10.1007/978-3-030-65584-6_4

Zuo, S., Liu, J., Yang, J., & Cai, X. (2009). Effects of the crystallinity of lignocellulosic material on the porosity of phosphoric acid-activated carbon. *Carbon, 47(15)*, 3578–3580. https://doi.org/10.1016/j.carbon.2009.08.026

Chapter 6 - Conclusions

6.1 Scientific Contributions

The impacts of TPT, HPT and APT on the characteristics of a single raw material (white spruce wood) were studied for the first time. The PT woods produced ACs with increased surface areas and adsorption capacities (on an IN basis). Of the PTs, HPT was the most effective and improved the IN and surface area to comparable levels with even the most popular commercially produced ACs used for water treatment. The pore size distribution of the produced ACs show the potential for them to remove taste and odour-causing compounds, certain cyanotoxins and NOM from potable water.

The PT ACs had improved surface areas and INs compared the Untreated AC due to enhanced pore widening. The improved pore widening was facilitated by the changes PTs induced to the crystalline, chemical and macroscopic properties of the white spruce wood precursor. The PT woods exhibited differing Changes to the crystallinity by the PTs proved to have the greatest impact on pore development during activation by governing the dominant pore development reaction mechanism during carbonization (i.e., acid-catalyzed hydrolysis of amorphous biopolymers versus cross-link formation). TPT caused a reduction in the mean size of cellulose crystallites leading to an increased propensity to form stable inter-crystalline cross-links that volatilize to a lesser degree, resulting in the formation of micropores. APT caused an increase in the mean size of crystallites resulting in the formation of larger pores due to cross-link formation. These larger crystallites were also more resistant to acid-catalyzed hydrolysis, resisting the formation of larger pores than in TPT AC. HPT provided the unique condition where the mildly increased mean crystallite size facilitated a balance between acid catalyzed-hydrolysis of amorphous biopolymers and inter-crystalline cross-link formation. The higher susceptibility to acid-catalyzed hydrolysis of HPT wood biopolymers combined with the increase in crystallite size both contributed to HPT AC having the highest average pore diameter, pore volume, specific surface area and IN of all ACs studied. All the PTs removed amorphous biopolymers (primarily hemicellulose) from the white spruce wood feedstock. The removal of these compounds decreased the apparent density of the wood which presumably facilitated increased

penetration of phosphoric acid into the wood's macrostructure. The removal of these compounds also increased the CrI of white spruce wood leading to phosphoric acid's preference for reaction with amorphous biopolymers, increasing the degree of pore widening across all PT ACs. Analysis of the gaseous products throughout the carbonization step supported the conclusion that variations in crystalline, chemical and macroscopic characteristics directly influenced the dominant reaction mechanisms shaping the final pore structure of the ACs.

6.2 Benefits for Use in Remote and Northern Canadian Communities

All studied PTs resulted in white spruce wood ACs with increased specific area, pore volume and iodine adsorption capacity. In fact, these metrics were brought into competitive ranges of commercially produced ACs for water treatment showing promise for their increased utility. Moreover, the PT ACs demonstrated potential for:

1. Reducing cost for producing high performing ACs for water treatment by showing potential to lower chemical and shipping frequency requirements (needs to be experimentally verified),
2. Benefitting the environment by converting waste material (i.e., white spruce wood) into a value-added product,
3. Improving the health of populations by sustainably manufacturing water treatment technology on site,
4. Strengthening local economies by increasing job opportunities in remote locations.

Ultimately, the study emphasized the potential to develop a solution to existing water treatment challenges experienced in remote and northern communities in a simple and cost-effective manner.

6.3 Recommendations for Future Work

The overwhelmingly positive results of this extensive study from both the practical and scientific lenses encourages research into the utility of PTs for the enhancement of AC porosity and aqueous-phase adsorption. However, the present study had three major limitations preventing its immediate application:

1. Only one PT condition was studied for each PT method.
2. Limited number of samples used for each characterization method.
3. The preparation of both PT white spruce wood and the subsequently prepared ACs was performed at the lab-scale. The limited mass of ACs produced in the present study (due to scale) would be insufficient for treating the volumes of water required by communities.
4. The aqueous-phase adsorption capacities of the ACs were determined in a single-solute (non-competitive) environment which does not depict realistic treatment application conditions.

Thus, the author would recommend further optimizing the PT conditions to produce AC. This recommendation may be most relevant for APT since of the lower energy requirement (compared to TPT and HPT) and the fact that NaOH is already commonly used in many water treatment plants for the management of alkalinity. Secondly, it would be recommended to study the impact of these PTs on a high number of samples (e.g., greater than 30) to gain a better understanding of the variability and statistical significance of the characteristic alterations. Third, it may be recommended to investigate options to scale up both the PT and AC production processes and compare AC properties to those produced at the bench-scale (i.e., those produced in the present study). It would also be recommended to carry out bench-scale tests using the PAC produced in the present study on waters extracted from various treatment phases in the targeted community to evaluate the PT ACs performance in an actual water treatment setting.

Other recommendations include:

1. Further analyzing the characteristic changes to white spruce wood due to the PTs (e.g., direct analysis of the specific surface area of the wood, wet chemical analysis of biopolymer components in the PT woods, etc.).
2. Bench-scale testing for the removal of NOM fractions (e.g., humic substances, phenolic compounds, etc.) from water in a single-solute system to identify potential preference for removal by the PT ACs.
3. Pore size distribution analysis of the PT woods to further study the impact of the PTs on potentially increasing the permeability of phosphoric acid into the wood macrostructure (as speculated by the change in apparent density due to the PTs).

DISCLAIMER: Note that the present work (and any writing presented in this thesis) is intended for research purposes ONLY and the activated carbons prepared in the study ARE NOT NSF/ANSI Standard 61 certified for Potable Water and DO NOT meet any regulatory requirements pertaining to potable water treatment.

Chapter 7 - References

Abolore, R. S., Jaiswal, S., & Jaiswal, A. K. (2024). Green and sustainable pretreatment methods for cellulose extraction from lignocellulosic biomass and its applications: A review. *Carbohydrate Polymer Technologies and Applications, 7*, 100396. https://doi.org/10.1016/j.carpta.2023.100396

Amarasekara, A. S., & Ebede, C. C. (2009). Zinc chloride mediated degradation of cellulose at 200 °C and identification of the products. *Bioresource Technology, 100(21)*, 5301. https://doi.org/10.1016/j.biortech.2008.12.066

Amarawansha, G., Zvomuya, F., Tomy, G., & Farenhorst, A. (2023). Trihalomethanes in drinking water from three First Nation reserves in Manitoba, Canada. *Environmental Monitoring and Assessment, 195(2)*, 341. https://doi.org/10.1007/s10661-022-10694-5

American Chemical Society. (2022). *3D model of cellulose*. American Chemical Society, Washington, D.C., USA. https://www.acs.org/education/resources/undergraduate/chemistryincontext/interactives/nutrition/3d-model-cellulose.html

Anderson, L. E., DeMont, I., Dunnington, D. D., Bjorndahl, P., Redden, D. J., Brophy, M. J., & Gagnon, G. A. (2023). A review of long-term change in surface water natural organic matter concentration in the northern hemisphere and the implications for drinking water treatment. *Science of The Total Environment, 858*, 159699. https://doi.org/10.1016/j.scitotenv.2022.159699

Ansell, M. P. (2015). Chapter 1 - Wood microstructure – A cellular composite. In *Wood Composites,* 3–26. Woodhead Publishing, Cambridgeshire, UK. https://doi.org/10.1016/B978-1-78242-454-3.00001-9

Arctic council. (2009). *Arctic Marine Shipping Assessment 2009 Report*. UNT Digital Library. https://digital.library.unt.edu/ark:/67531/metadc949512/m1/4/

Arzola-Villegas, X., Báez, C., Lakes, R., Stone, D. S., O'Dell, J., Shevchenko, P., Xiao, X., De Carlo, F., & Jakes, J. E. (2023). Convolutional neural network for segmenting micro-X-ray computed

tomography images of wood cellular structures. *Applied Sciences, 13(14)*, Article 14. https://doi.org/10.3390/app13148146

Assembly of First Nations Environmental Stewardship Unit. (2008). *Climate change and water: impacts and adaptations for First Nations communities*. https://books-scholarsportal-info.proxy.bib.uottawa.ca/en/read?id=/ebooks/ebooks0/gibson_cppc/2011-12-20/1/10507050

ASTM (2021) *D4607-14 standard test method for determination of Iodine Number of activated carbon*, ASTM International, West Conshohocken, PA, USA.

Ateia, M., Maroli, A., Tharayil, N., & Karanfil, T. (2019). The overlooked short- and ultrashort-chain poly- and perfluorinated substances: A review. *Chemosphere, 220*, 866–882. https://doi.org/10.1016/j.chemosphere.2018.12.186

Bai, X., Wang, G., Yu, Y., Wang, D., & Wang, Z. (2018). Changes in the physicochemical structure and pyrolysis characteristics of wheat straw after rod-milling pretreatment. *Bioresource Technology, 250*, 770–776. https://doi.org/10.1016/j.biortech.2017.11.085

Barakat, A., Mayer-Laigle, C., Solhy, A., Arancon, R. A. D., De Vries, H., & Luque, R. (2014). Mechanical pretreatments of lignocellulosic biomass: Towards facile and environmentally sound technologies for biofuels production. *RSC Advances, 4(89)*, 48109–48127. https://doi.org/10.1039/c4ra07568d

Barman, D. N., Haque, Md. A., Hossain, Md. M., Paul, S. K., & Yun, H. D. (2020). Deconstruction of pine wood (Pinus sylvestris) recalcitrant structure using alkali treatment for enhancing enzymatic saccharification evaluated by Congo red. *Waste and Biomass Valorization, 11(5)*, 1755–1764. https://doi.org/10.1007/s12649-018-00547-z

Barrera, J. (2019). *Attawapiskat declares state of emergency over water quality.* CBC News, Ottawa, Ontario, CA. https://www.cbc.ca/news/indigenous/attawapiskat-water-quality-emergency-1.5204652

Bedoui, A., Souissi-Najar, S., Idris, S. S., Rahman, N. A., & Ouederni, A. (2021). Thermal behaviour of impregnated olive stones with phosphoric acid via TGA-MS. *Chimie, 24(S1)*, 149–162. https://doi.org/10.5802/crchim.118

Berthouex, P. M. & Brown, L. C. (2002). Chapter 17 – Paired t-Test for assessing the average of differences. In *Statistics for Environmental Engineers (2nd ed.),* 147-154. Lewis Publishers, Boca Raton, Florida, USA.

Black and Veatch & AWWA. (2023). *WITAF 56 technical memorandum: PFAS national cost model report, prepared for American Water Works Association*. https://www.awwa.org/wp-content/uploads/WITAF-56-Final-Technical-Memorandum.pdf

Boundzanga, H. M., Cagnon, B., Roulet, M., de Persis, S., Vautrin-Ul, C., & Bonnamy, S. (2022). Contributions of hemicellulose, cellulose, and lignin to the mass and the porous characteristics of activated carbons produced from biomass residues by phosphoric acid activation. *Biomass Conversion and Biorefinery, 12(8),* 3081-3096. https://doi.org/10.1007/s13399-020-00816-9

Brigham, L. W. (2007, October). Thinking about the Arctic's future: Scenarios for 2040. *The Futurist, 41(5)*, 27-29,31-34.

Bulkowska, K. & Klimiuk, E. (2016). Chapter 6 - Pretreatment of lignocellulosic biomass. *Biomass for Biofuels, 1st Edition*, 121-153. CRC Press, Boca Raton, Florida, USA.

Calgon Carbon Corporation (2024). *Filtrasorb® granular activated carbon.* Calgon Carbon Corporation, Coraopolis, Pennsylvania, USA. https://www.calgoncarbon.com/app/uploads/F400-Final.pdf

Calgon Carbon Corporation (2017). *Acticarbone® activated wood carbon*. Calgon Carbon Corporation, Coraopolis, Pennsylvania, USA. https://www.calgoncarbon.com/acticarbone/

Canadian Wood Council. (2024). *Canadian species*. https://cwc.ca/articles/canadian-species/

Casimero, C., Hegarty, C., McGlynn, R. J., & Davis, J. (2020). Ultrasonic exfoliation of carbon fiber: Electroanalytical perspectives. *Journal of Applied Electrochemistry, 50(3)*, 383–394. https://doi.org/10.1007/s10800-019-01379-y

Chang, S., Zhao, Z., Zheng, A., He, F., Huang, Z., & Li, H. (2012). Characterization of products from torrefaction of sprucewood and bagasse in an auger reactor. *Energy & Fuels, 26(11)*, 7009–7017. https://doi.org/10.1021/ef301048a

Chen, C.X., Huang, B., Li, T., & Wu, G.-F. (2012). Preparation of phosphoric acid activated carbon from sugarcane bagasse by mechanochemical processing. *BioResources, 7(4)*, 5109–5116. https://doi.org/10.15376/biores.7.4.5109-5116

Chen, H., Ferrari, C., Angiuli, M., Yao, J., Raspi, C., & Bramanti, E. (2010). Qualitative and quantitative analysis of wood samples by Fourier transform infrared spectroscopy and multivariate analysis. *Carbohydrate Polymers, 82(3)*, 772–778. https://doi.org/10.1016/j.carbpol.2010.05.052

Chen, L., Wang, Q., Hirth, K., Baez, C., Agarwal, U. P., & Zhu, J. Y. (2015). Tailoring the yield and characteristics of wood cellulose nanocrystals (CNC) using concentrated acid hydrolysis. *Cellulose, 22(3)*, 1753–1762. https://doi.org/10.1007/s10570-015-0615-1

Chen, W.-H., Lin, B.-J., Lin, Y.-Y., Chu, Y.-S., Ubando, A. T., Show, P. L., Ong, H. C., Chang, J.-S., Ho, S.-H., Culaba, A. B., Pétrissans, A., & Pétrissans, M. (2021). Progress in biomass torrefaction: Principles, applications and challenges. *Progress in Energy and Combustion Science, 82*, 100887. https://doi.org/10.1016/j.pecs.2020.100887

Chen, Y., Liu, B., Yang, H., Yang, Q., & Chen, H. (2014). Evolution of functional groups and pore structure during cotton and corn stalks torrefaction and its correlation with hydrophobicity. *Fuel, 137*, 41–49. https://doi.org/10.1016/j.fuel.2014.07.036

Chin, K.L., Lee, C.L., H'ng, P.S., Rashid, U., Paridah, M.T., Khoo, P., Maminski, M. (2020). Refining micropore capacity of activated carbon derived from coconut shell via deashing post-treatment. *BioResources 15(4)*, 7749-7769.

Chowdhury, Z. K., Summers, R.S., Westerhoff, G.P., Leto, B.J., Nowack, K.O., Corwin, C.J. (2013). Chapter 4 – Activated carbon application approaches. In *Activated Carbon: Solutions for Improving Water Quality,* 31-72. American Water Works Association, Denver, Colorado, USA.

Collard, F.-X., & Blin, J. (2014). A review on pyrolysis of biomass constituents: Mechanisms and composition of the products obtained from the conversion of cellulose, hemicelluloses and lignin. *Renewable and Sustainable Energy Reviews, 38*, 594–608. https://doi.org/10.1016/j.rser.2014.06.013

Crittenden, J. C., Trussell, R.R., Hand, D.W., Howe, K.J. & Tchobanoglous, G. (2012). Chapter 15: Adsorption. In *MWH's Water Treatment: Principles and Design. (3rd ed.),* 1117-1263. John Wiley and Sons, Ltd., Hoboken, New Jersey, USA.

Danish, M., & Ahmad, T. (2018). A review on utilization of wood biomass as a sustainable precursor for activated carbon production and application. *Renewable and Sustainable Energy Reviews, 87*, 1–21. https://doi.org/10.1016/j.rser.2018.02.003

David Suzuki Foundation. (2017). *Glass half empty? Year 1 progress toward resolving drinking water advisories in nine First Nations in Ontario*. David Suzuki Foundation, Vancouver, British Columbia, CA. https://davidsuzuki.org/science-learning-centre-article/report-glass-half-empty-year-1-progress-toward-resolving-drinking-water-advisories-nine-first-nations-ontario/

Davoodbeygi, Y., Askari, M., Salehi, E., & Kheirieh, S. (2023). A review on hybrid membrane-adsorption systems for intensified water and wastewater treatment: Process configurations, separation targets, and materials applied. *Journal of Environmental Management, 335*, 117577. https://doi.org/10.1016/j.jenvman.2023.117577

De Oliveira Sampa, M. H., Rela, P. R., Casas, A. L., Mori, M. N., & Duarte, C. L. (2004). Treatment of industrial effluents using electron beam accelerator and adsorption with activated carbon: A comparative study. *Radiation Physics and Chemistry, 71(1–2)*, 459–462. Scopus. https://doi.org/10.1016/j.radphyschem.2004.03.023

Decker, K. C., & Long, B. W. (1992). Canada's cooperative approach to drinking water regulation. *American Water Works Association, 84(4)*, 120–28, https://doi.org/10.1002/j.1551-8833.1992.tb07337.x.

Delpla, I., Jung, A.-V., Baures, E., Clement, M., & Thomas, O. (2009). Impacts of climate change on surface water quality in relation to drinking water production. *Environment International, 35(8)*, 1225–1233. https://doi.org/10.1016/j.envint.2009.07.001

Demirbas, A. (2009). Agricultural based activated carbons for the removal of dyes from aqueous solutions: A review. *Journal of Hazardous Materials, 167(1)*, 1–9. https://doi.org/10.1016/j.jhazmat.2008.12.114

Diao, Y., Walawender, W. P., & Fan, L. T. (2002). Activated carbons prepared from phosphoric acid activation of grain sorghum. *Bioresource Technology, 81(1)*, 45–52. https://doi.org/10.1016/S0960-8524(01)00100-6

Dias, J. M., Alvim-Ferraz, M. C. M., Almeida, M. F., Rivera-Utrilla, J., & Sánchez-Polo, M. (2007). Waste materials for activated carbon preparation and its use in aqueous-phase treatment: A review. *Journal of Environmental Management, 85(4)*, 833–846. https://doi.org/10.1016/j.jenvman.2007.07.031

Dobele, G., Rossinskaja, G., Telysheva, G., Meier, D., & Faix, O. (1999). Cellulose dehydration and depolymerization reactions during pyrolysis in the presence of phosphoric acid. *Journal of Analytical and Applied Pyrolysis, 49(1)*, 307–317. https://doi.org/10.1016/S0165-2370(98)00126-0

El Qada, E. N., Allen, S. J., & Walker, G. M. (2008). Influence of preparation conditions on the characteristics of activated carbons produced in laboratory and pilot scale systems. *Chemical Engineering Journal, 142(1)*, 1–13. https://doi.org/10.1016/j.cej.2007.11.008

Fan, L. T., Lee, Y.-H., & Beardmore, D. H. (1980). Mechanism of the enzymatic hydrolysis of cellulose: Effects of major structural features of cellulose on enzymatic hydrolysis. *Biotechnology and Bioengineering, 22(1)*, 177–199. https://doi.org/10.1002/bit.260220113

Faust, S. D., & Aly, O. M. (1987a). Chapter 1 – Elements of surface chemistry. In *Adsorption Processes for Water Treatment,* 1-24. Butterworth Publishers, Stoneham, Massachusetts, USA.

Faust, S. D., & Aly, O. M. (1987b). Chapter 3 – Kinetics of Adsorption. In *Adsorption Processes for Water Treatment,* 65-122. Butterworth Publishers, Stoneham, Massachusetts, USA.

Faust, S. D., & Aly, O. M. (1987c). Chapter 5 – Physical and chemical properties of carbon. In *Adsorption Processes for Water Treatment*, 167-192. Butterworth Publishers, Stoneham, Massachusetts, USA.

Fengel, D., & Wegener, G. (1984a). Chapter 2 – Structure and ultrastructure. In *Wood: Chemistry, Ultrastructure, Reactions*, 6-25. W. de Gruyter, Berlin, DE.

Fengel, D., & Wegener, G. (1984b). Chapter 3 – Chemical composition and analysis of wood. In *Wood: Chemistry, Ultrastructure, Reactions*, 26-65. W. de Gruyter, Berlin, DE.

Fengel, D., & Wegener, G. (1984c). Chapter 3 – Cellulose. In *Wood: Chemistry, Ultrastructure, Reactions*, 66-105. W. de Gruyter, Berlin, DE.

Fengel, D., & Wegener, G. (1984d). Chapter 5 – Polyoses (hemicellulose). In *Wood: Chemistry, Ultrastructure, Reactions*, 106-131. W. de Gruyter, Berlin, DE.

Fengel, D., & Wegener, G. (1984e). Chapter 6 – Lignin. In *Wood: Chemistry, Ultrastructure, Reactions*, 132-181. W. de Gruyter, Berlin, DE.

Fengel, D., & Wegener, G. (1984f). Chapter 10 – Reactions in acidic medium. In *Wood: Chemistry, Ultrastructure, Reactions*, 268-295. W. de Gruyter, Berlin, DE.

Fengel, D., & Wegener, G. (1984g). Chapter 11 – Reactions in alkaline medium. In *Wood: Chemistry, Ultrastructure, Reactions*, 296-318. W. de Gruyter, Berlin, DE.

Fengel, D., & Wegener, G. (1984h). Chapter 12 – Influence of temperature. In *Wood: Chemistry, Ultrastructure, Reactions*, 319-343. W. de Gruyter, Berlin, DE.

Fitria, Ruan, H., Fransen, S. C., Carter, A. H., Tao, H., & Yang, B. (2019). Selecting winter wheat straw for cellulosic ethanol production in the Pacific Northwest, U.S.A. *Biomass and Bioenergy, 123*, 59–69. https://doi.org/10.1016/j.biombioe.2019.02.012

Flanagan, C. M. (2021). *Water Security on First Nations Reserves in Ontario: Exploring the Impact of Source Water Protection, Community Location, and Fiscal Capacity*, M.A. McGill University,

Montreal, Quebec, CA. https://www.proquest.com/docview/2652145851/abstract/A2ACB82237E14326PQ/1

Foo, P. Y. L., & Lee, L. Y. (2010). Preparation of activated carbon from Parkia speciosa pod by chemical activation. *Proceedings of the World Congress on Engineering and Computer Science 2010, Vol. II*, October 20-22, 2010. World Congress on Engineering and Computer Science, San Francisco, USA.

Franklin, R. E., & Randall, J. T. (1997). Crystallite growth in graphitizing and non-graphitizing carbons. Proceedings of the Royal Society of London. Series A. *Mathematical and Physical Sciences, 209(1097)*, 196–218. https://doi.org/10.1098/rspa.1951.0197

Ganjoo, R., Sharma, S., Kumar, A., & Daouda, M. M. A. (2023). Chapter 1 - Activated carbon: Fundamentals, classification, and properties. In *Activated Carbon: Progress and Applications*, 1-22. Royal Society of Chemistry, Piccadilly, London, UK. https://doi.org/10.1039/BK9781839169861-00001

Gao, X., Wu, L., Li, Z., Xu, Q., Tian, W., & Wang, R. (2018). Preparation and characterization of high surface area activated carbon from pine wood sawdust by fast activation with H3PO4 in a spouted bed. *Journal of Material Cycles and Waste Management, 20(2)*, 925–936. https://doi.org/10.1007/s10163-017-0653-x

Garrote, G., Domínguez, H., & Parajó, J. C. (1999). Hydrothermal processing of lignocellulosic materials. *Holz Als Roh- Und Werkstoff, 57(3)*, 191–202. https://doi.org/10.1007/s001070050039

Geczo, A., Giannakoudajis, D. A., Triantafyllidis, K., Elshaer, M. R., Rodriguez-Aguado, E., & Bashkova, S. (2020). Mechanistic insights into acetaminophen removal on cashew nut shell biomass-derived activated carbons. *Environmental Science and Pollution Research, 28,* 58969-58982. https://doi-org.proxy.bib.uottawa.ca/10.1007/s11356-019-07562-0

Georgiadis, A., Charisiou, N., & Goula, M. (2020). Removal of hydrogen sulfide from various industrial gases: a review of the most promising adsorbing materials. *Catalysts, 10(5)*, 521. https://doi.org/10.3390/catal10050521

Gobler, C. J. (2020). Climate change and harmful algal blooms: Insights and perspective. *Harmful Algae, 91*, 101731. https://doi.org/10.1016/j.hal.2019.101731

Gong, X.-J., Li, Y.-S., Dong, Y.-Q., & Li, W.-G. (2020). Arsenic adsorption by innovative iron/calcium in-situ-impregnated mesoporous activated carbons from low-temperature water and effects of the presence of humic acids. *Chemosphere, 250*, 126275. https://doi.org/10.1016/j.chemosphere.2020.126275

Government of Canada (2025a). *About drinking water advisories*. https://www.sac-isc.gc.ca/eng/1538160229321/1538160276874

Government of Canada. (2025b). *Drinking water advisories – Causes of boil water advisories*. https://open.canada.ca/data/en/dataset/0492d0f6-9d95-43e2-8db7-80751b18d6fc

Government of Canada. (2025c). *Map of long-term drinking water advisories on public systems on reserves.* https://sac-isc.gc.ca/eng/1620925418298/1620925434679

He, Z., Wang, Z., Zhao, Z., Yi, S., Mu, J., & Wang, X. (2017). Influence of ultrasound pretreatment on wood physiochemical structure. *Ultrasonics Sonochemistry, 34*, 136–141. https://doi.org/10.1016/j.ultsonch.2016.05.035

He, Z., Wang, Z., Qu, L., Qian, J., & Yi, S. (2019). Gaseous decomposition products from wood degradation via thermogravimetric and Fourier transform infrared analysis during thermal modification of beech and pine woods. *BioResources, 14(3)*, 6883–6894. https://doi.org/10.15376/biores.14.3.6883-6894

Ibrahim, R. H. H., Darvell, L. I., Jones, J. M., & Williams, A. (2013). Physicochemical characterisation of torrefied biomass. *Journal of Analytical and Applied Pyrolysis, 103*, 21–30. https://doi.org/10.1016/j.jaap.2012.10.004

Iroba, K. L., Soleimani, M., & Tabil, L. G. (2017). Chapter 14 - Compositional and structural modification of lignocellulosic biomass for biofuel production by alkaline treatment. *Biomass Preprocessing and Pretreatments for Production of Biofuels,* 384-412. CRC Press, Boca Raton, Florida, USA.

Jagtoyen, M., & Derbyshire, F. (1993). Some considerations of the origins of porosity in carbons from chemically activated wood. *Carbon, 31(7)*, 1185–1192. https://doi.org/10.1016/0008-6223(93)90071-H

Jeoh, T., Ishizawa, C. I., Davis, M. F., Himmel, M. E., Adney, W. S., & Johnson, D. K. (2007). Cellulase digestibility of pretreated biomass is limited by cellulose accessibility. *Biotechnology and Bioengineering, 98(1),* 112-122. https://doi.org/10.1002/bit.21408

Jiao, H., Guo, X., Shu, F., Zhang, Q., Wu, W., Jin, Y., & Jiang, B. (2025). Structure-property-function relationships of wood-based activated carbon in energy and environment materials. *Separation and Purification Technology, 353*, 128607. https://doi.org/10.1016/j.seppur.2024.128607

Jjagwe, J., Olupot, P. W., Menya, E., & Kalibbala, H. M. (2021). Synthesis and application of granular activated carbon from biomass waste materials for water treatment: A review. *Journal of Bioresources and Bioproducts, 6(4)*, 292–322. https://doi.org/10.1016/j.jobab.2021.03.003

Karthikeyan, T., Rajgopal, S., & Miranda, L. R. (2005). Chromium (VI) adsorption from aqueous solution by Hevea Brasilinesis sawdust activated carbon. *Journal of Hazardous Materials, 124(1–3)*, 192–199. Scopus. https://doi.org/10.1016/j.jhazmat.2005.05.003

Kemp, T. J. (2017). A brief 100 year history of carbon. *Science Progress, 100(3)*, 293–298. https://doi.org/10.3184/003685017X14994318577435

Kim, A., & Kim, N.-H. (2019). Effect of heat treatment and particle size on the crystalline properties of wood cellulose. *Journal of the Korean Wood Science and Technology, 47(3)*, 299–310. https://doi.org/10.5658/WOOD.2019.47.3.299

Kim, J.H., Jung, S.C., Lee, H.M., & Kim, B.J. (2022). Comparison of pore structures of cellulose-based activated carbon fibers and their applications for electrode materials. *International Journal of Molecular Sciences, 23(7)*, Article 7. https://doi.org/10.3390/ijms23073680

Kim, J. S., Lee, Y. Y., & Kim, T. H. (2016). A review on alkaline pretreatment technology for bioconversion of lignocellulosic biomass. *Bioresource Technology, 199*, 42–48. https://doi.org/10.1016/j.biortech.2015.08.085

Kim, T. H. (2021). Chapter 6 - Pretreatment of lignocellulosic biomass. In *Bioprocessing Technologies in Biorefinery for Sustainable Production of Fuels, Chemicals, and Polymers*, 91–110. John Wiley & Sons Ltd., Chichester, UK. https://doi.org/10.1002/9781118642047.ch6

Kota, K. B., Shenbagaraj, S., Sharma, P. K., Sharma, A. K., Ghodke, P. K., & Chen, W.-H. (2022). Biomass torrefaction: An overview of process and technology assessment based on global readiness level. *Fuel, 324*, 124663. https://doi.org/10.1016/j.fuel.2022.124663

Koutsianitis, D., Mitani, C., Giagli, K., Tsalagkas, D., Halász, K., Kolonics, O., Gallis, C., & Csóka, L. (2015). Properties of ultrasound extracted bicomponent lignocellulose thin films. *Ultrasonics Sonochemistry, 23*, 148–155. https://doi.org/10.1016/j.ultsonch.2014.10.014

Kozhevnikov, A. B. (2004). *Stalin's Great Science: The Times and Adventures of Soviet Physicists*. Imperial College Press, London, UK.

Kumar, A., & Jena, H. M. (2016). Preparation and characterization of high surface area activated carbon from Fox nut (Euryale ferox) shell by chemical activation with H3PO4. *Results in Physics, 6*, 651–658. https://doi.org/10.1016/j.rinp.2016.09.012

Kumar, S., Gupta, R., Lee, Y. Y., & Gupta, R. B. (2010). Cellulose pretreatment in subcritical water: Effect of temperature on molecular structure and enzymatic reactivity. *Bioresource Technology, 101(4)*, 1337–1347. https://doi.org/10.1016/j.biortech.2009.09.035

Lee, H. V., Yazid, N. A., & Bin Johan, M. R. (2024). Chapter two - Cellulose and hemicellulose: Types, cleavage, and depolymerization. In *Advances in Hydrotreating for Integrated Biofuel Production,* 51–75. Elsevier, Amsterdam, NL. https://doi.org/10.1016/B978-0-443-19076-6.00003-0

Li, M., Cao, S., Meng, X., Studer, M., Wyman, C. E., Ragauskas, A. J., & Pu, Y. (2017). The effect of liquid hot water pretreatment on the chemical–structural alteration and the reduced recalcitrance in poplar. *Biotechnology for Biofuels, 10(1)*, 237. https://doi.org/10.1186/s13068-017-0926-6

Lim, W. C., Srinivasakannan, C., & Al Shoaibi, A. (2015). Cleaner production of porous carbon from palm shells through recovery and reuse of phosphoric acid. *Journal of Cleaner Production, 102*, 501–511. https://doi.org/10.1016/j.jclepro.2015.04.100

Lobo, K. (2025). Chapter 4 – Materials and Methods. *Sustainable Pre-Treatments for White Spruce Wood-Based Activated Carbon: Impact on Porosity and Aqueous-Phase Adsorption [Unpublished Master of Applied Science Thesis]*, 58-91. University of Ottawa, Ottawa, Ontario, CA.

Lourenço, A., Araújo, S., Gominho, J., & Evtuguin, D. (2020). Cellulose structural changes during mild torrefaction of Eucalyptus wood. *Polymers, 12(12)*, 1–17. https://doi.org/10.3390/polym12122831

Lu, X., & Gu, X. (2022). A review on lignin pyrolysis: Pyrolytic behavior, mechanism, and relevant upgrading for improving process efficiency. *Biotechnology for Biofuels and Bioproducts, 15(106)*, 1-43. https://doi.org/10.1186/s13068-022-02203-0

Lu, H., Liu, S., Zhang, M., Meng, F., Shi, X., & Yan, L. (2016). Investigation of the strengthening process for liquid hot water pretreatments. *Energy & Fuels, 30(2)*, 1103–1108. https://doi.org/10.1021/acs.energyfuels.5b02658

Luo, Y., Li, D., Chen, Y., Sun, X., Cao, Q., & Liu, X. (2019). The performance of phosphoric acid in the preparation of activated carbon-containing phosphorus species from rice husk residue. *Journal of Materials Science, 54(6)*, 5008–5021. https://doi.org/10.1007/s10853-018-03220-x

Lv, P., Almeida, G., & Perre, P. (2015). TGA-FTIR analysis of torrefaction of lignocellulosic components (cellulose, xylan, lignin) in isothermal conditions over a wide range of time durations. *BioResources 10(3)*, 4239-4251. https://bioresources.cnr.ncsu.edu/

Lv, Y., Zhang, Y., & Xu, Y. (2024). Understanding and technological approach of acid hydrolysis processing for lignocellulose biorefinery: Panorama and perspectives. *Biomass and Bioenergy, 183*, 107133. https://doi.org/10.1016/j.biombioe.2024.107133

Maeda, M., Ito, T., Hori, M., & Johansson, G. (1996). The structure of zinc chloride complexes in aqueous solution. *Zeitschrift Für Naturforschung A, 51(1–2)*, 63–70. https://doi.org/10.1515/zna-1996-1-210

Mankar, A. R., Pandey, A., Modak, A., & Pant, K. K. (2021). Pretreatment of lignocellulosic biomass: A review on recent advances. *Bioresource Technology, 334*, 125235. https://doi.org/10.1016/j.biortech.2021.125235

Mansour, F., Al-Hindi, M., Yahfoufi, R., Ayoub, G. M., & Ahmad, M. N. (2018). The use of activated carbon for the removal of pharmaceuticals from aqueous solutions: A review. *Reviews in Environmental Science and Biotechnology, 17(1)*, 109–145. https://doi.org/10.1007/s11157-017-9456-8

Marsh, H., & Rodríguez-Reinoso, F. (2006a). Chapter 2 – Activated carbon (origins). In *Activated Carbon*, 13-86. Elsevier Science Ltd., Amsterdam, NL. https://doi.org/10.1016/B978-008044463-5/50016-9

Marsh, H., & Rodríguez-Reinoso, F. (2006b). Chapter 4 – Characterization of activated carbon. In *Activated Carbon*, 142-242. Elsevier Science Ltd., Amsterdam, NL. https://doi.org/10.1016/B978-008044463-5/50018-2

Marsh, H., & Rodríguez-Reinoso, F. (2006c). Chapter 5 – Activation processes (Thermal or physical). In *Activated Carbon*, 243-321. Elsevier Science Ltd., Amsterdam, NL. https://doi.org/10.1016/B978-008044463-5/50019-4

Marsh, H., & Rodríguez-Reinoso, F. (2006d). Chapter 6 – Activation processes (Chemical). In *Activated Carbon*, 322-365. Elsevier Science Ltd., Amsterdam, NL. https://doi.org/10.1016/B978-008044463-5/50020-0

Maurya, D. P., Singla, A., & Negi, S. (2015). An overview of key pretreatment processes for biological conversion of lignocellulosic biomass to bioethanol. *Biotech, 5(5)*, 597–609. https://doi.org/10.1007/s13205-015-0279-4

Molina-Sabio, M., Rodríguez-Reinoso, F., Caturla, F., & Sellés, M. J. (1995). Porosity in granular carbons activated with phosphoric acid. *Carbon, 33(8)*, 1105–1113. https://doi.org/10.1016/0008-6223(95)00059-M

Molina-Sabio, M., & Rodríguez-Reinoso, F. (2004). Role of chemical activation in the development of carbon porosity. *Colloids and Surfaces A: Physicochemical and Engineering Aspects, 241(1–3)*, 15–25. https://doi.org/10.1016/j.colsurfa.2004.04.007

Morales-delaRosa, S., Campos-Martin, J. M., & Fierro, J. L. G. (2014). Optimization of the process of chemical hydrolysis of cellulose to glucose. *Cellulose, 21(4)*, 2397–2407. https://doi.org/10.1007/s10570-014-0280-9

Mosier, N., Wyman, C., Dale, B., Elander, R., Lee, Y., Holtzapple, M., & Ladisch, M. (2005). Features of promising technologies for pretreatment of lignocellulosic biomass. *Bioresource Technology, 96(6)*, 673–686. https://doi.org/10.1016/j.biortech.2004.06.025

Nelson, M. L., & Conrad, C. M. (1948). Effect of grinding on the crystallinity of cellulose fibers, as indicated by the acid-hydrolysis and other techniques. *Textile Research Journal, 18(3)*, 155-164 https://journals-sagepub-com.proxy.bib.uottawa.ca/doi/abs/10.1177/004051754801800303

Neme, I., Gonfa, G., & Masi, C. (2022). Activated carbon from biomass precursors using phosphoric acid: A review. *Heliyon, 8(12)*, e11940. https://doi.org/10.1016/j.heliyon.2022.e11940

Ni, X., Cen, K., Li, X., Cui, D., Liu, M., Zhu, L., & Chen, D. (2025). Cellulose upgradation by torrefaction pretreatment and effect of torrefaction severity on the quality of pyrolysis products. *Industrial Crops and Products, 225*, 120516. https://doi.org/10.1016/j.indcrop.2025.120516

Nienstaedt, H., & Zasada, J. C. (1990). *Picea glauca (Moench) Voss*. https://www.srs.fs.usda.gov/pubs/misc/ag_654/volume_1/picea/glauca.htm

Niu, Y., Lv, Y., Lei, Y., Liu, S., Liang, Y., Wang, D., & Hui, S. (2019). Biomass torrefaction: Properties, applications, challenges, and economy. *Renewable and Sustainable Energy Reviews, 115*, 109395. https://doi.org/10.1016/j.rser.2019.109395

Office of the Parliamentary Budget Officer (2017). *Budget sufficiency for First Nations water and wastewater infrastructure*. https://publications.gc.ca/site/eng/9.848771/publication.html

Oginni, O., Singh, K., Oporto, G., Dawson-Andoh, B., McDonald, L., & Sabolsky, E. (2019). Effect of one-step and two-step H3PO4 activation on activated carbon characteristics. Bioresource Technology Reports, 8, 100307. https://doi.org/10.1016/j.biteb.2019.100307

Özgenç, Ö., Durmaz, S., Boyaci, I. H., & Eksi-Kocak, H. (2017). Determination of chemical changes in heat-treated wood using ATR-FTIR and FT Raman spectrometry. *Spectrochimica Acta Part A: Molecular and Biomolecular Spectroscopy, 171*, 395–400. https://doi.org/10.1016/j.saa.2016.08.026

Paredes, J. J., Jara, R., Shaler, S. M., & van Heiningen, A. (2008). Influence of hot water extraction on the physical and mechanical behavior of OSB. *Forest Products Journal, 58(12),* 56-62.

Park, M., Wu, S., Lopez, I. J., Chang, J. Y., Karanfil, T., & Snyder, S. A. (2020). Adsorption of perfluoroalkyl substances (PFAS) in groundwater by granular activated carbons: Roles of hydrophobicity of PFAS and carbon characteristics. *Water Research, 170*, 115364. https://doi.org/10.1016/j.watres.2019.115364

Pelaez-Samaniego, M. R., Yadama, V., Lowell, E., & Espinoza-Herrera, R. (2013). A review of wood thermal pretreatments to improve wood composite properties. *Wood Science and Technology, 47(6)*, 1285–1319. https://doi.org/10.1007/s00226-013-0574-3

Pfriem, A., Zauer, M., & Wagenführ, A. (2009). Alteration of the pore structure of spruce (Picea abies (L.) Karst.) and maple (Acer pseudoplatanus L.) due to thermal treatment as determined by helium pycnometry and mercury intrusion porosimetry. *Holzforschung 63(1)*, 94–98. https://doi.org/10.1515/HF.2009.027

Pivokonsky, M., Kopecka, I., Cermakova, L., Fialova, K., Novotna, K., Cajthaml, T., Henderson, R. K., & Pivokonska, L. (2021). Current knowledge in the field of algal organic matter adsorption onto activated carbon in drinking water treatment. *Science of The Total Environment, 799*, 149455. https://doi.org/10.1016/j.scitotenv.2021.149455

Prieto, M.J., Ellis, G., Budarin, V., Morales, E., Naffakh, M., & S. Shuttleworth, P. (2024). Understanding pore size relation in cellulose-derived, nitrogen-doped, hydrothermal carbons for improved supercapacitor performance. *Journal of Materials Chemistry, 12(43)*, 29698–29707. https://doi.org/10.1039/D4TA04477K

Qi, Y., Zhou, Z., Xu, R., Dong, Y., Zhang, Z., & Liu, M. (2023). Effect of NaOH pretreatment on permeability and surface properties of three wood species. *ACS Omega, 8(43)*, 40362–40374. https://doi.org/10.1021/acsomega.3c04745

Rehman, M. M., Zeeshan, M., Shaker, K., & Nawab, Y. (2019). Effect of micro-crystalline cellulose particles on mechanical properties of alkaline treated jute fabric reinforced green epoxy composite. *Cellulose, 26(17)*, 9057–9069. https://doi.org/10.1007/s10570-019-02679-4

Rissanen, J. V., Murzin, D. Yu., Salmi, T., & Grénman, H. (2016). Aqueous extraction of hemicelluloses from spruce – From hot to warm. *Bioresource Technology, 199*, 279–282. https://doi.org/10.1016/j.biortech.2015.08.116

Rodríguez-Reinoso, F., Molina-Sabio, M., & González, M. T. (1995). The use of steam and CO2 as activating agents in the preparation of activated carbons. *Carbon, 33(1)*, 15–23. https://doi.org/10.1016/0008-6223(94)00100-E

Rouquerol, J., Avnir, D., Fairbridge, C. W., Everett, D. H., Haynes, J. M., Pernicone, N., Ramsay, J. D. F., Sing, K. S. W., & Unger, K. K. (1994). Recommendations for the characterization of porous solids (Technical Report). *Pure and Applied Chemistry, 66(8)*, 1739–1758. https://doi.org/10.1351/pac199466081739

Rowell, R. M., Pettersen, R., & Tshabalala, M. A. (2012). Chapter 3 – Cell wall chemistry. In *Cell Wall Chemistry,* 34-70. Taylor & Francis, Oxfordshire, USA. https://www-taylorfrancis-com.proxy.bib.uottawa.ca/reader/download/55e8474f-5952-4c3a-8d36-4180507f1834/chapter/pdf?context=ubx

Ruhl, A. S., Altmann, J., Zietzschmann, F., Meinel, F., Sperlich, A., & Jekel, M. (2014). Integrating micro-pollutant removal by powdered activated carbon into deep bed filtration. *Water, Air, & Soil Pollution, 225(3)*, 1877. https://doi.org/10.1007/s11270-014-1877-1

Saha, B. C. (2003). Hemicellulose bioconversion. *Journal of Industrial Microbiology and Biotechnology, 30(5)*, 279–291. Scopus. https://doi.org/10.1007/s10295-003-0049-x

Santos, C. C., de Souza, W., Sant ’Anna, C., & Brienzo, M. (2018). Elephant grass leaves have lower recalcitrance to acid pretreatment than stems, with higher potential for ethanol production. *Industrial Crops and Products, 111*, 193–200. https://doi.org/10.1016/j.indcrop.2017.10.013

Sarko, A., & Muggli, R. (1974). Packing analysis of carbohydrates and polysaccharides. III Valonia Cellulose and Cellulose II. *Macromolecules, 7(4)*, 486–494. https://doi.org/10.1021/ma60040a016

Scherrer, P. (1918). Bestimmung der größe und der inneren struktur von kolloidteilchen mittels röntgenstrahlen. *Nachrichten von der Gesellschaft der Wissenschaften zu Göttingen. Mathematisch-Physikalische Klasse, 1918*, 98–100.

Segal, L., Creely, L. L., Martin Jr., A. E., & Conrad, C. M. (1959). An empirical method for estimating the degree of crystallinity of native cellulose using the X-Ray diffractometer. *Textile Research Journal, 29(10)*, 786-794. https://doi-org.proxy.bib.uottawa.ca/10.1177/004051755902901003

Seidel, H.F. (1985). Water utility operating data: An analysis. *Journal AWWA (77)*, 34-41. https://awwa-onlinelibrary-wiley-com.proxy.bib.uottawa.ca/doi/10.1002/j.1551-8833.1985.tb05536.x

Sharma, V., Yadav, J., Kumar, R., Tesarova, D., Ekielski, A., & Mishra, P. K. (2020). On the rapid and non-destructive approach for wood identification using ATR-FTIR spectroscopy and chemometric methods. *Vibrational Spectroscopy, 110*, 103097. https://doi.org/10.1016/j.vibspec.2020.103097

Sigma-Aldrich (2025a) *Phosphoric acid solution*. Sigma-Aldrich. https://www.sigmaaldrich.com/CA/en/search/phosphoric-acid-solutioon?focus=products&page=1&perpage=30&sort=relevance&term=phosphoric%20acid%20solutioon&type=product

Sigma-Aldrich. (2025b) *Zinc chloride solution*. Sigma-Aldrich. https://www.sigmaaldrich.com/CA/en/search/zinc-chloride-solution?focus=products&page=1&perpage=30&sort=relevance&term=zinc%20chloride%20solution&type=product

Sontheimer, H., Crittenden, J.C., & Summers, R.S. (1988a). Chapter 1: Water treatment through adsorption processes. In *Activated Carbon for Water Treatment (2nd ed.),* 1-49. DVGW-Forschungsstelle, Engler-Bunte-Institut, Universität Karlsruhe, Karlsruhe, DE.

Sontheimer, H., Crittenden, J.C., & Summers, R.S. (1988b). Chapter 2: The production and physical-chemical evaluation of activated carbon. In *Activated Carbon for Water Treatment (2nd ed.),* 51-103. DVGW-Forschungsstelle, Engler-Bunte-Institut, Universität Karlsruhe, Karlsruhe, DE.

Sontheimer, H., Crittenden, J.C., & Summers, R.S. (1988c). Chapter 3: Description of adsorption equilibria. In *Activated Carbon for Water Treatment (2nd ed.),* 106-237. DVGW-Forschungsstelle, Engler-Bunte-Institut, Universität Karlsruhe, Karlsruhe, DE.

Suffet, I. H. (Mel), Corado, A., Chou, D., McGuire, M. J., & Butterworth, S. (1996). AWWA taste and odor survey. *Journal AWWA, 88(4)*, 168–180. https://doi.org/10.1002/j.1551-8833.1996.tb06542.x

Svoboda, K., Pohořelý, M., Hartman, M., & Martinec, J. (2009). Pretreatment and feeding of biomass for pressurized entrained flow gasification. *Fuel Processing Technology, 90(5)*, 629–635. https://doi.org/10.1016/j.fuproc.2008.12.005

Sych, N. V., Trofymenko, S. I., Poddubnaya, O. I., Tsyba, M. M., Sapsay, V. I., Klymchuk, D. O., & Puziy, A. M. (2012). Porous structure and surface chemistry of phosphoric acid activated carbon from corncob. *Applied Surface Science, 261*, 75–82. https://doi.org/10.1016/j.apsusc.2012.07.084

Tchobanoglous, G., Burton, F. L., & Stensel, H. D. (2003). *Wastewater engineering: Treatment and reuse*. McGraw-Hill, Boston, Massachusetts, USA. http://archive.org/details/wastewaterengine0000unse

The Canadian Press. (2025). *Unsafe tap water is common in Newfoundland. This town just overcame a 1989 boil order.* CTVNews, Toronto, Ontario, CA. https://www.ctvnews.ca/canada/article/unsafe-tap-water-is-common-in-newfoundland-this-town-just-overcame-a-1989-boil-order/

Thermo-Fisher Scientific (2021) *269-2775—Nicolet iS50 ATR Module User Guide*, Thermo Fisher Scientific, Madison, Wisconsin, USA, 24-25.

USEPA (2025). *Summary of cyanotoxins treatment in drinking water.* USEPA, Washington, D.C., USA. https://www.epa.gov/ground-water-and-drinking-water/summary-cyanotoxins-treatment-drinking-water

USEPA (2018). *Reducing PFAS in Drinking Water with Treatment*. USEPA, Washington, D.C., USA. https://www.epa.gov/sciencematters/reducing-pfas-drinking-water-treatment-technologies

Vermeulen, T. (1958). Separation by Adsorption Methods. In *Advances in Chemical Engineering (Vol. 2),* 147-208. Academic Press, New York, New York, USA. https://doi.org/10.1016/S0065-2377(08)60228-8

Wan, J., Wang, Y., & Xiao, Q. (2010). Effects of hemicellulose removal on cellulose fiber structure and recycling characteristics of eucalyptus pulp. *Bioresource Technology, 101(12)*, 4577–4583. https://doi.org/10.1016/j.biortech.2010.01.026

Wang, Z., Chen, Z., & An, C. (2023). A review on solid waste management in Canadian First Nations communities: Policy, practices, and challenges. *Cleaner Waste Systems, 4*, 100074. https://doi.org/10.1016/j.clwas.2022.100074

Warade, H., Mukwane, S., Ansari, K., Agrawal, D., Asaithambi, P., Eyvaz, M., & Yusuf, M. (2025). Enhancing biogas generation: A comprehensive analysis of pre-treatment strategies for Napier grass in anaerobic digestion. *Discover Materials, 5(1)*, 1–30. https://doi.org/10.1007/s43939-025-00211-z

Woiciechowski, A.L., Dalmas Neto, C. J., Porto de Souza Vandenberghe, L., de Carvalho Neto, D. P., Novak Sydney, A. C., Letti, L. A. J., Karp, S. G., Zevallos Torres, L. A., & Soccol, C. R. (2020). Lignocellulosic biomass: Acid and alkaline pretreatments and their effects on biomass recalcitrance – Conventional processing and recent advances. *Bioresource Technology, 304*, 122848. https://doi.org/10.1016/j.biortech.2020.122848

Wu, F.-C., & Tseng, R.-L. (2006). Preparation of highly porous carbon from fir wood by KOH etching and CO2 gasification for adsorption of dyes and phenols from water. *Journal of Colloid and Interface Science, 294(1)*, 21–30. Scopus. https://doi.org/10.1016/j.jcis.2005.06.084

Xiao, R., Deng, Y., Xu, Z., & Chu, W. (2024). Disinfection byproducts and their precursors in drinking water sources: Origins, influencing factors, and environmental insights. *Engineering, 36*, 36–50. https://doi.org/10.1016/j.eng.2023.08.017

Xue, Z. H., Xie, Y. H., & Zhu, H. Z. (2013). The effect of alkali treatment on wood crystalline structure and micro-structural model. *Applied Mechanics and Materials, 423–426*, 1339–1343. https://doi.org/10.4028/www.scientific.net/AMM.423-426.1339

Yakout, S. M., & Sharaf El-Deen, G. (2016). Characterization of activated carbon prepared by phosphoric acid activation of olive stones. *Arabian Journal of Chemistry, 9*, S1155–S1162. https://doi.org/10.1016/j.arabjc.2011.12.002

Yang, H., Yan, R., Chen, H., Lee, D. H., & Zheng, C. (2007). Characteristics of hemicellulose, cellulose and lignin pyrolysis. *Fuel, 86(12)*, 1781–1788. https://doi.org/10.1016/j.fuel.2006.12.013

Yang, X., Wan, Y., Zheng, Y., He, F., Yu, Z., Huang, J., Wang, H., Ok, Y. S., Jiang, Y., & Gao, B. (2019). Surface functional groups of carbon-based adsorbents and their roles in the removal of heavy metals from aqueous solutions: A critical review. *Chemical Engineering Journal, 366*, 608–621. https://doi.org/10.1016/j.cej.2019.02.119

Yorgun, S., & Yıldız, D. (2015). Preparation and characterization of activated carbons from Paulownia wood by chemical activation with H3PO4. *Journal of the Taiwan Institute of Chemical Engineers, 53*, 122–131. https://doi.org/10.1016/j.jtice.2015.02.032

Young, G., & Funderlic, R. E. (1973). On the grain boundary diffusion theory of Fisher and Whipple. *Journal of Applied Physics, 44(11)*, 5151–5154. https://doi.org/10.1063/1.1662107

Yu, Y., Pei, W., Zhao, X., Cárdenas-Oscanoa, A. J., & Huang, C. (2025). Global evolution of research on autohydrolysis (hydrothermal) pretreatment as a green technology for biorefineries: A bibliometric analysis. *Journal of Bioresources and Bioproducts, 10(1)*, 92–110. https://doi.org/10.1016/j.jobab.2024.12.002

Yue, P., Hu, Y., Tian, R., Bian, J., & Peng, F. (2022). Hydrothermal pretreatment for the production of oligosaccharides: A review. *Bioresource Technology, 343*, 126075. https://doi.org/10.1016/j.biortech.2021.126075

Zhang, Y., Gao, Y., Zhao, M., Feng, X., Wang, L., Yang, H., Ma, H., & Zhou, J. (2021). Effects of torrefaction on the lignin of apricot shells and its catalytic conversion to aromatics. *ACS Omega, 6(39)*, 25742–25748. https://doi.org/10.1021/acsomega.1c04095

Zhang, J., Duan, C., Huang, X., Meng, M., Li, Y., Huang, H., Wang, H., Yan, M., & Tang, X. (2024). A review on research progress and prospects of agricultural waste-based activated carbon: Preparation, application, and source of raw materials. *Journal of Materials Science, 59(13)*, 5271–5292. https://doi.org/10.1007/s10853-024-09526-3

Zheng, Z., Lin, Q., Gao, Y., Ji, X., Sessler, J. L., & Wang, H. (2024). Recent advances in iodine adsorption from water. *Coordination Chemistry Reviews, 511*, 215860. https://doi.org/10.1016/j.ccr.2024.215860

Zhu, Y., Gao, J., Li, Y., Sun, F., Gao, J., Wu, S., & Qin, Y. (2012). Preparation of activated carbons for SO2 adsorption by CO2 and steam activation. *Journal of the Taiwan Institute of Chemical Engineers, 43(1)*, 112–119. https://doi.org/10.1016/j.jtice.2011.06.009

Zhuang, X., Wang, W., Song, B., & Yu, Q. (2021). Liquid hot water pretreatment for lignocellulosic biomass biorefinery. *Emerging Technologies for Biorefineries, Biofuels, and Value-Added Commodities (pp. 81–109)*. Springer International Publishing. https://doi.org/10.1007/978-3-030-65584-6_4

Zuo, S., Liu, J., Yang, J., & Cai, X. (2009). Effects of the crystallinity of lignocellulosic material on the porosity of phosphoric acid-activated carbon. *Carbon, 47(15)*, 3578–3580. https://doi.org/10.1016/j.carbon.2009.08.026

Appendix A – Supplementary Data: Apparent Density of Wood Blocks

Preliminary tests were performed for HPT and APT wherein different PT durations were used on groups of ten 30 x 15 x 15 mm wood block samples. These tests were carried out to identify a treatment duration under which the apparent density of the wood samples would be impacted consistently. The results for HPT and APT are shown in Table A-1 and Table A-2, respectively.

Table A-1. Reduction in apparent density of 30 x 15 x 15 mm wood block samples under different Hydrothermal Pre-Treatment times.

Duration (h)	95% Low (%)	Average, μ (%)	95% High (%)
0.5	- 0.008	0.007	0.022
1	- 0.021	0.313	0.647
2	1.445	1.482	1.520

Table A-2. Reduction in apparent density of 30 x 15 x 15 mm wood block samples under different Alkaline Pre-Treatment times.

Duration (h)	95% Low (%)	Average, μ (%)	95% High (%)
0.5	- 0.009	0.563	1.135
1	0.238	0.313	2.125
2	3.942	4.172	4.402

Based on these results, treatment durations of two hours were carried forward in the study for both HPT and APT. The complete statistical parameters for the two-hour apparent density tests are shown in Table A-3.

Table A-3. Statistical analysis parameters for the reduction in apparent density of 30 x 15 x 15 mm wood block samples under two hours of treatment.

Pre-Treatment	Variance, σ^2	Standard Deviation, σ	+/-, $\sigma/\sqrt{N} \cdot 2.262$	95% Low	Average, μ (%)	95% High
TPT	0.04396	0.210	0.066	1.400	1.466	1.532
HPT	0.01418	0.119	0.038	1.445	1.482	1.520
APT	0.52937	0.728	0.230	3.942	4.172	4.402

Appendix B – Supplementary Data: X-Ray Diffraction – Mean Size of Cellulose Crystallites and Crystallinity Index

Table B-1. Parameters used in the calculation of the Mean Size of Cellulose Crystallites.

Parameter	TPT		HPT		APT	
	Before	**After**	**Before**	**After**	**Before**	**After**
B (radians)	0.0491	0.0502	0.0488	0.0481	0.0578	0.5260
Θ_B (radians)	0.3874	0.3877	0.3870	0.3901	0.3863	0.3894
T (nm)	3.187	3.121	3.210	3.260	2.706	2.979

Table B-2. Parameters used in the calculation of the Crystallinity Index.

Parameter	TPT		HPT		APT	
	Before	**After**	**Before**	**After**	**Before**	**After**
I_{002}	5635	9638	5888	8055	16551	15018
I_{am}	1875	2971	1957	2384	6101	5031
CrI	66.7	69.2	66.8	70.4	63.1	66.5

Appendix C – Supplementary Data: Thermogravimetric Analysis and Fourier Transform -Infrared Spectroscopy of Produced Off-Gases

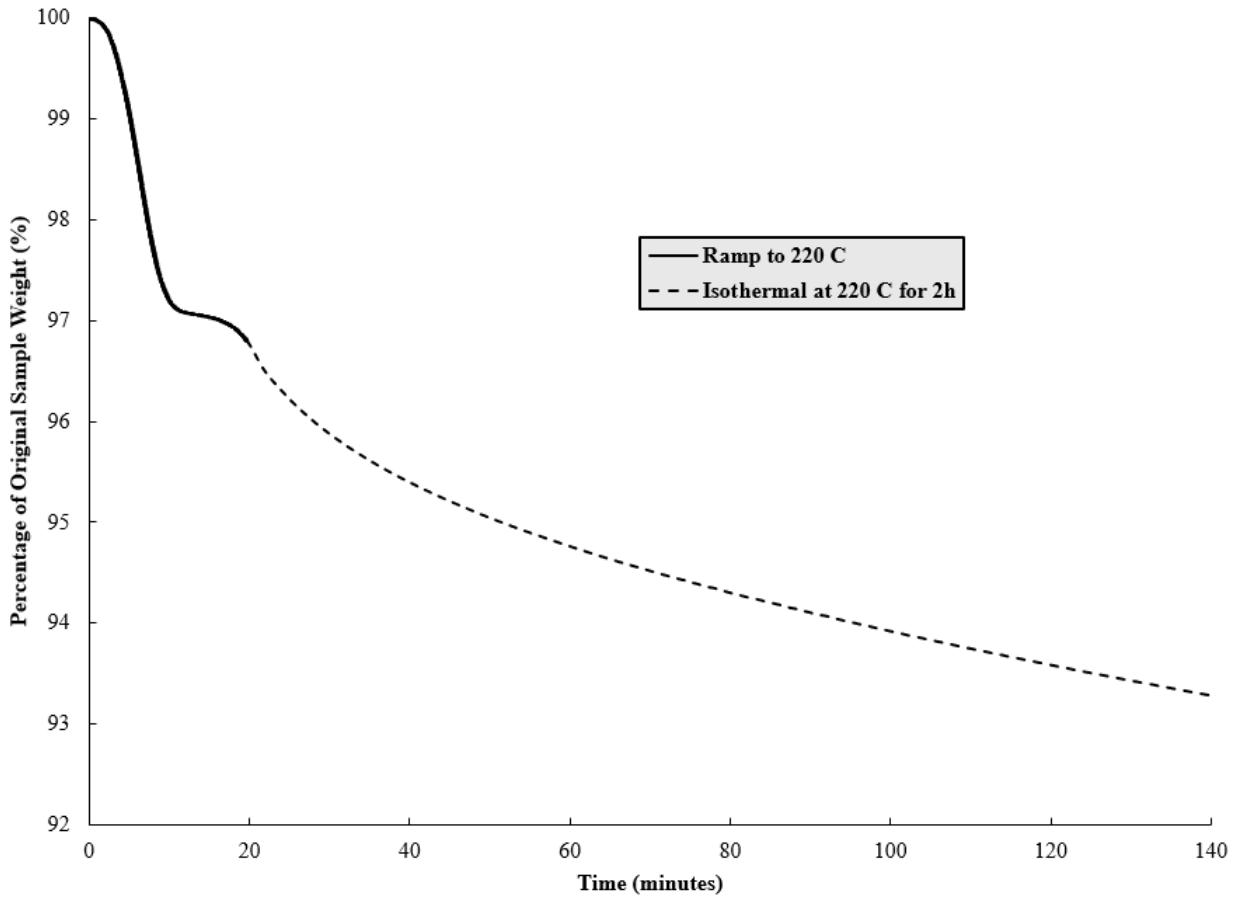

Figure C-1. Thermogravimetric analysis of Torrefaction Pre-Treatment process.

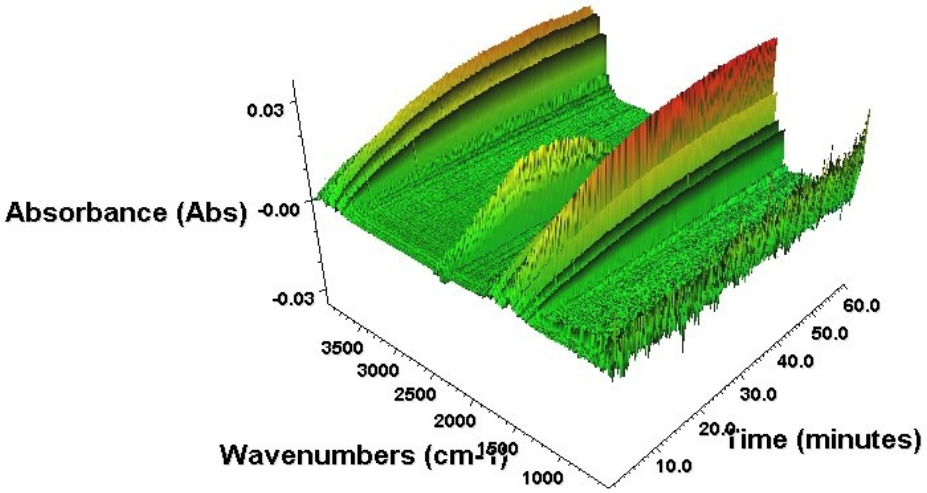

Figure C-2. Fourier Transform – Infrared Spectroscopy of off-gases produced during the Torrefaction Pre-Treatment of 5 x 5 x 2 mm sample.

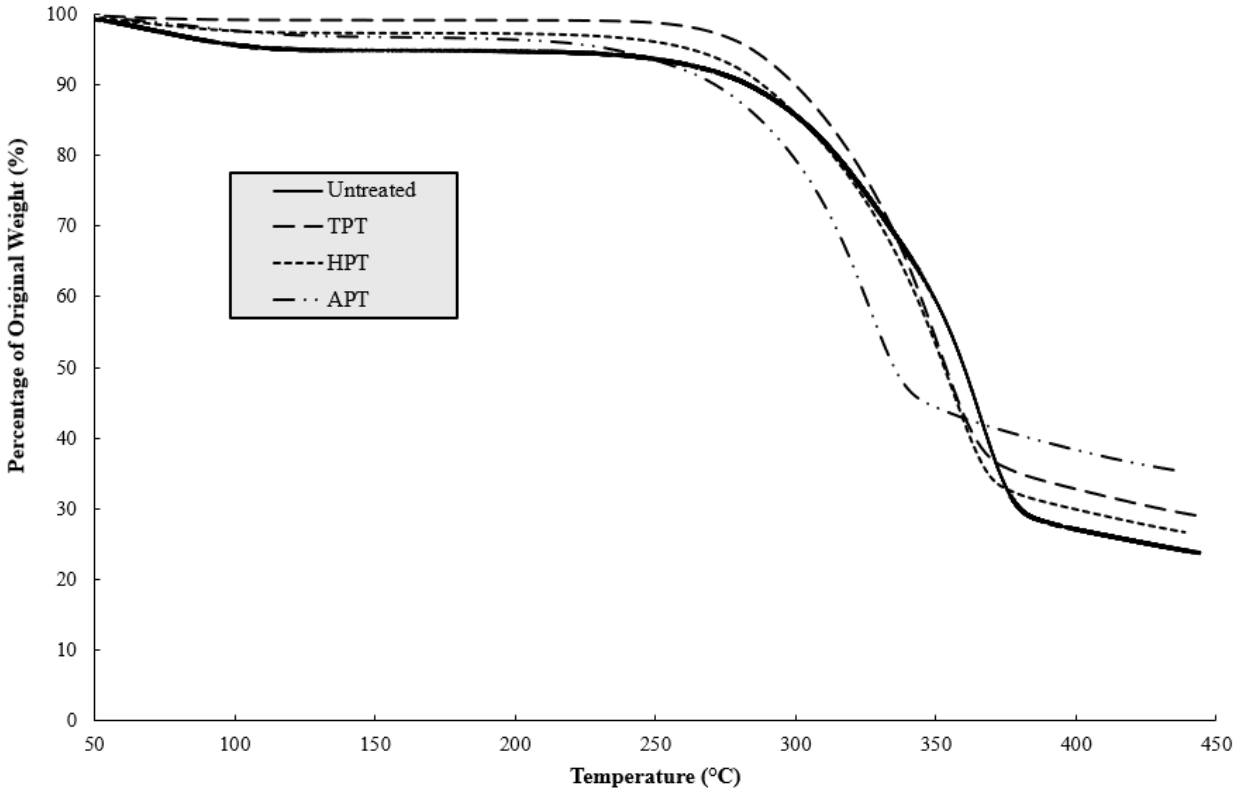

Figure C-3. Thermogravimetric analysis of Untreated and Pre-Treated, dry samples.

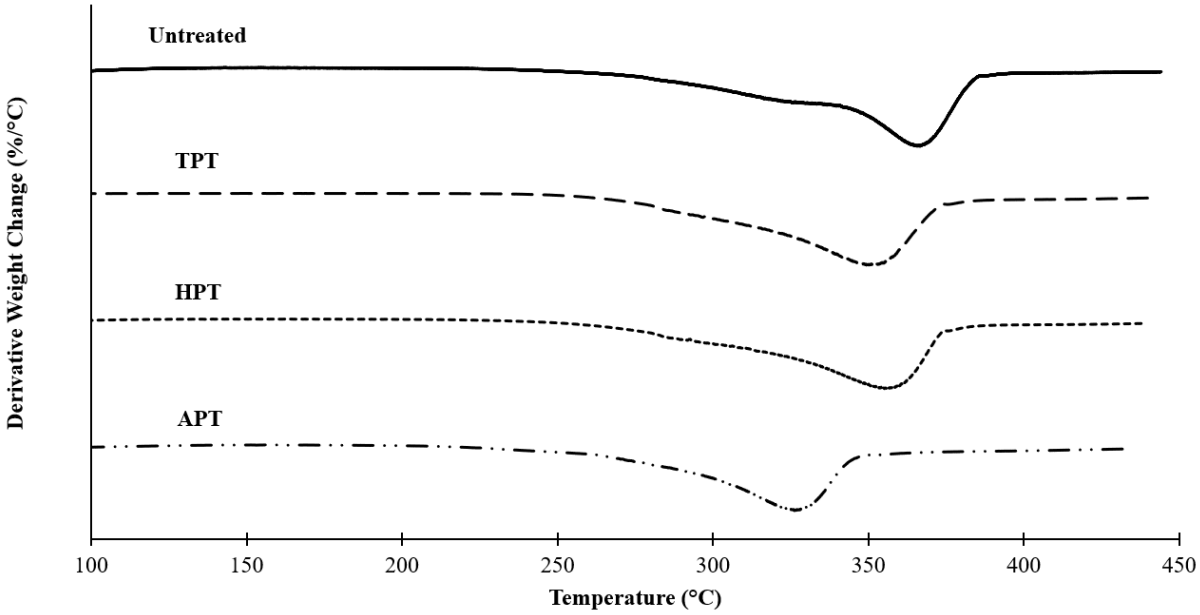

Figure C-4. Differential thermogravimetric analysis of Untreated and Pre-Treated, dry samples.

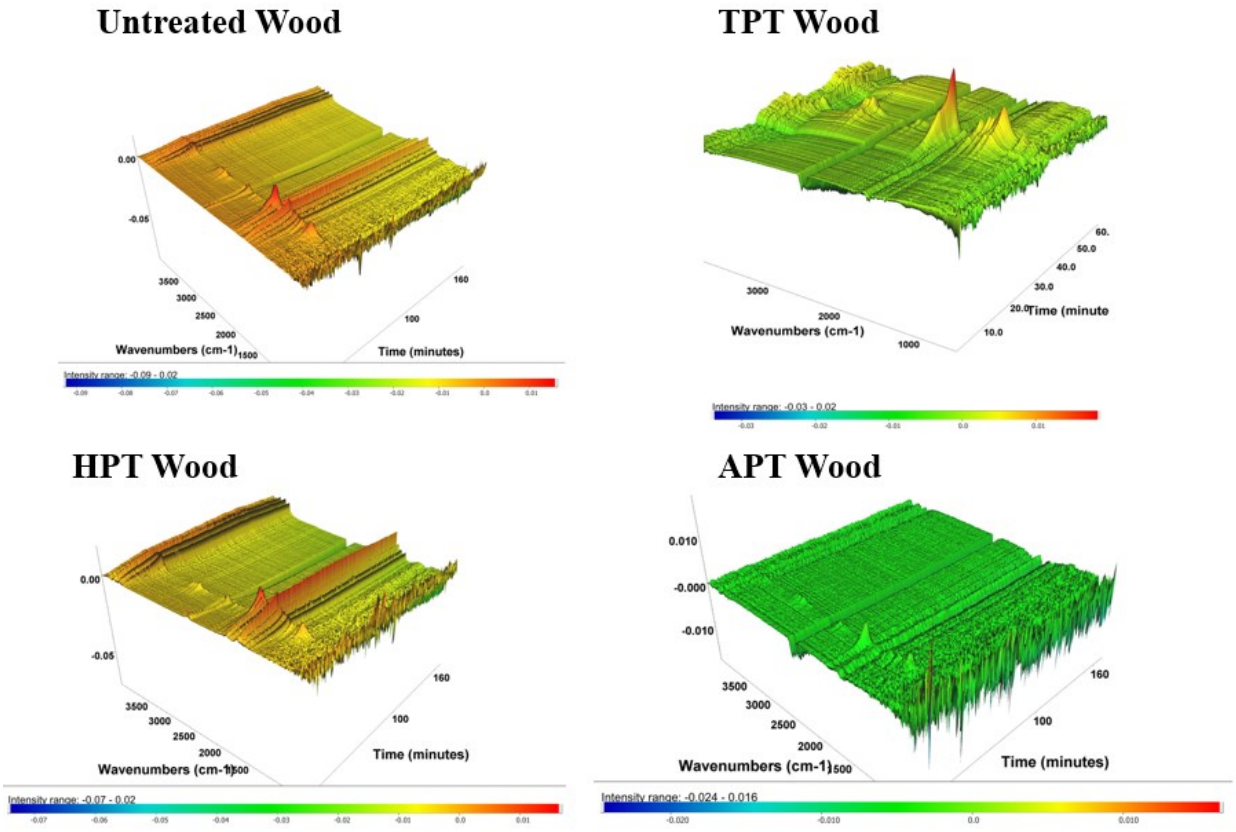

Figure C-5. Fourier Transform – Infrared Spectroscopy of off-gases produced during the thermogravimetric analysis of Untreated and Pre-Treated, dry samples.

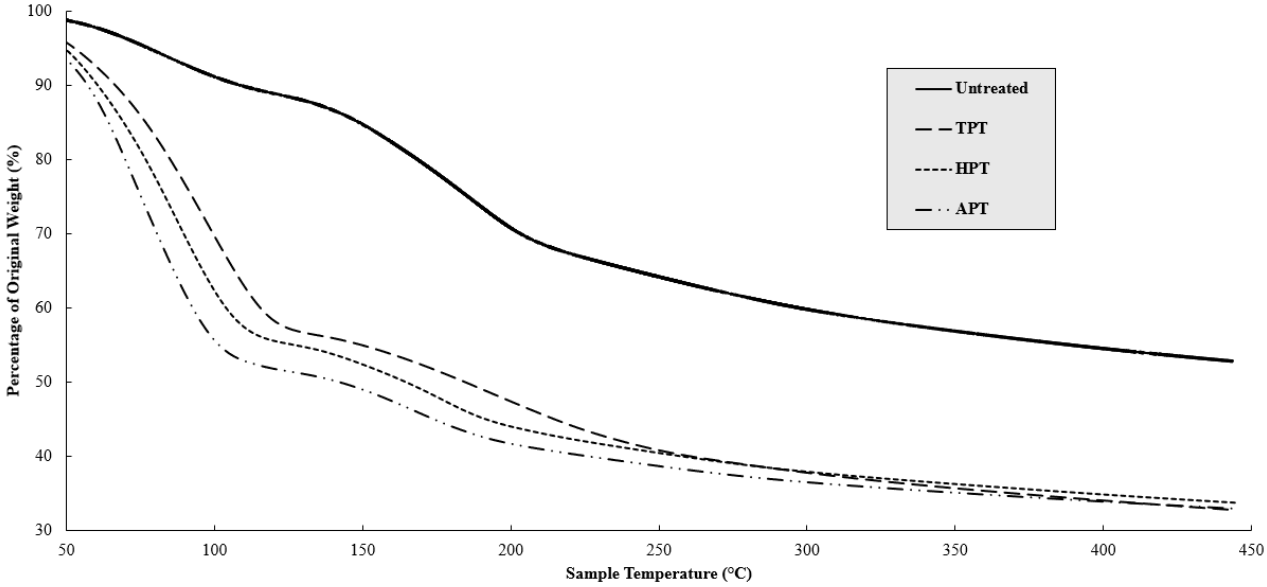

Figure C-6. Thermogravimetric analysis of Untreated and Pre-Treated H_3PO_4 impregnated samples.

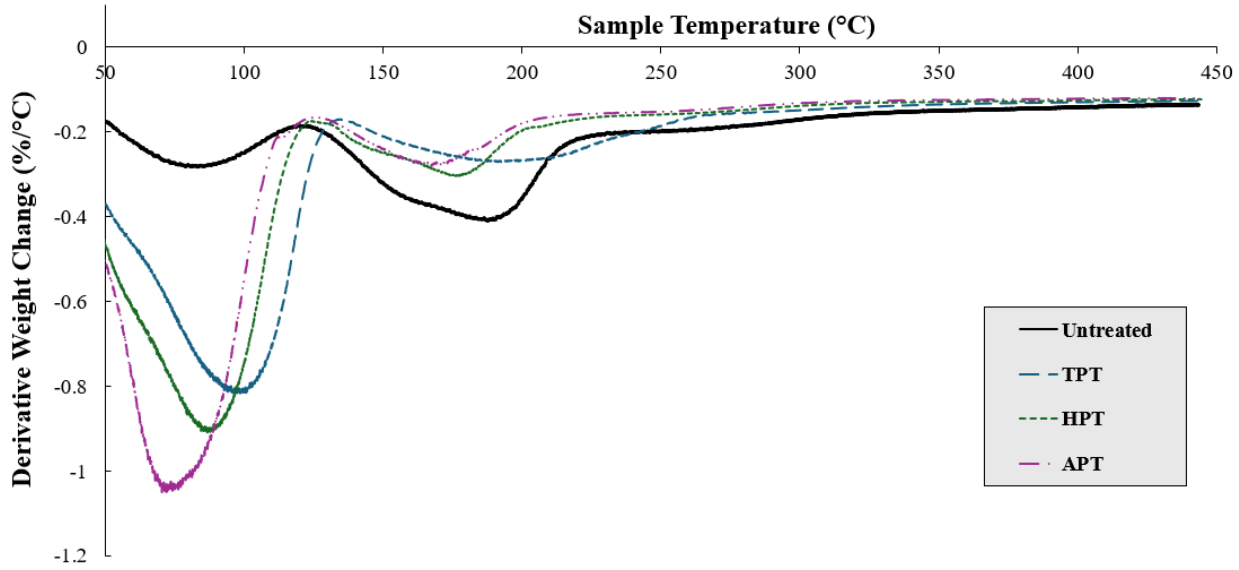

Figure C-7. Differential thermogravimetric analysis of Untreated and Pre-Treated H_3PO_4 impregnated samples.

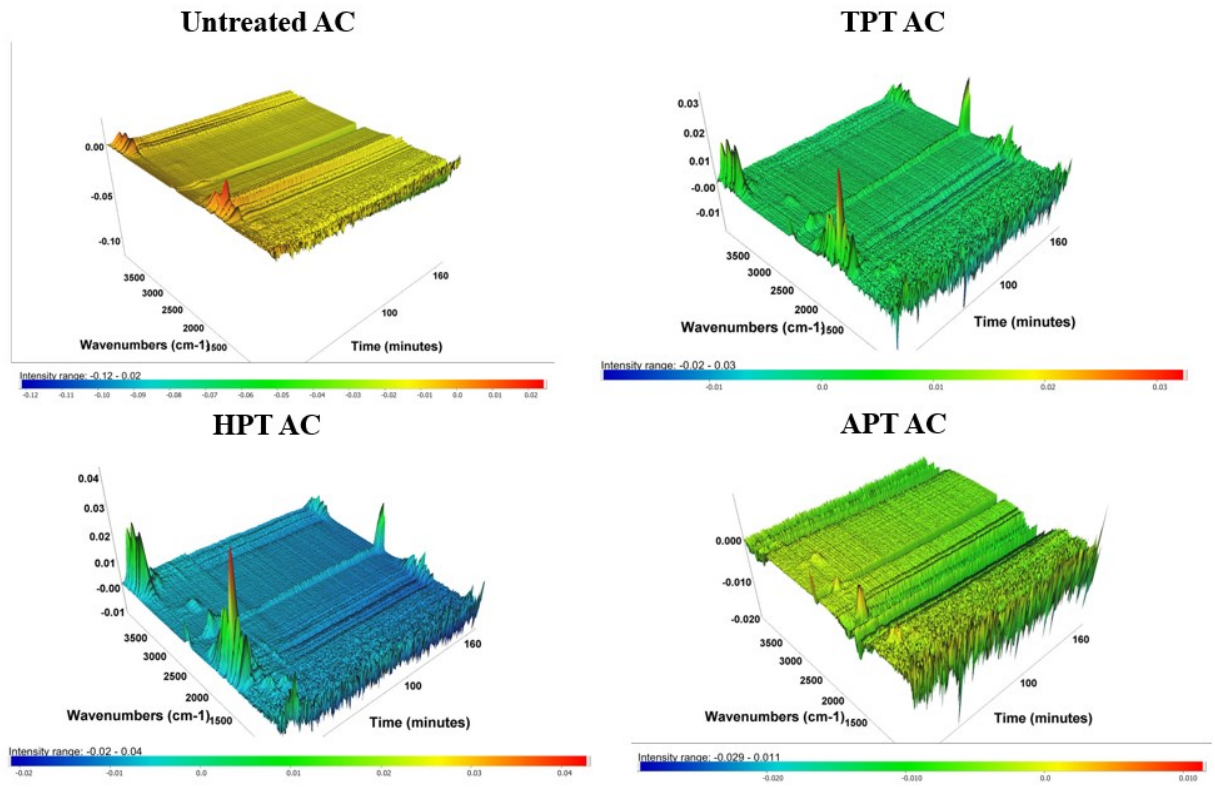

Figure C-8. Fourier Transform – Infrared Spectroscopy of off-gases produced during the thermogravimetric analysis of the H_3PO_4 impregnated samples.

Appendix D – Supplementary Data: Nitrogen Gas Adsorption Test

IUPAC recognizes several isotherm classifications (Type I through Type VI) which generally describe the nature of the porous material in question. Using this classification system, the ACs produced in this study most-closely align with Type IV which is commonly identified by a hysteresis loop. For example, the adsorption-desorption isotherm for the Untreated AC sample is shown in Figure D-1 below. The hysteresis loop is caused by a difference in the adsorption and desorption curves and is indicative of mesoporosity as the evaporation of nitrogen from these pores is laboured during the desorption phase. Thus, it may generally be expected that AC produced from white spruce wood using phosphoric acid would be mesoporous.

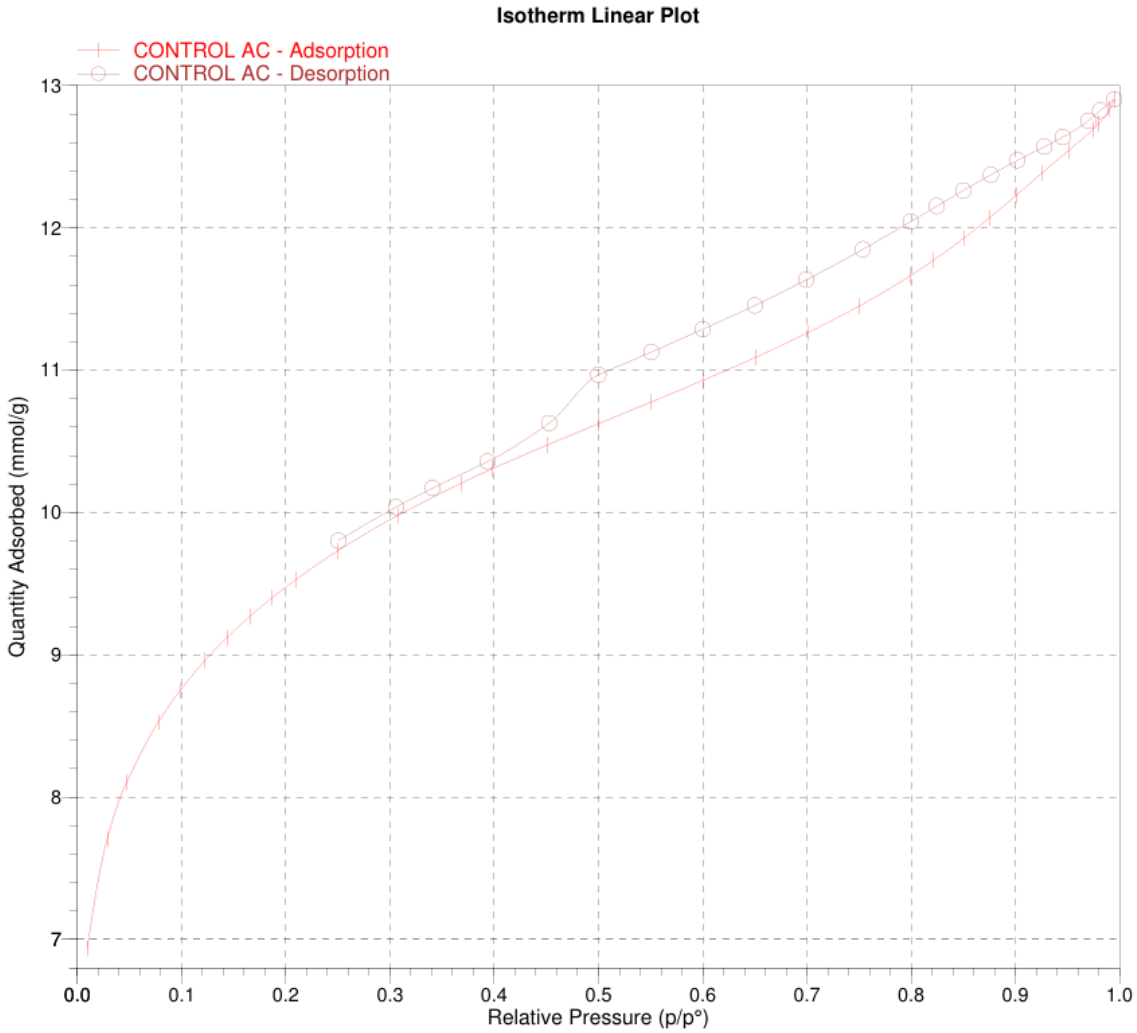

Figure D-1. Nitrogen gas adsorption-desorption isotherm plot for Untreated AC.

When comparing the adsorption-desorption isotherm of the Untreated AC sample with the HPT AC sample (the sample with the greatest specific surface area and pore volume), one key difference is recognizable (Figure D-2). At lower partial pressures (< 0.3), where micropore adsorption occurs during the test, the adsorption curve for the Untreated sample is visibly steeper than for the HPT sample. This observation implies that the HPT AC sample was less microporous than Untreated AC sample and is consistent with the quantitative results presented in Chapter 5.

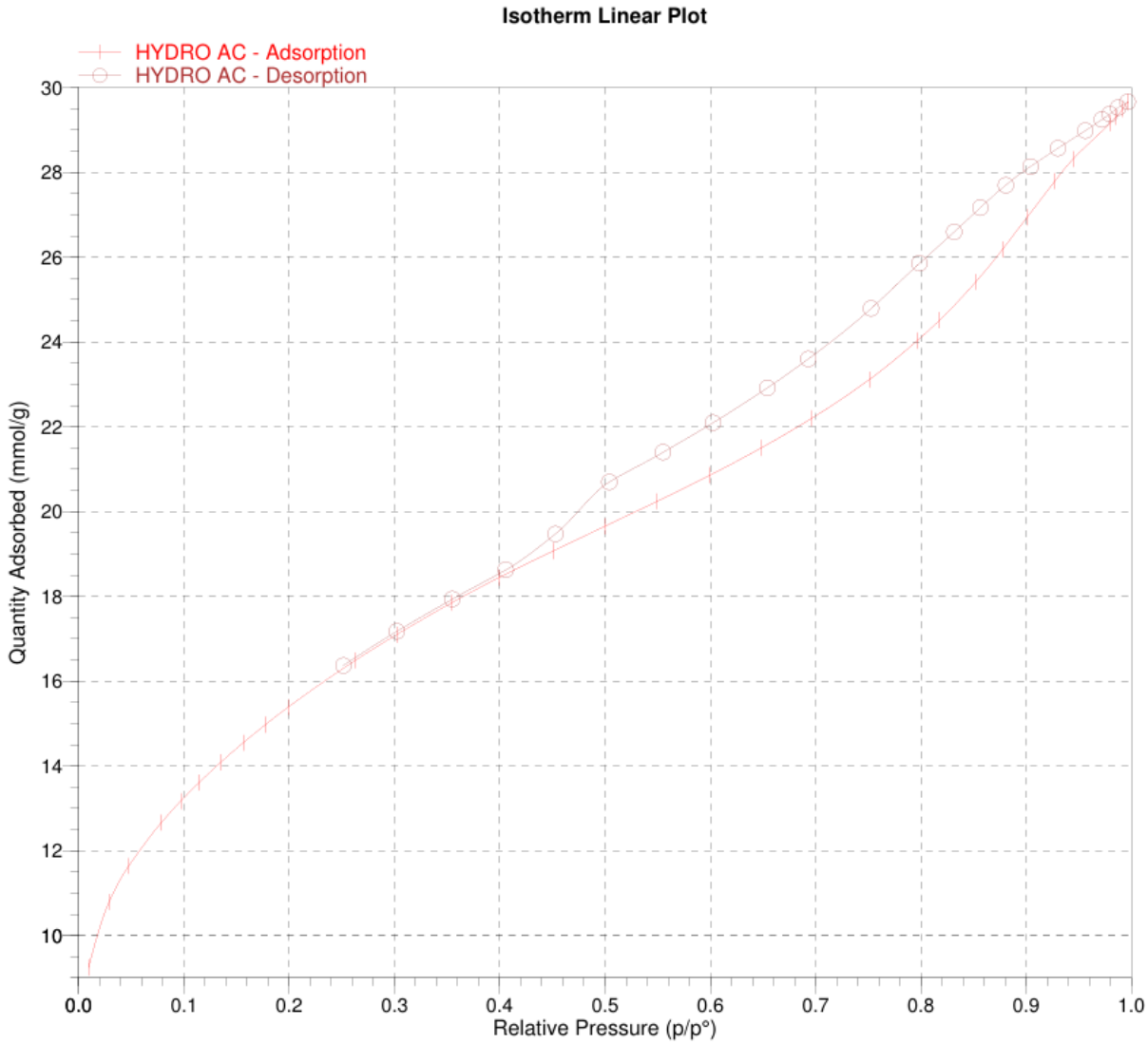

Figure D-2. Nitrogen gas adsorption-desorption isotherm plot for HPT AC.